Optical Wireless Channel Characterisation in Guided Structures (vehicle applications)

By

Zeina Safwan Rihawi

A thesis submitted in partial fulfilment of the requirements for the degree of

Doctor of Philosophy

School of Engineering

April 2016

For the martyrs of Syria 2011

&

for my family

Table of Contents

List of Figures

List of Tables

List of Abbreviations

4G – Fourth Generation

ABS - Antilock Braking Systems

ADAS - Advanced Driver Assistance Systems

AEL - Acceptable Exposure Limit

APD - Avalanche Photodiodes

BRDF - Bidirectional Reflectance Distribution Function

CAN - Controller Area Network

CDMMC - Combined Deterministic and Modified Monte Carlo

DMR - Diffuse-to-Mirror Ratio

ECU - Electronic Control Units

EMI - Electro-magnetic Interference

FOV – Field Of View

FOV- Field Of View

FSO – Free Space Optics

I2V - Infrastructure to Vehicle

IM/DD - intensity modulation direct detection

IR - Infrared

ISI - Inter Symbol Interference

ITS - Intelligent Transportation System

IVC – Intra-Vehicle Communications

LD - Laser Diode

LED - Light Emitting Diode

LIN - Local Interconnect Network

LOS – Line Of Sight

MCA - Monte Carlo Algorithm

MCA – Monte Carlo Algorithm

MMCA - Modified Monte Carlo Algorithm

MOST - Media Oriented Systems Transport

NLOS – Non Light Of Sight

OSI - Open System Interconnection

OW - Optical Wireless

OWC - Optical Wireless Communications

OWLS – Optical Wireless Links for Intra-Satellite

POF - Plastic Optical Fiber

RF – Radio Frequency

RFID - Radio Frequency ID

RMS - Root Mean Square

SAE - Society of Automotive Engineers

TDMA - Time Division Multiple Access

TS – Training Sequence

TTCAN - Time Triggered CAN

TTP - Time-Triggered Protocol

UAV - Unmanned Air

UTP - Unshielded Twisted Pair

UUV - Underwater Vehicles

UV – Ultra Violet

UWB - Ultra-Wide Band

V2I - Vehicle to Infrastructure

V2V - Vehicle to Vehicle

VLC – Visible Light Communication

Acknowledgments

The work which lies between these two covers was the most challenging academic project I have ever faced. Without the guidance, support and assistance of the following people, I would have never been able to complete it.

I am heartily thankful to my supervisors, Roger Green and Mark Leeson, for their support, understanding and guiding through the years. Without their encouragement through good and hard times I went through, I would not be able to reach this stage. Their academic support from the initial to the final level enabled me to develop an understanding of the subject and get more ideas to implement.

I would like to thank my family inspired, encouraged and fully supported me for every trial that comes my way, *Safwan ,Bouchra, Hazem,* and *Samer*.

I am pleased to gratefully thank all my friends inside and outside Syria for their kindness, support and being beside me in spite of the distance, *Dunia, Rahaf, Eman, Nour, Aya* and *Ahmad*

My friends in UK who gave me support, I am so proud to know you all, *Kifaya, Freeha, Maria, Aljalilah, Gulnaz, Aya, Dr. Alaa, Dr. Abdulqader, Amira, Monia, and Hiba (including Rand and Rana ☺).*

Lastly, I offer my regards and blessings to all of those who supported me in any respect during the completion of the project.

Declaration

This thesis is submitted in partial fulfilment for the degree of Doctor of Philosophy under the regulations set out by the Graduate School at the University of Warwick. This thesis is solely composed of research completed by Zeina Rihawi, except where stated, under the supervision of Prof. Roger Green and Dr. Mark Leeson. No part of this work has been previously submitted to any institution for admission to a higher degree.

Zeina Rihawi

April 2016

Abstract

The field of automotive electronics is growing exponentially in terms of devices related to safety, driver assistance and a variety of other nodes connected to infotainment systems which become standards with every automobile. Networking protocols connect these systems to provide assistance to drivers. However, the demand of high-bandwidth to serve applications lead to the necessity of a more flexible communication network within the vehicle

This thesis proposes using optical wireless links in intra-vehicle applications where different parts of the vehicle can form signal transferring media. A vehicle chassis can be represented as an optical wireless waveguide, where Line-of-sight (LOS) or a diffuse optical wireless link exists.

In order to predict the validity of the idea, optical wireless channel characteristics should be determined. This thesis describes the design of a modified Monte Carlo simulation tool for modelling a waveguide optical wireless channel. The simulator has the ability to determine the channel characteristics, and it can also be used more generally for indoor systems. The simulator studies the effect of purely diffuse and purely reflective materials as well as mixed diffuse-specular materials. The program was validated by comparing it with other indoor simulation studies and with a laboratory experiment for straight waveguide.

Emphasis was placed on understanding the requirements of LOS and diffusing optical wireless communication links. Results are presented for straight and bent waveguides received power, path loss and bandwidth for a series of receiver areas and fields-of-view. Studying the coupling effect between two waveguides which are different in dimensions has been assessed for series of transmitter directions. All studies have been undertaken for two types of materials (scattered and reflective) and two kinds of transmitters (omnidirectional and directional).

The study shows that the waveguides are plausible candidates to convey signals with high bandwidth, but a high power transmitter or an array of Light Emitting Diodes (LEDs) is needed due to power limitations.

List of Publications

R. J. Green, Z. Rihawi, Z. Abdul Mutalip, M. S. Leeson and M.D. Higgins, "Networks in automotive systems: the potential for Optical Wireless integration", 15th IEEE International Conference on Transparent Optical Networks (ICTON 2012), paper Tu.D3.1, Coventry, UK, July 1-5 2012.

M. D. Higgins, Z. Rihawi, Z. A. Mutalip, R. J. Green and M. S. Leeson, "Optical Wireless Communications in Vehicular Systems", *Communication in Transportation Systems*, O. Strobel (ed.), IGI Group, ISBN 978-14-666-2976-9, Chapter 7, pp. 209-222, 2013.

Z. Rihawi, M. S. Leeson and R. J. Green, "Free-Space Optical Communications in Vehicular Networks Using Rectangular Guiding Models", *IEEE Photonics Technology Letters,* vol. 28 (13), 2016

Z. Rihawi, M. S. Leeson and R. J. Green, "Path Loss and Coupling Efficiency between waveguides of Different Dimensions for the Optical Wireless Channel", *in preparation for IET Communications.*

Chapter 1: Introduction

1.1 Introduction

Optical Wireless Communications (OWC) have turned out to be more mainstream in current correspondence frameworks, with numerous applications in various media. Few but not all of the advantages which OWC systems carry, compared to Radio Frequency (RF) system, include the license-free high bandwidth as the RF spectrum is currently experiencing congestion. Besides, optical links in both the infrared and the visible spectrum are not regulated, which has recently allowed to demonstrate Visible Light Communication (VLC) system at speeds in excess of3 Gb/s utilizing single LED [1]. OWC systems are recognized to have a high level of security for indoor applications where the optical beam stays within the room and does not pass through wall. Another point of preference is the ease of the framework since it benefits from modest Infrared (IR) components which can be utilized for enlightenment at the same time.

Although practically OWC will not totally supplant RF frameworks such as fourth-generation (4G) wireless networks which can serve 100 Mb/s download data rate for

high mobility and it can reach 1Gb/s for low-versatility, during the last decade OWC technology proved its capability for handling short-range communication applications such as indoor environment and proceeded onward to Optical Wireless Links for Intra-Satellite communications (OWLS) [2].

1.2 Optical wireless communication systems

OWC systems cover Ultra-Violet (UV), Visible Light (VL) and Infrared (IR) communication systems each with better performance in a specific application. Figure 1-1 presents the basic components in an OWC system. For example, recently, VL communication is proposed to be an alternative to IR systems for indoor applications where white LEDs are used for both illumination and data transmission. In hospitals, where using RF devices is critical due to the probability of interference with other medical equipment, OW can be implemented with interference being risk-free. This idea can be expanded to any environment where RF interference can cause problems. However, a number of challenges should be considered: the high data rate required for transferring big data which might be limited by LEDs, the effect of the artificial light in the room which might cause Inter Symbol Interference (ISI) and the eye and skin safety regulations which might limit the value of the transmitted power.

Terrestrial Free Space Optics (FSO) communication is an outdoor communication system used for various applications. Basically, it is a LOS link which can be established

between buildings, between buildings and optical fibre networks and the last-mile access network [3]. Usually, lasers are used in FSO instead of LEDs. A full duplex FSO system between two nodes, which operates in different weather conditions, is becoming more popular in the market, for example [4] proposes a high speed system (80 Gb/s) using wavelength division multiplexing. The main challenge which OWC systems face in FSO lies basically in the weather conditions such as rain and fog which cause signal attenuation. It is important to keep the LOS link between the transmitter and the receiver in order to receive signal successfully with low error probability.

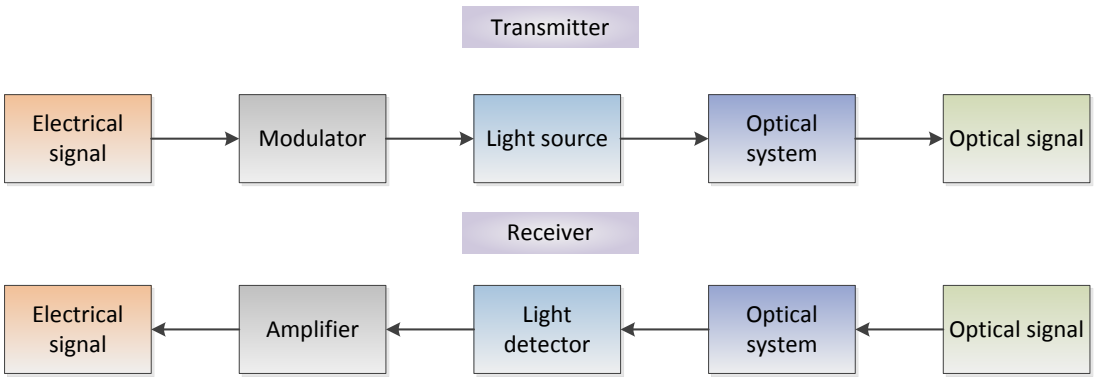

Figure 1-1 Basic components in an OWC system (adapted from [2])

Underwater OWC systems become an interesting domain for research and exploration [6]. Wire-line systems might offer real-time communications but with high cost and less flexibility, which open the window for light to be an important candidate as a communication medium [3]. Absorption and scattering affect the quality of the link where absorption tends to attenuate the signal and weaken it while the scattering might

distort and deviate the signal from its original path which results in poor received signal.

Another application domain where OW can perform well is Intelligent Transportation System (ITS). Two vehicles can communicate with each other and/or with road infrastructure using traffic lights, street lamps and vehicles light to send real time information to avoid accidents, help in detecting blind spots and connect to the internet for example.

1.3 Research motivation and contributions

The main application which drives this work is intra-vehicle communication and integrating OWC within this domain. Intra-vehicle communication is considered as one of the ongoing developed domains. The demand for high bandwidth links in order to serve multimedia and video signals in addition to the importance of secure connections has increased. Generally, the trend is towards replacing the mechanical mechanism with electronics and integrated circuits. The main parts of electronics for the car are: power-train management, body electronics, infotainment and communications with the outside world [7]. The sensors and processors can be connected through wires or wirelessly using RF signals.

As stated before, the transportation systems take place in OW applications, however, integrating OW into the body of the vehicle to transmit and receive different control

and multimedia signals has not been investigated widely. Other research which proposes using OW within the vehicle limits the application to use OW in the vehicle cabin [8] which offers a number of advantages, such as avoiding the RF interference, getting the benefit of high bandwidth availability and decreasing the necessity of using wires through the vehicle.

However, other vehicle parts can be used as a medium to transmit the OW signals through, an aspect that has not been reported yet. A vehicle chassis can be considered as a series of hollow waveguides which allow the light to travel through. Using the in-built material to transfer different signals will help in lowering the complexity of the overall vehicle system.

No work in the literature has investigated light transmission inside confined environments in vehicle; therefore, the fundamental goal of this work is to investigate another medium for OWC frameworks, in particular waveguides. Channel demonstrating will prompt better comprehension of OW channel which helps in designing and building reliable communication system.

The contribution of the thesis can be summarised as follows:

- It explores a new application area for OWC systems and fill a research gap in vehicular communication systems. It introduces new systems which can fulfil

different applications requirements within the vehicle.

- This thesis designs and validates a modified Monte Carlo simulation tool for waveguide-based OWC systems which can be used particularly for vehicular application. The simulation tool can be also used more generally for other systems with different configurations. The program takes into account the Phong model [9] where both scattered and specular components of reflected rays are considered, which adds to previous indoor OWC research where either of these components is measured.

Emphasis was placed on understanding the requirements of waveguide media to transmit OW signals. Therefore, results are presented for different parameters, namely received power, path loss, root mean square delay spread and bandwidth for a series of receiver areas, receiver FOVs and transmitter directions. Impulse response and frequency response of specific channels based on specific configurations are also presented. The effect of the material type is explored beside the transmitter level of directivity within the following environments:

- The OWC link through a straight waveguide has been studied in addition to studying the effect of the bent, and how it shifts the system from a LOS system to a diffusing system.

- Coupling two waveguides with different dimensions is explored in detail.

- An analytical study of connecting two waveguides without the use of a coupler is provided, including a study of transmitter directivity.

1.4 Thesis outline

The thesis consists of three parts: Introduction to Intra-Vehicle Communication (IVC) systems and to OWC systems and how it can be implemented in transportation systems. Building a simulator in order to study and model OW channels through the proposed environment is the second part. The last part simulates various scenarios and studies the effects of parameters on channel performance.

Chapter 2 reviews current IVC systems both wired and wireless systems, with an emphasis on technologies' physical layer. Within this chapter lies the motivation to conduct the research in detail. It concentrates on the IVC requirements and current systems drawbacks. Then, a new technology, the OWC systems, is proposed to complement the current systems.

Chapter 3 presents an up-to-date detailed study about various channel models developed for indoor OWC links. For diffused system, where non-line-of-sight (NLOS) exists between the transmitter and the receiver, reflections play the key role in conveying

the signal resulting in multipath behaviour. The studied models investigate the multipath and its effect on the system accuracy and computational efficiency. The chapter illustrates the theory behind OWC channel modelling which will be the basis for building the simulator needed to undertake the research.

Chapter 4 discusses the methodology used for the subsequent chapters along with the Monte Carlo Algorithm (MCA) in more detail to build the simulator. This simulator is programmed to cover all the scenarios that have been studied over in this research. It also provides all the fundamental equations required to study the channel performance. The simulation is based on ray tracing theory to capture the light travel from the transmitter to the receiver through the environment. Within the chapter, the primary results are presented by comparing the simulation results with a simple experiment study for a simple case.

Chapter 5 analyses the first group of scenarios. It studies the effect of curvature on OWC link performance in waveguides. To begin with, since most of the links are NLOS, It has been proved that a high number of reflections is essential, which differs from other indoor OW channels where normally 3-5 reflections are applied. Then the main characteristics of the channel (power distribution, RMS delay spread distribution and bandwidth distribution) over the end of the waveguide have been studied. The research moves on to study different parameters affects which are the receiver FOV and receiver aperture. The study is divided into four groups where two waveguides

material and two types of transmitter are used.

Chapter 6 presents the validity of connecting two waveguides which have different dimensions. The coupler behaviour on the light transmission is studied by defining the channel characteristics when using short and long couplers and how it affects the received power and bandwidth. The transmitter direction plays an important role in the quality of the received signal; therefore, it is included in the study.

Chapter 7 concludes the exploration and reveals insights into conceivable future work. Imperative results obtained from previous chapters are condensed and the feasible outcomes for future bearings are discussed.

Chapter 2: Background and Literature Review[1]

2.1 Introduction

Various sectors, from electronic systems through to communication technologies, automotive control systems or network topology developers, are finding vehicular communications attractive. Current protocols integrate different systems, for example Advanced Driver Assistance Systems (ADAS), infotainment devices and Antilock Braking Systems (ABS), into the vehicle. However, different requirements such as high-bandwidth and more secure and privacy connections make more reliable and flexible communication systems vital.

This chapter deals with the intra-vehicle network technologies presently employed, essentially wired and wireless systems. First, it highlights the technologies' physical layer, and second, it looks into the shortcomings in the current systems. This is followed by an overview of Optical Wireless (OW) communication systems, which explores the system configurations together with their components plus the fundamentals

[1] This chapter was partly published in [72] and [118]

of the channel theory. The chapter ends with a debate on the issue of the possible implementation of OW links replacing or complementing the designs now existing in intra-vehicle networks.

2.2 Intra-Vehicle Communication System Overview

The upgrading of automobile design has brought with it noticeable increase in vehicle electronics. The trend today is for cars to be equipped with electronic systems, which are becoming an integral part of the entertaining system, rather than mechanical and hydraulic ones. Along with controlling the movements of a car, they set up global connections with the help of a range of network technologies [7][10].

Generally, the applications in a vehicle can be divided into five subsystems or fields as shown in Figure 2-1, [11][12][13][14][15]. The powertrain subsystem has an intricate and fixed timed set of mechanisms controlling the engine and transmission. A remarkably consistent network with a high bandwidth is a prerequisite for this occurrence of frequent data transmission so that this real-time information can be communicated accurately.

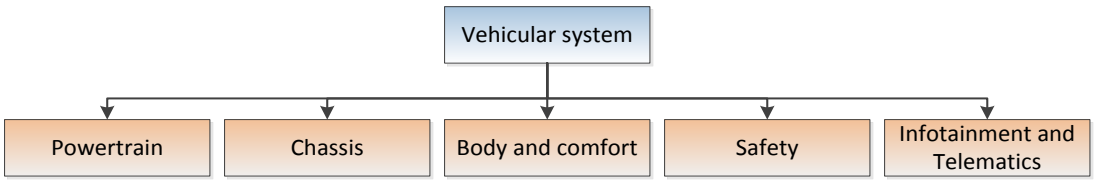

Figure 2-1 The five embedded vehicular subsystems (adapted from **[16]**)

Real-time, high bandwidth and safety critical networks are also present within the

chassis domain, and they are generally thought of as encompassing the suspension, steering and brakes.

The body and comfort subsystem includes electronics such as lighting, cruise control, air-conditioning, wipers, and locking mechanisms. Although it is important that the functionality of these components should be reliable, it is not of critical safety and thus does not require a high bandwidth network for which there are a number of elements thought of as lesser with respect to cost.

The safety subsystem is created when a sensor network is connected to impact and rollover zones, airbags and seatbelts. The success of a vehicle in delivering quality in this network is ultimately a factor into the overall success of its ability to provide the driver and/or passengers with information from any unpredictable and perhaps severe events. Even though the bandwidth is not an issue (because some of the actuators and the sensors are relatively simple), its high availability is of great importance.

The infotainment and telematics subsystem handles the multimedia and communications devices such as GPS or computer consoles and audio visual units. Yet, this subsystem differs from the chassis subsystem since many vehicle manufacturers do not consider several of the devices mandatory/compulsory, or they are installed and maintained by third parties. It is expected that a network subsystem will mostly require a high bandwidth for video and music streaming. Keeping in mind the advancement of entertainment and data requirements, which are developing faster than the time between the purchase of vehicles, subsystems will have to be dependable and to a large extent upgradable.

2.2.1 Physical Layer Technologies

Many years ago, there were typically up to 70 Electronic Control Units (ECUs) exchanging data in a vehicle [11]. Newer vehicles came with increased functionalities giving rise to greater demand on vehicular networks. The need of the hour was higher network bandwidth and more reliability but at a lower cost, which is true even today. From an engineering point of view, it became clear that with the reduction of the complexity of the network/s and the size, this problem could be solved. This would have to be achieved by maintaining or enhancing the capabilities of the requirements of the overall network given above [12][15]. In recent years, there have been some proposals for wired and wireless solutions or candidate solutions. A broad view of the various technologies is shown in Figure 2-2 [16].

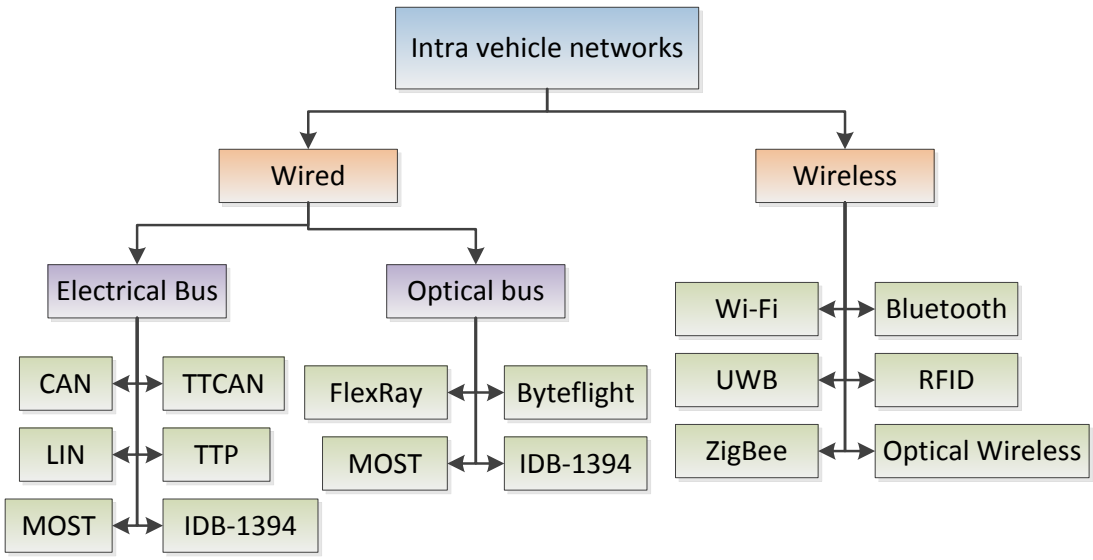

Figure 2-2 Intra-vehicle networks

Looking at Figure 2-2, one can observe that the names of the wired networks seem to be specific to the vehicular markets, which only vehicular engineers can understand. On the other hand, the names that the wireless networks have are commonplace names,

often widely recognized by the public. A short account of each of the matured wired technologies is provided below.

2.2.1.1. Intra-Vehicle Wired Networks

Controller Area Network (CAN)

Robert Bosch GmbH created the CAN protocol, an event driven communication protocol, in the mid 1980's [11]. It works at the physical and data link layer of the Open System Interconnection (OSI) Reference model. There are different data rates for the different versions of CAN, 125 kbps and 1 Mbps, normally 500 kbps, (low and high speed CAN protocols respectively) with the two-wire balanced signalling method being applied [17]. The Society of Automotive Engineers (SAE) classifies the third version of CAN as utilizing a single-wire plus-ground as a physical layer. CAN is mainly applied in non-automotive applications such as engine management, door and roof, air conditioning and lighting (power train applications). It seems to be the most popular in-vehicle network protocol. There have been a series of upgrades and advancements [18], one of the most important is the Time Triggered CAN protocol TTCAN. This lays emphasis on safety critical applications such as fly-by-wire sensors and actuators. It uses a bus network topology that operates at 1Mbps [10].

Local Interconnect Network (LIN)

A time-triggered network, the LIN protocol was created in 1999. It employs the master/slave mechanism. It is a low speed serial bus in-vehicle communication network (25 kbps) resulting in a low cost network. It is primarily used in body applications. Being a physical medium, the LIN protocol makes use of a single conductor wire to form a 12-V bus [17] and can be made a substitute to CAN when a low data rate is

adequate [19]. Basically, the use of LIN exists in simple applications in the body and in the comfort electrical subsystems joining the simple sensors and actuators over a single wire. Based on a master-slave protocol, LIN can take on unconditional, random, event triggered, diagnostic or under defined frame specifications [11]. The Ford Motor Company builds network architectures for next generation vehicles of multi levels: level one buses are usually for low data rate where LIN can be used, and level two buses connect level one buses [20].

Media Oriented Systems Transport (MOST)

In the car manufacturing sector, multimedia has evolved from a plain radio to refined entertainment systems that call for the interconnection of CD player, rear-view camera, and the navigation display [21]. MOST and CAN may be used together to realise an integrated in-vehicle audio and video communication [22].

MOST was built so that fast and short-delay networking with high bandwidth for infotainment applications would be possible. It aimed at providing real-time networking for safety applications and adopted a logical ring as its topology, which could be instrumental on physical or star networks [23].

MOST versions

MOST 25: Employing three channels (asynchronous, synchronous and control information) this version can reach maximum data rate of 25 Mbps. MOST 25 uses optical physical layer: Plastic Optical Fiber (POF) [24], which has resistance against Electromagnetic Interference (EMI), is lightweight and has low heat emission.

MOST50: This has more flexibility in channel assignment than MOST25, reaching the maximum data rate of 50 Mbps. Unlike MOST25, it employs the electrical transmission over Unshielded Twisted Pair (UTP).

MOST150: Being the latest version of MOST protocol, its maximum data rate is 150 Mbps. Like MOST25, MOST150 uses the same physical layer (POF) thus making MOST150 the new version of MOST25. MOST150 fully supports real time radio, compressed video and asynchronous data to transport simultaneously [25][26].

FlexRay

The first version of this protocol was published in 2004. It is a general purpose, high speed and fault tolerant protocol developed for time-sensitive and safety critical applications. It is sometimes deployed with CAN when there is need for a larger data rate of up to 20 Mbps, although it is flexible enough to be extended across all subsystem applications within the vehicle. The high point of the flexibility of the protocol is the capacity to configure a bus, star or multiple star topologies over copper or optical layers [27]. It consists of event-triggered and time-triggered communications. The protocol is used for safety applications and can be said to be the backbone that connects heterogeneous networks.

Time-Triggered Protocol (TTP)

TTP was developed for those devices that needed time-triggered event solutions. It has two versions, TTP/A and TTP/C. While the former is based on a Time Division Multiple Access (TDMA) master-slave topology, the latter is based on a fully distributed TDMA topology. TTP/C has been the most popular variant in recent years. It is set up

with a star bus for fault tolerant applications up to 10Mbps [19][28].

IDB – 1394

The ITS Data Bus employing IEEE 1394 (IDB-1394) technology has been designed as a high performance bus useful in multimedia applications. It is presently able to transfer at rates of up to 400 Mbps with a possible 1600 Mbps version on the horizon. It is capable of both isochronous and asynchronous modes, with the former designed for use with high speed cameras and video streaming [29].

Byte flight

Designed by BMW, this 10Mbps optical data bus is meant for applications that combine time sensitive or safety critical operations, for example, airbags. Its flexibility makes it deployable in less safety critical electronics within the body and comfort subsystem [30]. It is, in part, also used in the FlexRay protocol as the protocol can incorporate both time and event driven mechanisms and is based upon single point to point links [31].

Table 2-1 summarizes some information on the physical layer specifications of specific intra-vehicle wired networks

Table 2-1 Some Automotive Physical Layer Technologies (adapted from **[14]**)

Protocol	**Bitrate**	**Medium**
LIN	19.2 kbps	Single Wire
CAN	1 Mbps	Twisted Pair
FlexRay	20 Mbps	Twisted Pair/Optical Fibre
MOST	150 Mbps	Optical Fibre

2.2.1.2. Intra-Vehicle Wireless Networks

Looking at the maturity of the wired networks above, researchers are now also focusing their studies upon wireless methods for a number of reasons. Firstly, with the rise in the degree of complexity of the vehicles, with more sensors and actuators present, more wires are required. At this simple level, the wider audience sees this vehicle as both heavier and harder to manufacture; its making and working will cost more. Secondly, end users today are more involved in interactions with wireless networks and so wish to have these included in the vehicular experience too.

Researchers are focusing on general purpose technologies such as Bluetooth [32], specific technologies such as a full ZigBee stack [33] and the latest works on the use of Ultra-wide band UWB links [34].

Bluetooth

Bluetooth, which is the most commonly used standard today [32], is cheap and capable of transmitting voice and data. Its power requirements are low and it can penetrate obstacles. However, it cannot handle high data rates making it ineffective for video transfer.

ZigBee

ZigBee provides high-performance short-range communication with low power consumption. This is the reason why it is a good candidate for automotive applications. However, working in the same frequency range as Bluetooth (the ISM Band), there is a possibility that these two networks will interfere with each other in the vehicle net-

work. De Francisco et al. [35] studied how a ZigBee network can simultaneously co-exist with Bluetooth. Unfortunately, ZigBee is not capable of transmitting video signals as it can only transfer signals at low to medium data rates.

Ultra-Wide Band (UWB)

UWB technology shows promises of a worthy candidate with a capacity of solving multipath fading and also with its available spectrum [34]. It is mostly used in indoor or confined spaces being of utility in short range applications that have low transmission power requirements.

UWB can be used for telematics, multimedia and infotainment applications within the vehicle. It is also employed in vehicular radar systems [36][37]. The restrictions of UWB arise from the challenge of designing an antenna and a receiver for the different applications knowing that UWB is particularly vulnerable to the interference of noise coming from other vehicular elements, especially from the engine [38].

Radio Frequency ID (RFID)

RFID networks are formed by tagging objects within the vehicle that need to be acknowledged such as safety harnesses and spare wheels. It is possible to communicate via a radio frequency signal to the tag on the system the object to be detected by a transponder. Even though there have been several ideas proposed in the past, the limitations of power efficiency and the locations of tags within the vehicle cannot be overlooked [39].

2.2.2 Discussion

In 1994, the SAE published a classification of in-vehicle networks. It stated that networks are only categorized based on bandwidth (data rate) and functions of networks [40]. The first category includes low speed/low cost networks with data rates less than 10 kbps (LIN as an example). The applications of this group are mostly committed to the body domain. The second category networks are those operating at data rates of between 10 and 125 kbps and are used for general information exchange (low speed Controller Area Network (CAN-B) [41] as an example). Differing from the above, the third and fourth groups of networks require high speed communication. The data rates of the third group of networks range from 125 kbps to 1Mbps. They are used in a wide range of applications, especially in powertrain and chassis domains. On the other hand, data rates in the fourth group are up to or more than 1 Mbps. They are primarily used for telematics (MOST and Bluetooth as wireless communication [42] are the main examples of networks for telematics data transmission). Furthermore, there are networks that provide high data rates (greater than 1 Mbps) such as the TTP/C, FlexRay [43] and Byteflight [42][44] protocols mainly applied to in-vehicle safety applications.

The cost and weight of a modern automobile's cable harness is substantial as it may weigh up to 30kg. Also, cable connections need space, and this has to be taken from either the doors, columns or the firewall between the engine and the passenger compartment [45].

The system performance becomes limited due to some shortcomings of intra-vehicle networking systems. Some examples are: electrical buses are prone to electromagnetic disturbances, the bus line must not be very long, only low signal quality is available

and electrical buses are generally unsuitable for high speed data transmission. This results in the use of an optical data bus, which is generally insensitive to electromagnetic disturbances and cross talk effect between lines, significantly higher transmission speeds, and also cost and weight savings by the reduction of wiring [24].

On the other hand, the radio frequency (RF) wireless medium overcomes few of the mentioned disadvantages; however, RF susceptibility restricts the system performance.

2.3 OW Communication System Overview

The physical layer of an OW communication system depends on optical signals in the 400-3000 nm band [46]. In communication systems based on RF, the carrier frequency ranges from 30 MHz to 5 GHz, while it can go up to 300 GHz for satellite and other pointed communication systems [47].

An OW communication system making use of an IR carrier is a technology capable of bringing together the high bandwidth opportunities within optical fibre systems. Such systems have the added benefit of mobility which is a characteristic within RF systems. The difference between the RF and OW systems is that the latter has the benefit of high speed short to medium range communications operating within a theoretically unlimited and unregulated bandwidth spectrum with lower cost components. Table 2-2 compares radio and IR indoor wireless communications [48].

Moreover, OW systems are capable of secure deployments with immunity to adjacent

communication cell interference as a result of light's inability to pass through many obstacles [49].

Table 2-2 Properties of Radio and IR Wireless (adapted from **[48]**)

Property	**Radio**	**IR**	**Implication for IR**
Bandwidth regulated	Yes	No	Approval not required Worldwide compatibility
Passes through walls	Yes	No	Inherently secure Carrier reuse in adjacent rooms
Multipath fading	Yes	No	Simple link design
Multipath dispersion	Yes	Yes	Problematic at high data rates
Path loss	High (frequency dependent)	High	Short range
Dominant noise	Other users (EMI)	Background light	Short range
Average power proportional to	$\int \lvert f(t)\rvert^2 \, dt$	$\int f(t)dt$	*F(t)* is the input signal with high peak-average ratio

However, the capabilities of OW are not without limitations. It does have some disadvantages. With the carrier unable to pass through opaque barriers, it becomes important to have a potentially larger number of base stations as they can avoid issues in shadowing. In general, the photodetectors are greatly susceptible to concentrated levels of background light from the sun or ambient lighting. Another important issue is the need to operate a transmitter within an Acceptable Exposure Limit (AEL) so that the users' sight is not affected [50].

2.3.1 Link types in IR systems

Links can be classified based on two parameters: the angle of the transmitted beam and the receiver field of view (FOV), and the relative positions of the transmitter and receiver. A directed transmitter comprises a narrow-beam radiation pattern and a directed receiver has a narrow FOV. Similarly, non-directed transmitter consists of a broad-beam radiation pattern, whereas non-directed receiver has a wide FOV. A LOS exists between them if the receiver gets direct radiation from the transmitter. If this direct radiation is not obtained from the transmitter, the receiver gets the radiation from reflecting objects, then it is non-LOS [51]. Figure 2-3 illustrates OW link configurations in a room.

Directed LOS link is used for point-to-point communication links in outdoor environments, but in certain instances it is used in the indoor environment, too. The source transmits an intense narrow beam displaying low power requirements and also creating a high-power flux density at the photo detector. Moreover, the LOS link has the ability to provide the high data rate (hundreds of Mbps) for up to 5 km distance [52]. In a directed LOS link, the noise emitted from the ambient light sources is to a great extent rejected when used with a narrow FOV receiver [52] and the signal distortion due to multipath dispersion is almost neglected. Thus, the data rate is restricted by free-space path loss [52][53][54]. Turning now to the disadvantages: the coverage area of a signal channel could be very small for indoor applications; therefore, it can pose a problem while providing area coverage and roaming. As receiver and transmitter modules have to be aligned, directed LOS links cannot support mobile users when using wide FOV receiver, the configuration is called hybrid configuration.

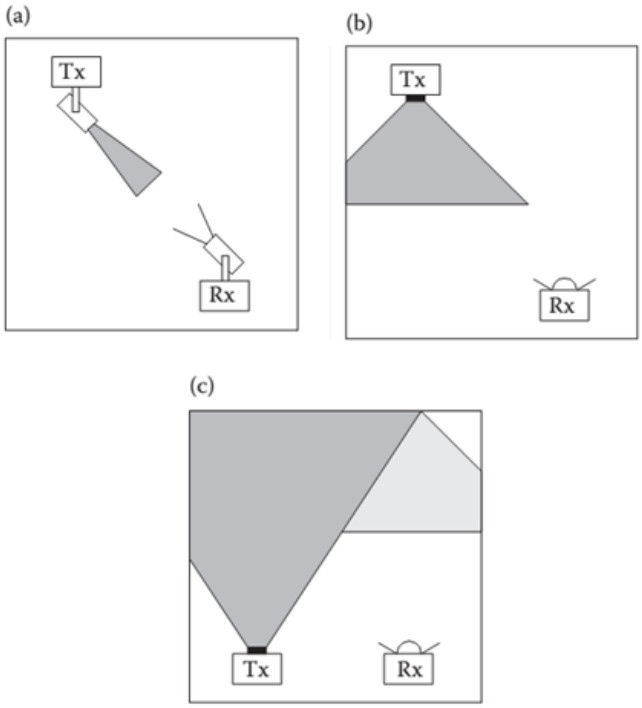

Figure 2-3 OW Link configurations (a) Directed LOS, (b) Non directed LOS, (c) Diffused, (adapted from **[48]**)

Non-directed LOS links which are widely known as the most flexible configuration for indoor applications use wide beam transmitters and wide FOV receivers. The beam scatters from surfaces within the room (indoor environment) for a wider coverage area, consequently giving an optical medium similar to RF, offering data rates in excess of 150 Mbps. Non-directed links are appropriate for point to multipoint broadcast applications providing the ability to overcome shadowing and blockage; not needing any alignment or tracking. Most of the received power comes from reflections from object surfaces within rooms, which allows the photodetector to detect the transmitted light from diverse directions. On the other hand, they face a high optical path loss (thus higher transmit power is needed) and must also cope with multipath-induced dispersion. Multipath propagation gives rise to (ISI); however, as a result of the large detector

sizes when compared with the wavelength, it does not lead to multipath fading in indoor IR systems resulting in limiting the data rate to around a few Mbps in a normal size room.

A diffuse configuration is also identified as nondirected NLOS proposed in [55]. In the indoor environment, the transmitter direction is straight towards the ceiling emitting a wide IR beam. It does not require perfect alignment of the transmitter and receiver modules. Neither does it require a LOS path to be maintained being almost immune to blockage of the transmission path. Besides, it is also very flexible and can be efficiently used for both infrastructure and ad hoc networks [52][55].

Unfortunately, diffuse links have to withstand high path loss, usually 50–70 dB for a horizontal separation of 5 m [56]. This path loss can be even more if a temporary obstruction (for example a person) obscures the receiver blocking the main signal path; this situation is known as shadowing [56]. Furthermore, a wide FOV photodetector normally gathers signals that have undergone one or more reflections from ceilings, walls and other room objects. The received signal may have to experience severe multipath dispersion with the transmitted pulses spreading out across alternative routes of varied lengths.

2.3.2 OW system hardware

Transmitter: The transmitter converts the electrical signal into an optical signal. It comprises an interface circuit and source drive circuit where the drive circuit transforms the electrical signal into an optical one with the help of light source. There are two options in practical circuits for a light source, Light Emitting Diodes (LEDs) and

Laser Diodes (LDs). Both are useful in specific systems [57].

Broad bandwidths and high launch powers make LDs fit for outdoor applications. As they produce narrow optical beams, they may need a diffuse lens if a wide beam is required. LDs provide a larger modulation bandwidth and higher optical power output than LEDs. Also, LDs that are commercially available have a fairly linear and efficient electrical to optical conversion (conversion efficiency ranges from 30-70%) above the lasing threshold [58]. This allows multilevel modulation schemes to be applied in the indoor OW link. Yet, for obtaining a wider scale employment the following issues have to be considered: cost, the need to render the LDs eye safe and further requirements of threshold and temperature control [2]. The consideration of safety issues is of importance as LDs emit high power making it imperative to consider the LED alternative.

Normally, LEDs are inexpensive and not easily damaged [59]. Safety standards uphold the use of all indoor applications with Class 1 eye safe, and so LEDs are mainly used in indoor systems rather than LDs.

The choice between these two light sources actually depends on the particular application requirements.

Receiver: The receiver comprises an optical detector and signal conditioning circuit. Its role is that of converting the transmitted optical power into electrical signals.

The two options for a photodetector are PIN diodes and Avalanche Photodiodes APD. A PIN is often preferred as it has good quantum efficiency and is low-cost whereas an

APD 10-15 dB is more sensitive but has little tolerance to temperature fluctuations [60].

While designing an OW system, apart from the safety issues, *noise* is another important factor that has to be taken into consideration. Out of the many sources of noise, the ones having the greatest impact are the thermal noise or receiver noise and the background noise. Sunlight and light from incandescent and fluorescent lamps are the sources of background noise. These are known to be the major sources of noise due to their radiation being in the same wavelength as the IR data signal. Thermal noise is generated at the receiver's side and depends on the type of preamplifier used.

Channel: In nearly all short range and confined deployments, such as indoors, or as will be seen, in-vehicle, the single practical transmission technique is intensity modulation direct detection (IM/DD), as shown in Figure 2-4.

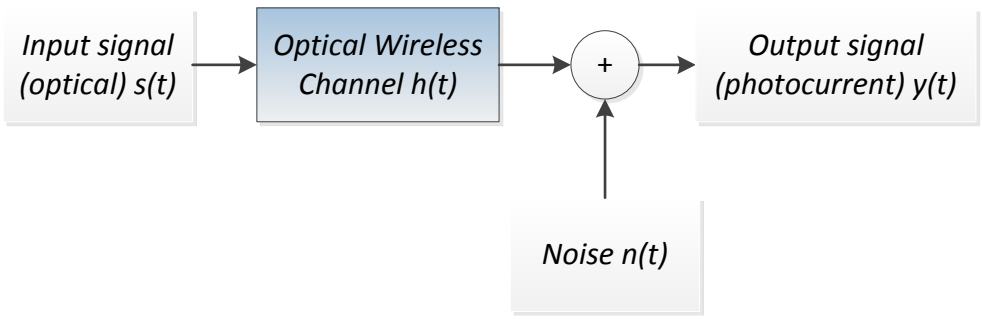

Figure 2-4 IM/DD Equivalent Baseband Model of an OW System (adapted from **[49]**)

This has a suitable device such as an LD or LED for emitting an instantaneous optical power *s(t)* that propagates through a linear channel with impulse response *h(t)* until

the time it is incident upon an optical detector at the receiver. The photodetector normally has a surface area of between 10^6 and 10^8 square wavelengths, and this makes it is possible to assume optical incoherence. Thus, the received signal *y(t)* is nothing but the integration of the detected optical power over the surface of the detectors, multiplied by its responsivity, *R*. Besides, if one assumes that the system is operating in the presence of intense IR and possible background radiation, *y(t)* will also comprise an additive white Gaussian noise term *n(t)* such that:

$$y(t) = R\, s(t) * h(t) + n(t) \quad (2.1)$$

where * denotes convolution. As *s*(*t*) is a power quantity, it cannot be negative, such that the average transmitted optical power, P_t , is proportional to the time integral of *s*(*t*):

$$P_t = \lim_{T\to\infty} \frac{1}{2T} \int_{-T}^{T} s(t)dt \quad for\ t \geq 0 \quad (2.2)$$

Assuming *h(t)* is known, the total optical path gain is given by:

$$H(0) = \int_{-\infty}^{\infty} h(t)dt \quad (2.3)$$

Such that the received power is given by

$$P_r = H(0)P_t \quad (2.4)$$

where from Equation 2.4 it is possible to see that the aim should be to maximise P_r by

a combination of minimising the path loss and increasing the average transmitted power, yet remaining within the maximum permissible AEL. An OW system designer finds it very challenging to determine or predict the impulse response, *h(t)* since this is unique to a given source and receiver configuration within the environment in which they are deployed. Thus, the position and orientation of the transmitter and receiver, and its respective properties of radiation emission pattern, FOV and active collection area, are all factors of *h(t)*. There is an endless number of potential responses when one combines these with the dimensions of the environment and any object enclosed, together with their respective reflectivity properties.

2.4OW applications in automotive Systems

OW communication systems have found their way into aerospace applications, air craft environment and transportation systems and are considered to be strong candidates to be applied in both Unmanned Air and Underwater Vehicles (UAV and UUV) after intensive improvements to optoelectronic parts, circuits and front-end electronics reported by Arruego *et al*. [61]. Their study reports ten years of research and developments in OW Links to intra-Spacecraft communications (OWLS) which took place in the early 2000s. Several communication protocols were adapted to OWLS (for example, CAN). Another study presents OW link performance between Low Earth Orbit satellites [62].

Several studies have been performed to evaluate the availability of OW links in aircraft cabins [63]-[66]. Such links benefit from the freedom of interference with avionics. However, eye safety regulations should be considered while designing the system.

Moving towards vehicle communication systems, OW links have been found useful in terms of vehicle to vehicle (V2V) networks, Vehicle to Infrastructure networks (V2I) and Infrastructure to Vehicle networks (I2V) [67]-[70]. Visible Light Communications (VLC) has been integrated into Intelligent Transportation Systems (ITS) using LEDs existing in vehicles while it offers both safer and faster systems in vehicles.

2.4.1 OW application in intra vehicle environment

Looking at all the constraints on an OW communication system, one might wonder how it would be feasible for it to compete with the conventional methods described earlier for intra-vehicle communications

In effect, [71] and [72] suggested building OW links within the vehicle to take advantage of their positive characteristics; high security, high bandwidth, low-cost system and immunity to EMI. Higgins *et al.* [73] provides an initial analysis into the feasibility of implementing an OW communication system for IVC. The study shows the possibility of offering a high bandwidth system within an empty car cabin with negligible delay. The study is improved to incorporate passenger presence [74] and all results support the possibility of employing OW in intra-vehicle applications.

Other vehicle parts can be used as pathways for the OW signal; for example, the vehicle frame or the engine compartment. Both the doors and the vehicle frame form potential waveguiding structures that are free of sun and ambient light. Concentrating on the vehicle frame as a transmission medium, a waveguide in a vehicle can be defined by a sequence of tubes with different shapes; straight, bent and T- shaped, with rectangular and circular cross sections as shown in Figure 2-5. The metal structure is assumed

to be clean with smooth polish inner surfaces so manufacture faults are not affecting the optical transmission

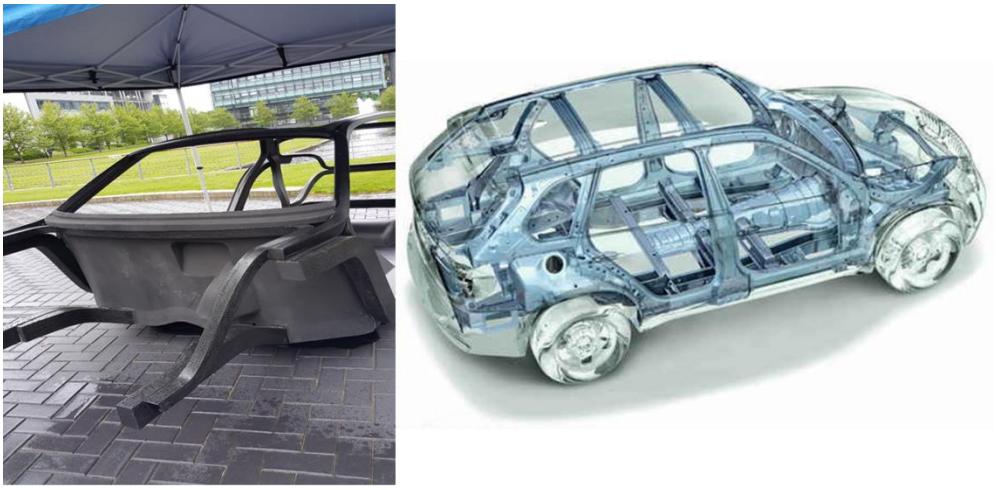

(a) (b)

Figure 2-5 Vehicle chassis (a) general vehicle frame (b) BMW X5 frame

This application in particular drives the motivation of this study. An OW infrastructure can be built within vehicles in order to benefit from the free-space propagation of light waves in the near IR band as a transmission medium for communication. As the distance between transmitter and receiver is relatively short, high data rates can be easily achieved in cars. Furthermore, if OW is going to be used in the car structure (doors or engine compartment), then eye safety constraints should not be a limiting factor. However, the nature of the vehicle frame as a sequence of waveguides might not allow for LOS system which decreases the maximum data rate the system can serve. Another challenge OW system faces in this environment is signal-to-ratio (SNR) value which depends on the optical signal power.

2.5 Conclusions

In this chapter, an overview study of intra-vehicle communication system and OW communications have been presented. Protocols presently used in vehicles have been studied emphasising on the physical layer used and the requirements for each protocol. Wires (electrical and optical) or a wireless medium (RF domain) are used to transfer the signals.

The general OW communication system has been studied starting from the link configurations via a transmitter/receiver overview to end with a presentation of the OW channel. This leads to the next chapter, where an intensive review of OW channel models is presented.

Chapter 3: Indoor Optical Wireless Channel Models

3.1. Introduction

In the previous chapter, the concept of an OWC system as well as the fundamentals of relevant transmitters and receivers were discussed. The main and proposed applications of an OWC system in transportation systems have been addressed.

Since the main application which drives the motivation of this work is studying the possibility of integrating OW communication systems in intra-vehicle networks, then we need to model the channel through which the OW signal is passing. As discussed earlier, the vehicle frame potentially constitutes a series of optical waveguides due to its structure. The light can be transmitted from one end, travelling through the frame until it reaches the receiver in the other end of the frame. The frame can be considered as hollow tubes with specific shapes; straight, bent, and T-shaped with rectangular and circular cross sections.

In order to build the channel model, firstly in this chapter, an intensive up-to-date study

of different OW channel models is presented. This study is quite important because of the significance the channel impulse response has in evaluating the performance of the system. Several algorithms have been suggested to calculate the impulse response and its related characteristics (Root Mean Square (RMS) delay, bandwidth, received power, and data rate) which define the link performance.

Channel models are compared in terms of computation speed, complexity and accuracy.

3.2. System model

A vehicle frame constitutes a structure which can be viewed as an optical waveguide. An optical beam will reach the receiver after undergoing quite a number of reflections. Therefore, a relatively high power is required at the transmitter. The signal is dispersed in time due to multipath propagation which results in reduced pulse amplitude and increased delay spread and causes ISI.

The vehicle frame environment is similar to an indoor environment, as it forms a closed medium. In addition, it benefits from the absence of sun and ambient light, which leaves the noise sources to be only the component noise. The channel configuration mainly consists of non-directed diffused links, where LOS and NLOS paths exist.

3.3. System characterization

In order to study channel models, first, we need to define the system elements. Source, detector and reflector (environment) mathematical characteristics are explained in the following subsections.

3.3.1. Source model

An optical source may be represented mathematically by a number of factors: a unit-length orientation vector $\widehat{\boldsymbol{o}}_S$, a position vector $\boldsymbol{p}_S$, a transmitted power P_s, and an emission pattern $I(\phi,\theta)$, where ϕ and θ are azimuth and polar angles respectively. The emission pattern refers to the light strength in any direction from the light source.

In a conventional OWC channel, the source follows a Lambertian radiation pattern model, where it has uniaxial symmetry and it means that it is independent of ϕ and proportional to the viewing angle:

$$I(\theta) = \frac{n+1}{2\pi} \; P_s \cos^n(\theta) \quad for\ \theta \in \left[-\frac{\pi}{2}, \frac{\pi}{2}\right] \qquad (3.1)$$

where n is the mode number of the radiation lobe, which specifies the directionality of the source. The higher the n, the higher the directionality. $n=1$ corresponds to a conventional Lambertian source:

$$n = -\frac{0.693}{ln[cos(\mho)]} \qquad (3.2)$$

where ʊ is the LED half power transmission angle.

Commercial LEDs such as the NSPW345CS from Nichra and the LUXEON Rebel from Lumileds/Philips, have rotational asymmetries appearing in the emission pattern. Therefore, a more general mathematical model is needed. The radiation pattern can be modelled by using analytical approximations or Monte Carlo ray tracing [75][76][77], or by using a more recent analytical model whereby emitting surfaces are taken into consideration [78]. The sum of two or three Gaussian or cosine-power functions [79] represents the LED radiation pattern. For the aforementioned LEDs the radiation patterns are illustrated in Figure 3-1, and can be expressed respectively [80]:

$$I(\theta,\phi) = \sum_i g1_i \, exp\left[-(|\theta| - g2_i)^2 \left(\frac{cos^2\phi}{(g3_i)^2} + \frac{sin^2\,\phi}{(g4_i)^2}\right)\right] \qquad (3.3)$$

where $g1_1$= 0.13, $g2_1$ = 45˚, $g3_1$= g4$_1$ =18˚, $g1_2$ = 1, $g2_2$= 0, $g3_2$ =38˚, $g4_2$ =22˚, and ϕ is the azimuth angle off the initial direction within the plane that is parallel to the emitting surface of LED, and

$$I(\theta) = \sum_i g1_i \, exp\left[-\left(\frac{|\theta| - g2_i}{g3_i}\right)^2\right] \qquad (3.4)$$

where $g1_1$ = 0.76, $g2_1$ = 0˚, $g3_1$ =29˚, $g1_2$ = 1.10, $g2_2$ =45˚, and $g3_2$ = 21˚.

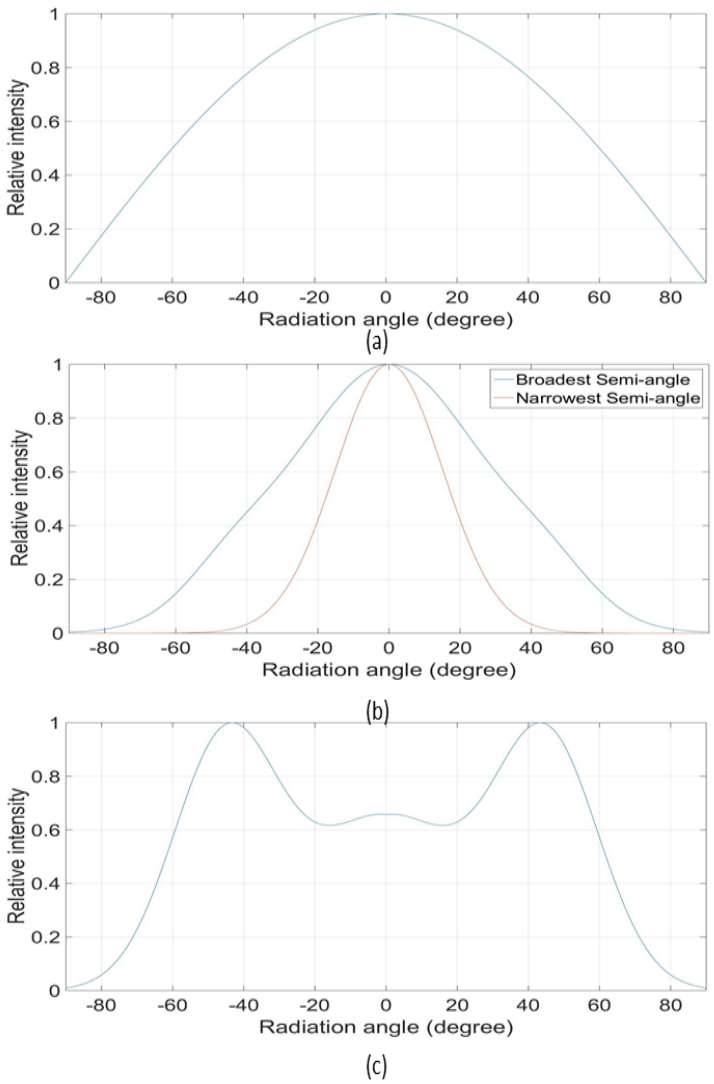

Figure 3-1 2-D radiation pattern of (a) Lambertian; n=1, (b) NSPW345CS from Nichia, (b) LUXEON Rebel from Lumileds Philips **[80]**

The optical source has a direct effect on the indoor OWC channel performance and by optimizing the source Lambertian order the transmission bandwidth will be improved in an NLOS OWC system [81]. In addition, using a tuned elliptical Lambertian beam model instead of a conventional circular Lambertian beam offers higher transmission bandwidth [82]. An IR source is modelled by a Lambertian model which will be used

in this work.

3.3.2. Detector model

At the receiver side, the receiver is defined mathematically by four of parameters; the orientation vector $\hat{\boldsymbol{o}}_R$, the position vector $\boldsymbol{p}_R$, the area A_R, and the FOV. The receiver senses the light whose angle of incidence is less than FOV:

$$D(\theta, FOV) = \begin{cases} A_R \cos(\theta) & for\ \theta \leq FOV \\ 0 & for\ \theta > FOV \end{cases} \quad (3.5)$$

3.3.3. Reflector model

Reflectors are points within environments receiving light rays which either absorb or reflect them. Therefore, they act as a receiver when the light hits the surface, and then they act as a transmitter if they reflect the light. The area of a reflector element is dA. Reflections can contain specular and diffusive components. When the specular component is dominant the reflection pattern is approximated by the model of Phong [9]. When the diffusive component is dominant, the reflection pattern is approximated by a Lambertian model.

The reflection characteristics of any surface depend on several factors, such as the surface material, the wavelength of the incident radiation, and the angle of incidence. Specular reflection results from a smooth surface, whereas diffuse reflection results from a rough surface. The roughness is determined according to the Rayleigh criterion

[9]:

$$\zeta < \frac{\lambda}{8 \sin \theta_i} \qquad (3.6)$$

where ζ is the maximum height of the surface irregularities, λ is the wavelength of the incident radiation and θ_i is the angle of incidence. For IR radiation with $\lambda = 800\ nm$ and for normal incidence, a surface is rough for $\zeta > 0.1\ \mu m$.

Lambertian model: The reflection pattern for rough surfaces is modelled using a Lambertian model which is defined by:

$$E(\theta_0) = \rho\, E_i \frac{1}{\pi} \cos(\theta_0) \qquad (3.7)$$

where ρ is the surface reflection coefficient, E_i is the incident optical power and θ_o is the observation angle.

Phong model: The reflection pattern for smooth surfaces is approximated using the Phong model by:

$$R(\theta_i, \theta_0) = \rho\, R_i \left[\frac{n+1}{2\pi}\, r_d \cos^n(\theta_0) + (1 - r_d)\, \frac{m+1}{2\pi}\, \cos^m(\theta_0 - \theta_i)\right] \qquad (3.8)$$

where r_d is the percentage of incident signal that is reflected diffusely ($r_d \epsilon$ [0,1]), and *m* represents the directivity of the specular component.

3.4. Channel models

3.4.1. Gfeller model

The first OW link was described by Gfeller *et al.* [55] in 1979. The authors proposed a wireless broadcast/multi-access channel in an empty rectangular room in an in-house environment. The transmission medium used of radiation at 950nm wavelength and the study showed that using an optical wireless channel is feasible for low-to-medium speed at low error rates for a range of up to 50m.

Both theoretical analysis and experimental demonstrations were presented in the work. A bandwidth-distance product was approximated in the presence of multipath propagation for a specific room size and specific system configuration taking into account single reflections only. It was shown that for a small room (5m diameter), the transmission speed could reach 52 Mbit/s and the bandwidth-distance product was 260 Mbit.m/s. The experiments used digital links for baseband PCM and PSK modulations at 125 Kbit/s and 64 Kbit/s respectively.

Gfeller *et al.* simulated a basic diffuse OW channel in an office room as illustrated in Figure 3-2. The transmitter was an LED and its radiation characteristics were modelled by a generalized Lambertian law:

$$dP_{\varsigma} = \frac{n+1}{2\pi} \cos^{n}(\theta) P_{s}\, d\varsigma \qquad (3.9)$$

where *Ps* represents the total transmitted power, dP_ς is the power radiated into the solid angle $d\varsigma$, *n* is the mode number and θ is the polar angle.

The power transmitted from the LED hit the surface *A* (with reflection coefficient ρ) and was reflected from the surface element *dA* which emits radiation *E,* given by:

$$E = \frac{dP_A}{dA} = \frac{n+1}{2\pi D_1^2} P_s \rho \cos^n(\theta_i)\cos(\beta) \qquad (3.10)$$

where:

$$d\varsigma = \frac{dA}{D_1^2}, D_1^2 \gg dA \qquad (3.11)$$

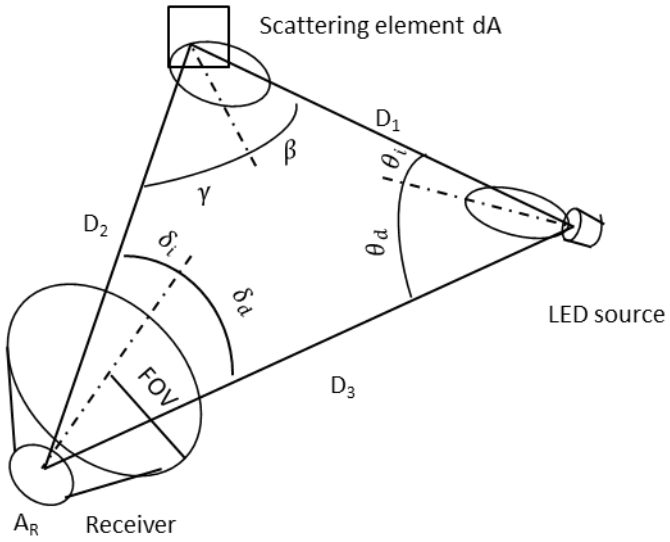

Figure 3-2 Simulation model of the diffuse optical channel (adapted from **[55]**)

The receiver was a photodiode with a photosensitive area A_R, and *FOV*. The collected power dP_{RA} from *dA* is:

$$dP_{RA} = E\ \frac{A_R}{D_2^2\,\pi}\ \cos(\gamma)\cos(\delta_i)\,rect(\delta_i)dA \qquad (3.12)$$

where

$$rect(\delta_i) = \begin{cases} 1, & if\ |\delta_i| \le FOV \\ 0, & if\ |\delta_i| > FOV \end{cases} \quad (3.13)$$

To find the total received power from the first and only reflections, the equation (3.12) is integrated over the reflecting area A:

$$P_{RA} = \frac{n+1}{2\,\pi^2}\ P_T \int \rho\ cos^n(\theta_i)\cos(\beta)\ \cos(\gamma)\cos(\delta_i)\,rect(\delta_i)\ \frac{A_R}{D_1^2\,D_2^2}\ dA \quad (3.14)$$

If the transmitter is located within the receiver FOV then the power which reaches the photodiode through LOS is given by:

$$P_{Rd} = \frac{n+1}{2\,\pi}\ P_T\ cos^n(\theta_d)\cos(\delta_d)\,rect(\delta_d)\ \frac{A_R}{D_3^2} \qquad (3.15)$$

The total received power is:

$$P_R = P_{RA} + P_{Rd} \qquad (3.16)$$

The Gfeller model can be used to predict the total received power in order to analyse the link budget, but getting further useful results (such as: bandwidth, data rate and RMS delay spread) is not possible.

3.4.2. Recursive model

The previous model is not enough to analyse the impulse response of an OW channel due to the limitation of the number of reflections. The signal which undergoes several reflections will experience multipath propagation, which causes a spread of the transmitted pulse over time. This temporal spread could cause ISI and signal distortion. Therefore, after presenting experimental measurements [83] [84], Barry et al. proposed a general computational method which theoretically can cover any number of reflections for the OW channel.

Similar to the Gfeller model, Barry *et al* limited the model to that for an empty rectangular room [85], where the transmitter and receiver were arbitrarily placed in fixed positions and reflecting surfaces (ceiling, walls and floor) were purely diffusive; an ideal Lambertian situation. Simulation and experimental results were compared in order to verify the reliability of the proposed algorithm.

The system elements: source, detector and reflectors are defined in section 3.1. The radiation pattern of the source and the reflectors followed a Lambertian model, where $n=1$ which made the reflected radiation independent of the angle of the incident radiation. Each surface in the room was divided into N numbers of reflectors, each with an area = dA.

When an LOS link between the transmitter and receiver exists, Figure 3-3, the signal

will reach the receiver virtually instantly. The impulse response is given by:

$$h_0(t;S;R) \approx \frac{n+1}{2\pi} cos^n(\phi) \cos(\theta) \frac{A_R}{D^2} rect\left(\frac{\theta}{FOV}\right) \delta(t - \frac{D}{c}) \qquad (3.17)$$

where the distance between the transmitter and receiver is *D,* the rectangular function is defined in equation 3.13 and *c* is the speed of light.

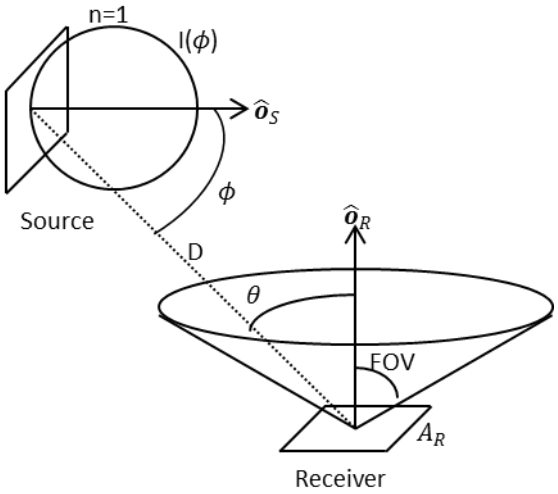

Figure 33-3 Geometry of LOS link between source and receiver (adapted from **[85]**)

When light reaches the receiver after a number of reflections, it suffers from path loss and multipath dispersion. Barry *et al* derived the impulse response for an infinite number of reflections as

$$h(t;S,R) = \sum_{k=0}^{\infty} h_k(t;S,R) \qquad (3.18)$$

where $h_k(t)$ is the response of the light undergoing *k* reflections:

$$h_k(t;S,R) \approx \frac{n+1}{2\pi}\sum_{i=1}^{N}\frac{\rho_i cos^n(\phi)cos(\theta)}{D^2}\, rect\left(\frac{2\theta}{\pi}\right) h_{k-1}\left(t-\frac{D}{c};\{\boldsymbol{r},\hat{\boldsymbol{n}},1\},D\right) dA \quad (3.19)$$

Figure 3-4 shows both frequency and impulse responses for diffused configurations. The accuracy of the algorithm increases by increasing the number of reflectors, which leads to decreases in the reflector area *dA*. This spatial discretization causes temporal discretization, too. Therefore, the time is divided into time bins of width Δt*:*

$$\Delta t = \frac{\sqrt{dA}}{c} \quad (3.20)$$

From the point of view of the computational complexity, the total number of basic calculations needed to find the impulse response is N^k, while the number of unique basic calculations is $(N+1)^2$. Despite the algorithm's ability to find the impulse response for an infinite number of reflections, only 3 reflections can be considered practically, because of the running time required to run the simulation.

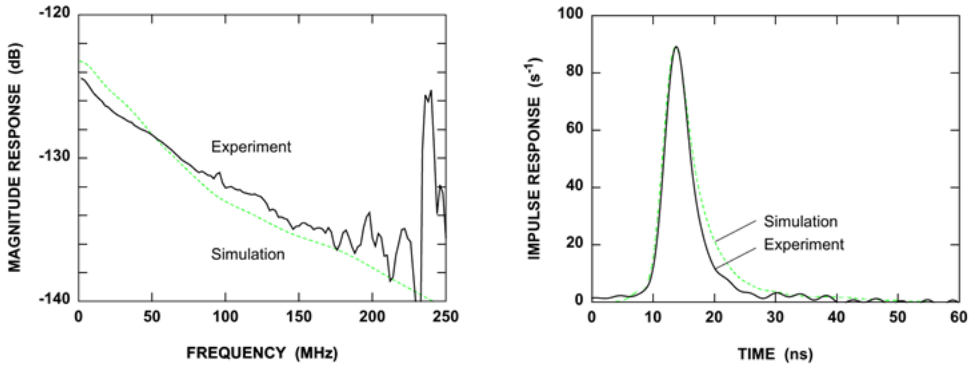

Figure 3-4 Experimental and simulated frequency response and impulse response for a diffused configuration **[85]**

This model was improved to implement the effect of furniture and people in a room [86]. The furniture was assumed to have a rectangular shape and the surface areas were parallel with room walls. All surfaces which cannot receive any light were eliminated from calculations. It was found that the existence of furniture had a great impact on the impulse response. It might make it better or worse depending on the relative positions of source, receiver and furniture. People were represented by rectangular-shaped boxes with appropriate dimensions in the model. In order to simulate an irregular room shape, the author replaced any irregularity with large boxes which also had a rectangular shape and modelled the room in the same manner. Another method to simulate asymmetrical rooms was proposed in [87]. Lomba *et al.* developed a simulation which evaluated and optimized the power distribution by selecting the appropriate parameters for the transmitter and receiver [88]. Other studies based on the Barry model approach are [89][90][91][92].

3.4.3. Ceiling bounce model

The main approach when characterising an infrared link in an indoor environment is to define the average transmitted power required to achieve a certain bit-error rate for a specific modulation scheme. [93] shows that the normalized delay spread and optical path loss are enough parameters to predict the channel performance.

For a channel with impulse response *h(t),* the optical gain G_o is:

$$G_o = \int_{-\infty}^{\infty} h(t)dt \qquad (3.21)$$

and the optical path loss is:

$$OP_L = -10 \log_{10} G_o \qquad (3.22)$$

RMS delay spread is calculated from the impulse response:

$$\Gamma = \left[\frac{\int (t-\mu)^2 h^2(t)dt}{\int h^2(t)dt}\right]^{1/2} \qquad (3.23)$$

where μ is the mean delay:

$$\mu = \frac{\int t\, h^2(t)dt}{\int h^2(t)dt} \qquad (3.24)$$

Carruthers *et al*. in [93] used a ceiling-bounce model to derive a comparatively simple equation to represent the impulse response for a specific indoor environment. The transmitter and receiver were located in the same horizontal plane at a distance *H* from the ceiling, which is the sole Lambertian-reflector surface in the system. The time origin is shifted by *b=2H/c,* which is the minimum time required for the light to reach the receiver after one reflection from the reflector surface. Assuming an optical gain $G_o=1$, the OWC channel impulse response and RMS delay spread are:

$$h_c(t,b) = \frac{6b^6}{(t+b)^7}\, p(t) \qquad (3.25)$$

where *p(t)* is a unit step function.

$$\Gamma\big(h_c(t,b)\big) = \frac{b}{12}\sqrt{\frac{13}{11}} \qquad (3.26)$$

This model is simple and shows the effect of multipath dispersion in spite of the inaccuracy of the impulse response. However the power requirement for a specific modulation scheme can be predicted.

3.4.4. DUSTIN algorithm

In 1997, Lopez-Hernandez developed a new algorithm named DUSTIN to calculate the impulse response for an IR wireless channel in an indoor environment [94]. This algorithm is faster than previous methods because it uses a smaller number of calculations, and most calculations can be done in parallel. In addition, it can handle more than one receiver. The main concept of the algorithm is that instead of dividing the process into specific number of reflections it defines time steps.

Before starting calculations, the basic parameters are defined. The environment (walls, ceiling and floor) is divided into small square cells (with dimensions $d \times d$) and N_x, N_y, N_z are the number of cells along the *x, y, z* axis. The total number of cells is *N*:

$$N = 2\left(N_x.N_y + N_x.N_z + N_z.N_y\right) \qquad (3.27)$$

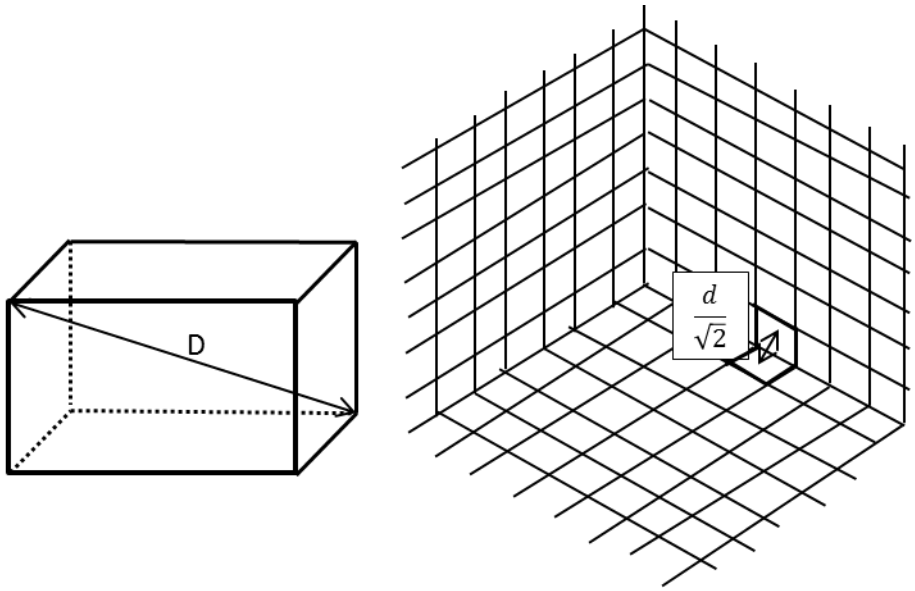

Figure 3-5 Room configuration (adapted from DUSTIN algorithm **[94]**)

The shortest delay between the cells centres is:

$$\delta = \frac{d}{\sqrt{2}\,c} \qquad (3.28)$$

where c is the speed of light.

The longest delay in the environment is:

$$t_{max} = \frac{D}{c} = \frac{\sqrt{W_x^2+W_y^2+W_z^2}\,d}{c} \qquad (3.29)$$

where *D* is the distance between the far corners in the room, as shown in Figure 3-5. Any interaction between cells will take less than *M* time slots, where *M* is the lowest integer number larger than the ratio between *D* and *d*.

The workspace is defined as $M \times N$ matrix. The element *(q,b)* represents the power impinging on the b^{th} cell during q^{th} time slot.

The algorithm is divided into three stages: 1- initialisation, 2- wall processing, 3- calculation of the photodiode response.

The first stage fills the first row of the workspace with the value of the power reaching the cells from the emitter.

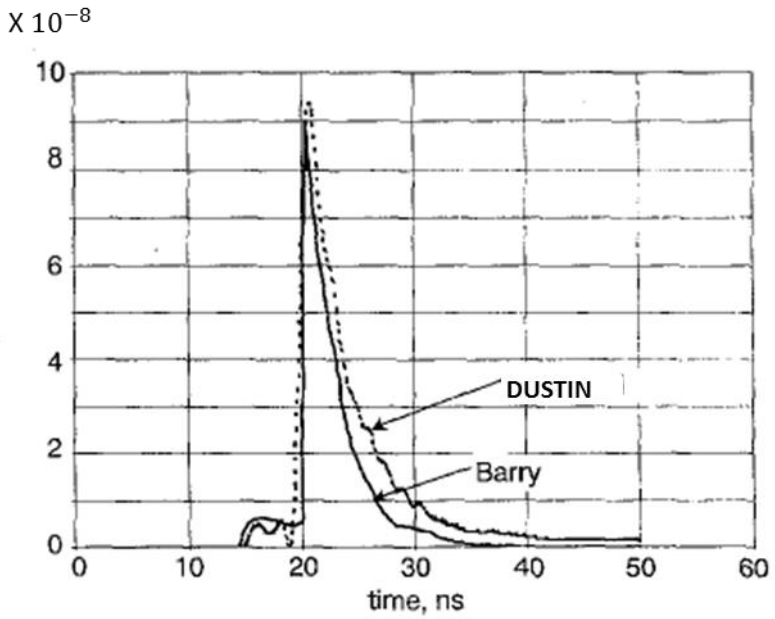

Figure 3-6 Impulse response comparison (Barry model and DUSTIN model) **[94]**

The second stage fills the rest of the workspace matrix and works basically with the cells. We have the initial value for each cell in the first row. The contribution of each cell to another is calculated in this stage and saved in the workspace matrix (in the row

given by the delay normalised to δ and in the column of the target cell).

The third stage calculates the received power to each receiver.

After filling the workspace matrix properly, another matrix is generated with the number of columns equal to the number of receivers and the number of rows equal to the number of time slots. For each time slot, the power contribution from all cells is known from the workspace matrix and the contribution from each cell to the receiver can be calculated and summed in order to find the channel impulse response.

The method is faster than the recursive model and less complex, and a comparison with the Barry model is shown in Figure 3-6.

3.4.5. Statistical model

Because of the computational complexity of Barry's method, Perez-Jimenez *et al.* proposed a statistical model to estimate the impulse response of an optical wireless channel [95]. The model estimates the delay parameters (τ_{rms} and τ_m), then these values are used to fit the *h(t)* shape with Rayleigh or Gamma distributions and finally the received power is calculated using a power budget approximation. The studied indoor environment is a square room and similarly to the previous study the reflectors are assumed to be Lambertian reflectors, as in Figure 3-7.

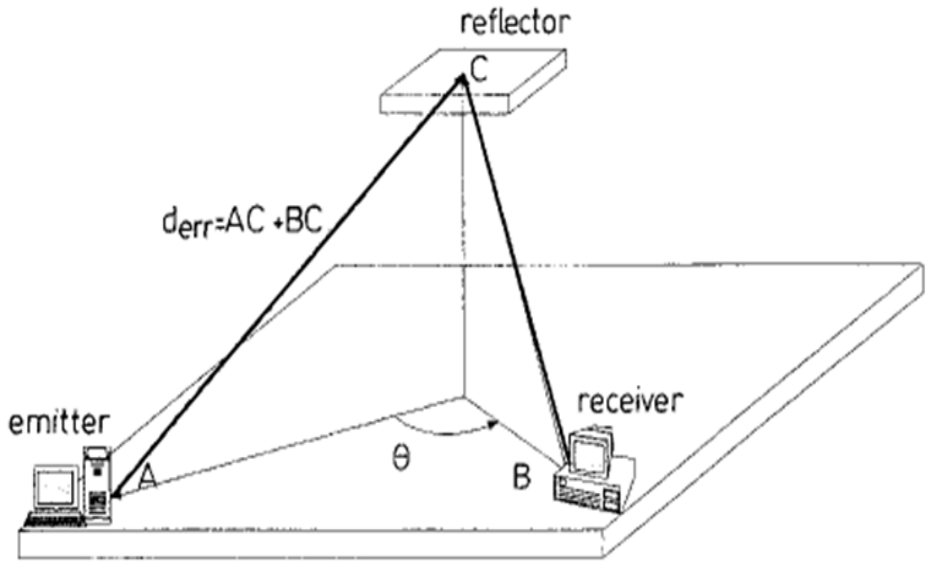

Figure 3-7 Link configuration **[95]**

Several channel configurations were tested with total of 1400 measures for the fitting process considering two cases: first, the emitter and receiver are pointing to the centre of the ceiling and second, the emitter and receiver are pointing vertically. The study showed a dependence of the delay parameters with the propagation characteristics (especially the emitter-reflector-receiver distance d_{err}, the angle between transmitter and receiver θ, and the mode number n of the infrared LED radiation pattern). The general expression for the delays is:

$$\tau\,(ns) = a + b\cos(c\theta + d) \quad (3.30)$$

For the first case, the delays can be expressed as:

$$\tau_{rms}(ns) = -0.82\,n^{0.03} + 0.58\,n^{-0.11}d_{err} + (-0.54 + 0.19\,d_{err})\,\cos(0.019\,\theta - 0.32) \quad (3.31)$$

$$\tau_m(ns) = -0.46\, n^{0.28} + 0.33\, n^{-0.17} d_{err} + (-0.17\, n^{0.41} + 0.18\, n^{0.26} d_{err})\, \cos(0.018\, \theta - 0.012)$$

(3.32)

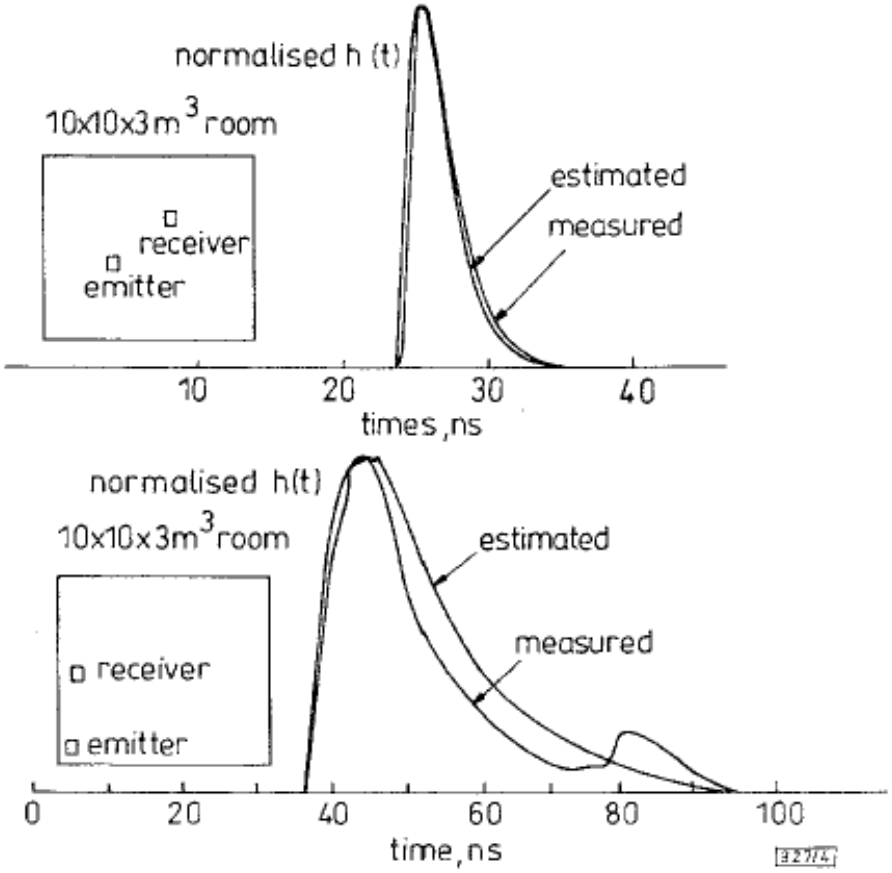

Figure 3-8 Comparison of measured and estimated normalised impulse response **[95]**

While for the second configuration case:

$$\tau_{rms}(ns) = -2.37 + 0.007n + (0.8 - 0.002\, n) d_{err} \quad (3.33)$$

$$\tau_m(ns) = -3.26\, n^{-0.04} + (1.12\, n^{-0.03})\, d_{err} \quad (3.34)$$

The estimated parameters are compared with known distribution functions (Rayligh

and Gamma) to fit the shape of the impulse response.

3.4.6. Monte Carlo and modified Monte Carlo algorithms

All previous simulation studies are sliced either into the number of reflections or into time steps. Both of which require relatively long times in which to perform the computational operations and reflectors are assumed to be purely Lambertian. The Monte Carlo algorithm overcomes these negative points [96].

The method basically generates random rays from the emitter which follow the radiation pattern, then the rays pass through several reflections and a particular ray might be captured by the receiver. The algorithm keeps tracing the ray until it either reaches the receiver or misses it, as Figure 3-9 illustrates.

In a similar way to the DUSTIN algorithm, it is first important to define and save all basic parameters (environment configuration, emitter, receiver and reflectors parameters). Additionally, a new ratio is defined: Diffuse-to-Mirror Ratio (DMR) which specifies whether the incident ray will be secularly reflected or scattered depending on the incident angle. The algorithm is divided into three stages: ray generation, wall processing and calculation of the photodiode response. For a Lambertian radiation profile, if $n = 1$, a unitary ray-direction vector is defined (x_1, y_1, z_1). If the mode number >1 then the random unitary vector (x_2, y_2, z_2) follows the radiation pattern $cos^n\varphi$, after finding (x_1, y_1, z_1):

$$z_2 = \sqrt[n]{z_1}\,, x_2 = k.x_1, y_2 = k.y_1 \qquad (3.35)$$

where:

$$k = ((1 - z_2^2)/(1 - z_1^2)) \qquad (3.36)$$

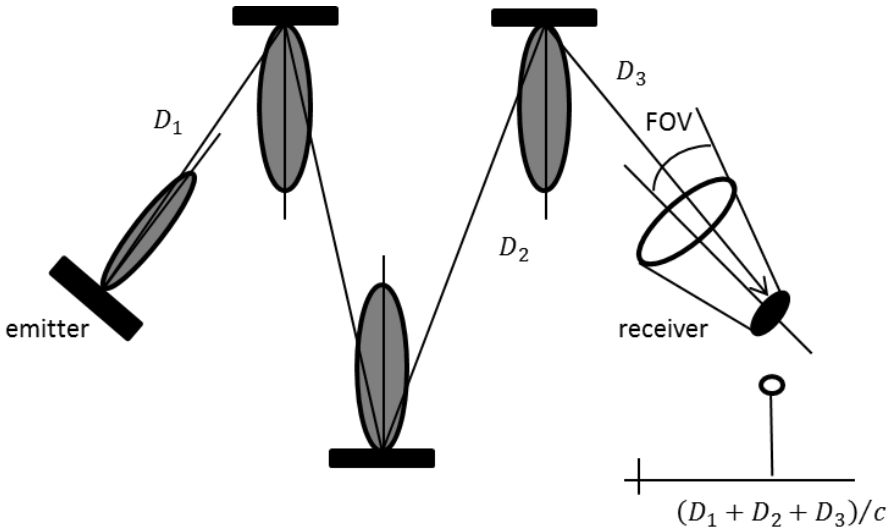

Figure 3-9 IR link (Monte Carlo algorithm) **[96]**

In the second phase; the intersection point between the ray and an obstacle is studied whether it is on the receiver or on a wall. If it is on a wall a decision should be made as to whether it will be reflected or scattered. The output power is calculated by multiplying the input power by ρ. If the ray is reflected the output direction is strictly defined, whereas if it is scattered the new direction will be defined in the same procedure explained above.

In the last phase the matrix with number of columns equals the number of receivers, and the number of rows equals the number of time slots defined and filled with the power contributions for each ray. The ray simulation runs until the delay is longer than the specified simulation time.

Later on this method was modified to make it faster and more accurate [97]. The main improvement in the modified Monte Carlo Algorithm (MMCA) is by calculating the contribution to the receiver from each ray after each rebound or reflection as Figure 3-10 represents. Figure 3-11 compares the Barry model with the MMCA for two configurations. Both MC and MMC methods have been used widely to calculate the channel impulse response for different indoor environments [98][99][100].

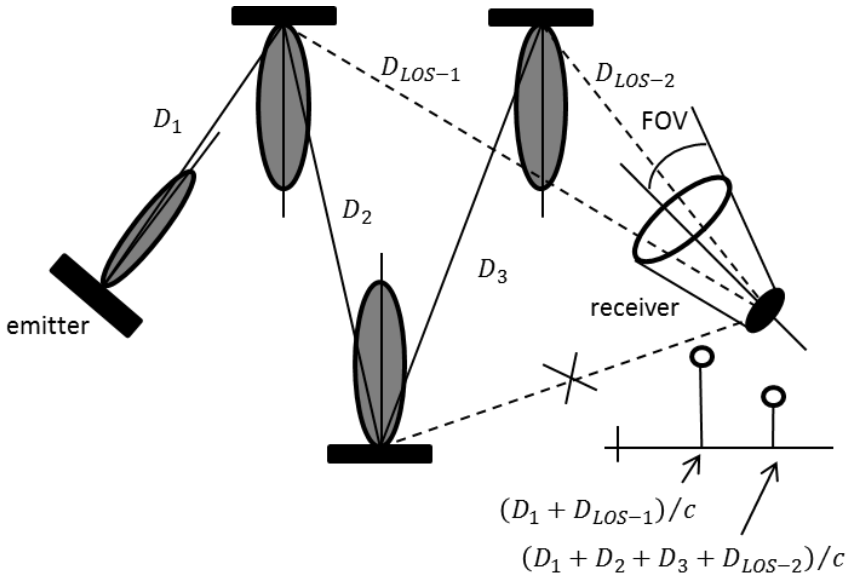

Figure 3-10 IR link (modified Monte Carlo algorithm) **[97]**

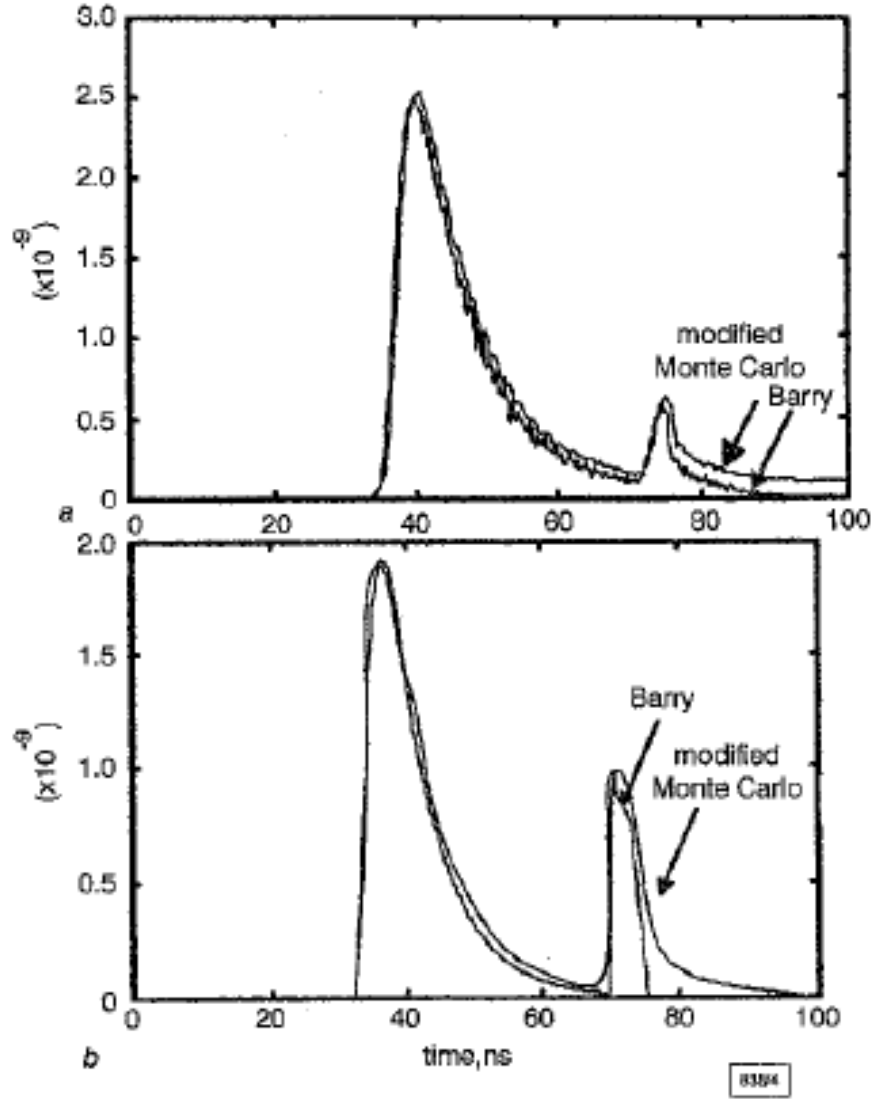

Figure 3-11 Comparison of simulated impulse response for the Barry and the modified Monte Carlo algorithm **[97]**

3.4.7. Sphere model

In this model individual photons are sent from the transmitter to the receiver [101]. Their path is tracked until the photon either is absorbed by the room surface or has reached the receiver. The path loss *a* is defined:

$$a = -10 \log \frac{N_{Rx}}{N_0} \qquad (3.37)$$

where N_0 is the number of the transmitted photons, and N_{Rx} is the number of received photons.

The impulse response for a diffuse link is very similar to one for Integrating Surface and the transfer function is defined as:

$$H_{diff}(jf) = \frac{\eta}{1+j\frac{f}{f_0}} \qquad (3.38)$$

with:

$$f_0 = \frac{1}{2\pi\tau} \qquad (3.39)$$

and the optical power efficiency is related to the path loss by:

$$a = -10 \log \eta \qquad (3.40)$$

The total received signal amplitude:

$$\left| H_{diff} + H_{LOS} \right| = \sqrt{A_{diff}^2(f) + A_{LOS}^2 + 2\, A_{diff}(f) A_{LOS} \cos[2\pi f \Delta T + \Phi_{diff}} \qquad (3.41)$$

where

$$\Phi_{diff} = -\arctan(\frac{f}{f_0}) \qquad (3.42)$$

Based on this model, work has been done to determine the degree of directivity required to achieve the optimum data rate [102] [103].

3.4.8. Iterative site-based model

This model was reported in 2002 [104] by Carruthers. It defines the transmitter and receiver with the same parameters defined by Barry. The difference is in the way in which Carruthers has modelled the environment. He modelled it as a set of *W* rectangular boxes $\{B_1, B_2, \ldots, B_W\}$, Figure 3-12. The first box B_1 represents the universe box which contains all other boxes, emitters and receivers. Other boxes define the objects in the room. Each box is defined by one corner position vector $\overrightarrow{p_{B_i}}$ and a size vector $\{L_{x,B_i}, L_{y,B_i}, L_{z,B_i}\}$. Only the interior surfaces of the universe box and the exterior surfaces of all other boxes receive and reflect the light so only these surfaces are considered in the calculations.

The LOS impulse response $h_0(t; S; R)$ is given by:

$$h_0(t; S; R) = V(\overrightarrow{r_s}, \overrightarrow{r_r}, E)T(\phi)(A_r\ g(\theta)/D^2)\ \delta(t - D/c) \qquad (3.43)$$

where $D = |\overrightarrow{r_s} - \overrightarrow{r_r}|$ is the distance between the source and the receiver. The visibility function $V(\overrightarrow{r_s}, \overrightarrow{r_r}, E)$ is 1 when the LOS path between S and R is unobstructed, and is zero otherwise.

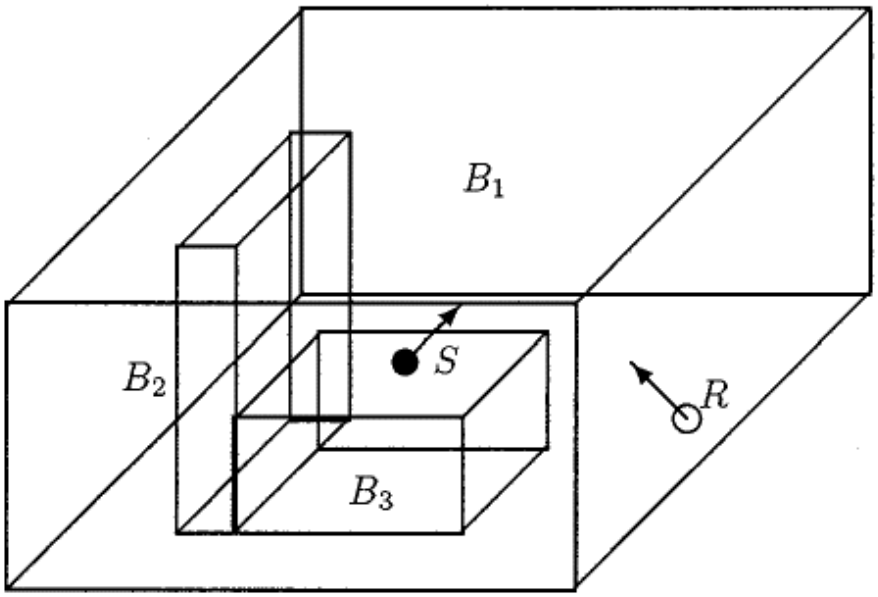

Figure 3-12 Environment configuration (Iterative site based model) **[104]**

The impulse response due to reflections is approximated by:

$$h_k(t;S,R) \approx \sum_{j=1}^{W} \rho_{\varepsilon_j^r}\, h_{k-1}(t;S,\varepsilon_i^r) * h_0\left(t;\varepsilon_j^s,R\right) \qquad (3.44)$$

where ε_i^r and ε_i^s represent element i acting as a receiver and a source respectively.

$$h_k(t;S,\varepsilon_i^r) \approx \sum_{j=1}^{W} \rho_{\varepsilon_j^r}\, h_{k-1}(t;S,\varepsilon_i^r) * h_0\left(t;\varepsilon_j^s,\varepsilon_i^r\right) = \sum_{j=1}^{W} \alpha_{ij}\, h_{k-1}(t-\tau_{ij};S,\varepsilon_i^r)$$

where:

$$\alpha_{ij} = V\left(\vec{r}_{\varepsilon_j^r}, \hat{n}_{\varepsilon_j^r}, E\right) \frac{\rho_{\varepsilon_j^r}\, T(\phi_{ij}) g(\theta_{ij})}{P^2\, D_{ij}^2} \qquad (3.45)$$

where:

$$\tau_{ij} = D_{ij}/c \qquad (3.46)$$

W impulse responses $h_1(t; S, \varepsilon_j^r)$ will be calculated and used to calculate $h_2(t; S, \varepsilon_j^r)$ and so forth until $h_{k-1}(t; S, \varepsilon_j^r)$ is found, and then they will be applied in the equation for the intended receiver. Figure 3-13 compares impulse responses produced from the Barry model and the Iterative site-based model.

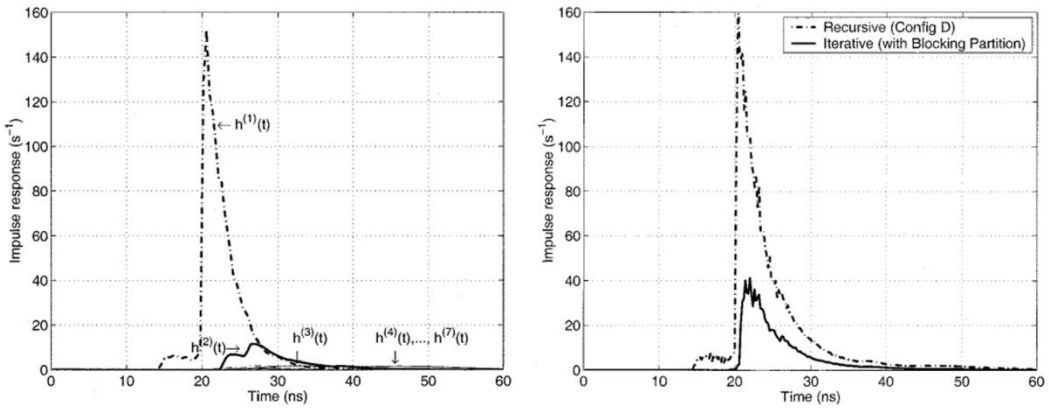

Figure 3-13 Comparison of channel impulse responses for the Barry model and the Iterative site-based model **[104]**

This method allows for less computational complexity and less simulation time. The 4-bounce impulse response can be calculated in 90.7s using 1992-vintage Sun Sparc station. Using this model, complex reflection environments can be modelled. This method is used to demonstrate empty and complex rooms with furniture and people and where multiple receivers are used [105].

3.4.9. Photon model

In 2009, a new direction towards simulating optical wireless links was introduced. Instead of simulating the light as bundle of rays, it was simulated as group of photons. In [106] the photon mapping method was adopted. The emitter is defined by the number of photons and their angular distribution.

The emitted photons travel from the source until they hit an object, and either a given photon will be absorbed or it will be reflected. If the object surface is specular, the reflected photon direction is specified, whereas if it is diffuse then one reflected direction will be chosen according to the distribution function of the diffuse light, which relates to the surface material and property, the function being called the Bidirectional Reflectance Distribution Function (BRDF). Unless the photon is absorbed, the number of photons stays constant during the process. As a result, the number of computational processes is the product of the number of generated photons multiplied by the number of reflections.

To model the emitter, it is necessary to define the spectrum and radiation patterns of the source. Then the light intensity is defined from the photon density by counting the number of photons which intersect a reception sphere, Figure 3-14.

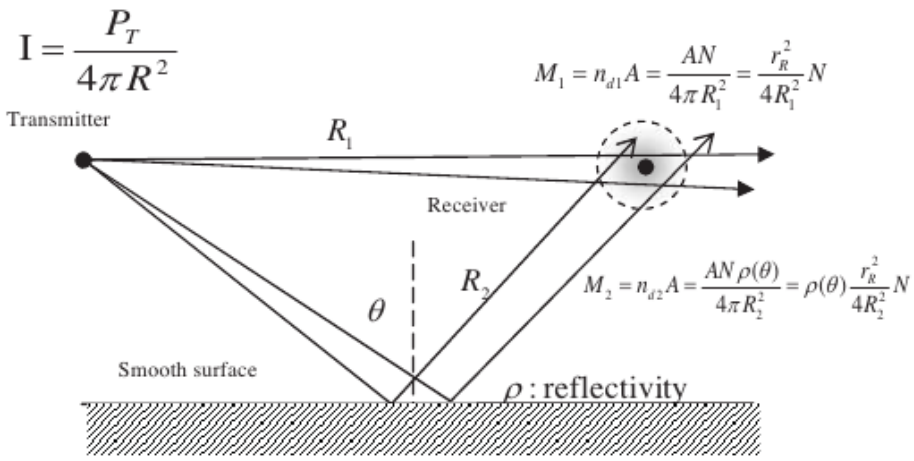

Figure 3-14 Calculation of light intensity using a reception sphere **[106]**

The number of photons M_1 which follow an LOS path, is given by:

$$M_1 = \frac{r_R^2}{4\,R_1^2}\,N \qquad (3.47)$$

Where R_1 is the distance between the transmitter and the reception sphere, r_R is the receiver diameter, and N is the number of the transmitted photons.

The power received from one photon:

$$P_{R1} = M_1 \frac{P_T}{N} = \frac{r_R^2}{4\,R_1^2}\,P_T \qquad (3.48)$$

where P_T is the transmitted power.

After one reflection from a surface with reflectivity ρ, the photon power is:

$$P_{R2} = \rho(\theta)\ \frac{r_R^2}{4\ R_2^2}\ P_T \qquad (3.49)$$

where θ is the angle between the incident direction and the normal vector of the surface.

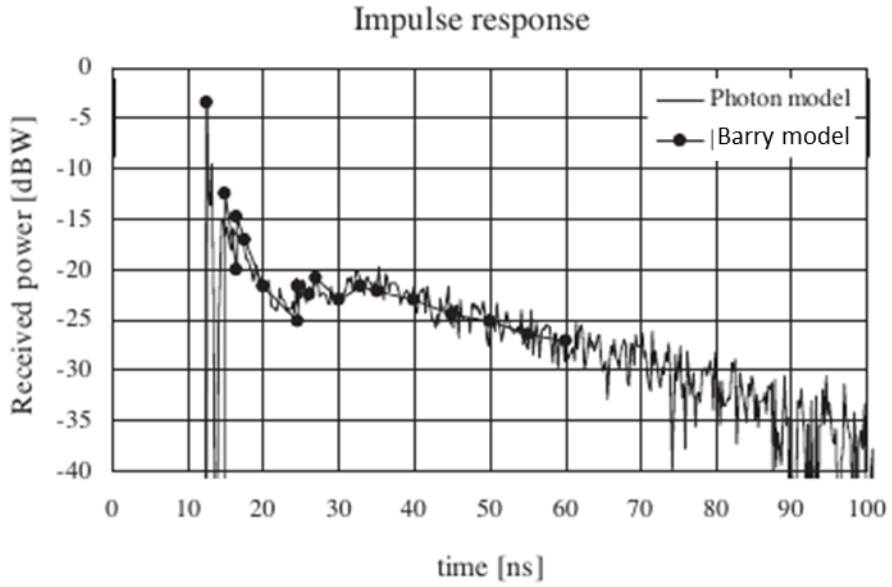

Figure 3-15 Impulse response comparison between the Barry model **[85]**and the photon model **[104]**

3.4.10. Photon tracing model

One year later, another model was defined [107]. It is based on sending photons instead of rays. The main difference with the modified Monte Carlo algorithm is in the reflection stage. In this model, when the photon reaches the object, instead of reflecting with power reduction, it has two cases: either (a) it will be reflected (with a probability of ρ) with its full power, or (b) it will be absorbed (with a probability of [1-ρ]).

The transmitter, receiver and reflector are defined in Chapter 3, section 3.1. The line-of-sight impulse response is given by:

$$h^{(0)}(t;S,R) \approx \frac{m+1}{2\pi}(\cos(\theta))^m \frac{A_R}{d^2} \cos(\Psi)\ rect\left(\frac{\Psi}{FOV}\right)\ \delta\left(t-\frac{d}{c}\right) \qquad (3.50)$$

At the k^{th} reflection, the number of photons arriving to one reflector is M/ρ at a time T_{pl}. After the reflection, the number of reflected photons is M. The contribution from one photon in this reflection is:

$$h_i^{(0)}(t;dA,R) \approx \frac{1}{\pi N}\cos(\theta)\frac{A_R}{d^2} \cos(\Psi)\ rect\left(\frac{\Psi}{FOV}\right)\ \delta\left(t-T_{PI}-\frac{d}{c}\right) \qquad (3.51)$$

and the contribution from all photons is in the k^{th} reflection:

$$h^{(k)}(t;S,R) = \sum_{i\epsilon P^{(k)}} h_i^{(0)}(t;dA,R) \qquad (3.52)$$

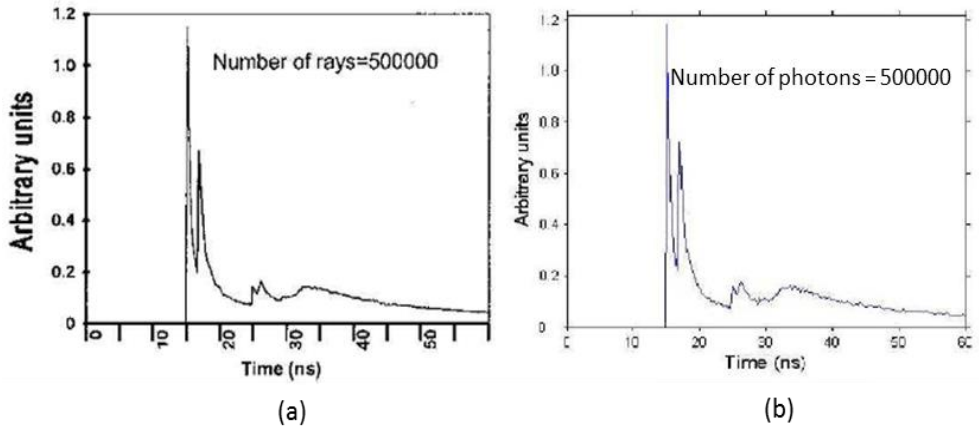

Figure 3-16 Impulse response obtained from (a) modified Monte Carlo algorithm and (b) photon tracing method **[107]**

3.4.11. Training sequence

In [108] an optimal Training-Sequence (TS) based channel estimation was introduced for the first time in OWC systems. Data frame consist of precursor, training sequence and the data as illustrated in Figure 3-17. *J-1* symbols are required in the beginning of the preamble and they are followed by the TS data (*N* symbol) directly before the transmitted data.

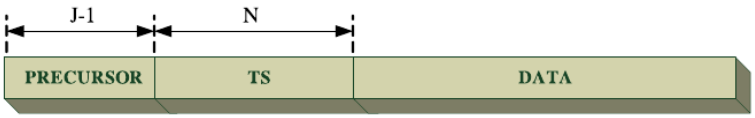

Figure 3-17 The structure of the data frame with a TS [108]

The signal on the receiver side is expressed by:

$$y(t) = a(t) * h(t) + n(t) \quad t \geq 0 \qquad (3.53)$$

where * represents convolution, *a(t)* represents the instantaneous optical power in the transmitter, *h(t)* is the channel impulse response, and *n(t)* refers to the optical channel noise. After sampling:

$$t(iT_s) = \sum_m h(mT_s)\, a(i\,T_s - mT_s) + n(iT_s) \qquad (3.54)$$

To simplify the previous expression:

$$y_i = \sum_m h_m \, a_{i-m} + n_i \qquad (3.55)$$

From the known information, and by analysing the relationship between the received signal and the training sequence, the channel impulse response can be estimated. In [109] three methods have been used for the estimation (correlation method, the least square method and the minimum square error) and a further study was undertaken to find the optimal training sequence using the Cramer-Rao Bound in [108].

3.4.12. Ray gathering

For systems with multiple sources, [110] presents an optimised simulation algorithm to calculate the impulse response. The algorithm is based on the MC method but by reversing the ray directions where they are reflected back from the receiver towards the transmitter, this idea reduces the computation time about 100 times for the systems where there are multiple sources and single receiver. The authors use only three reflections.

$$E_k(t) = \frac{|\overrightarrow{\omega_0}.\overrightarrow{n_0}|}{p_0(x_0,\overrightarrow{\omega_0})}.A_{R_x}\sum_{i=1}^{l}\left(L_i(x_i,\overrightarrow{\omega_i},t)\prod_{j=1}^{i-1}\frac{f_r\left(x_j,\overrightarrow{\omega_j}\rightarrow\overrightarrow{\omega_{j-1}}\right).\left|\overrightarrow{\omega_j}.\overrightarrow{n_j}\right|}{p_j(x_j,\overrightarrow{\omega_j})}\right)$$

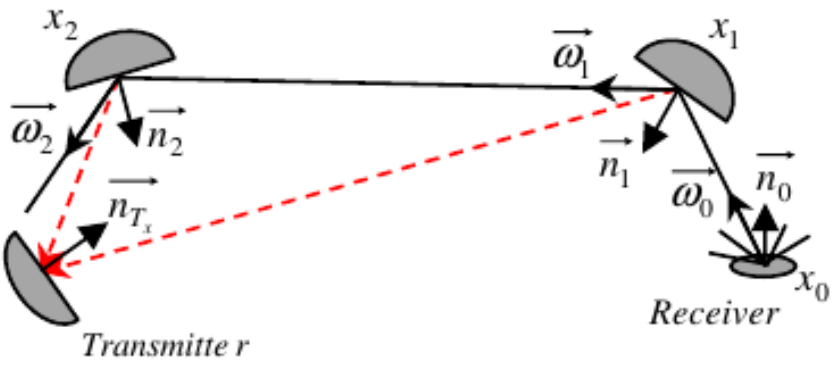

Figure 3-18 OW link in the ray gathering algorithm **[110]**

3.4.13. Combined deterministic and modified Monte Carlo method

The most recent method proposed to find the impulse response in an indoor environment was proposed by Chowdhury *et al.* in 2014 [111]. This combines both the Barry model and the MMC algorithm to benefit from their particular advantages in order to reach less relative estimated errors in less computational time. The method takes a large number of reflections into account in order to calculate the impulse response. The contribution of the first reflection is calculated by using the Barry model, whereas for the contributions of the second, and the rest of the reflections all are calculated using the MMC algorithm.

This combination has advantages over the MMC for NLOS links and when there are multiple sources where less relative estimated error can be achieved. For single source configurations, more rays are needed to calculate the impulse response in Combined Deterministic and Modified Monte Carlo (CDMMC).

Another advantage of CDMMC is the ability of implementing it for parallel computation which reduces the simulation running time. Only the MMC part of the algorithm takes advantage of multi-core computer processors.

3.5. Comparison of models

The channel modelling started with a simple configuration in an empty rectangular room by implementing a single reflection. Then it was improved by considering a number of reflections. The number of reflections was restricted by the computational efficiency. In some environments with a low required data rate, high order reflections can be ignored because there is no useful information carried by the signals after a specific number of bounces. In contrast, for high speed channels, high order reflections have a direct impact and should be considered in calculations [112]. The earlier algorithms were based on the concept of slicing, either the space into a number of reflectors, or the time into time steps. The main drawback of these algorithms is the computational complexity and the memory required for the calculations. Another improvement has been achieved by considering more complex environments and by taking furniture and people effects into consideration.

Models which are classified under this category are the Gfeller model, the Barry model, the DUSTIN algorithm, and the iterative site-based model.

In the Barry model there are N^k elementary computations and the memory required to

run the simulation is $8N^2$. The model can handle practically up to 3 reflections because the run time is exponential in k. In comparison, the DUSTIN algorithm is less complex in terms of the computation process, and the memory required handling the simulation is N^2. It can be used with several emitters and receivers in the environment. The simulation takes less time because the algorithm has parallel processes.

Another type of OW channel modelling was introduced later. This type depends on the ray tracing concept. Instead of tracking all possible paths for rays in the indoor environment, only a bundle of rays would be generated. This bundle would follow the transmitter radiation pattern. At this stage, implementing the Phong model, which represents specular reflection, was possible. This model allows for higher computational efficiency and less time consumption for running the simulation.

Models classified under this category are: the Monte Carlo algorithm, the modified Monte Carlo algorithm, the sphere model, ray gathering and CDMMC.

In the Monte Carlo algorithm specular reflections can be considered beside diffuse reflections. In terms of the required memory, only N^2 is needed. In terms of computational complexity, it is only kNN_s, where k is the number of reflections, N is the number of generated rays and Ns is the number of surfaces in the environment. Ray gathering and CDMMC perform more accurately than other algorithms under specific conditions.

Later on, models depending on simulating transmitted photons from the emitter instead of rays were proposed. Models under this category differ from each other in the way the photons are processed. This type includes the following models: the photon and the photon tracing model.

In the photon model, the computation time increases linearly with the number of reflections. In photon tracing the computational complexity equals $\tilde{k}NN_s$ where $\tilde{k}$ is constant. A comparison between the modified Monte Carlo algorithm and the photon tracing algorithm in terms of error analysis and computational efficiency has been demonstrated in [113].

3.6. Conclusions

An extensive review regarding the channel modelling of indoor optical wireless communication systems has been presented. Since the accuracy of the channel model is important in order to build a reliable system, the mathematical model, which is considered the first step in modelling, behind each method, was explained. In addition, a comparison between the most applied methods from different points of views was drawn.

Recursive and ray tracing methods are widely used for channel modelling because of the accuracy of the former and the practicality of the latter. While training sequence, photon tracing and ray gathering methods are less used because of the lack of optimal

training sequence, higher error of photon tracing method compared to MC and the complexity of ray gathering method.

Chapter 4: Simulation of the OW Waveguide Channel

4.1. Introduction

In the previous chapter, the different models for indoor OW channels have been discussed. Using recursive models can give relatively accurate results but at the price of computational complexity. It is not practical to use such methods when a high number of reflections (three or more) is essential to assess the system performance. On the other hand, the MC and MMC algorithms are able to deal with this high number of reflections in practical time with reduced accuracy results depending on the number of rays generated from the source.

In this chapter, a simulator is built to predict the OW channel performance in waveguides. Models have been implemented and improved for indoor OW channels (room and office size) [92] and for fibre optic media [114]. However, waveguides lie in the research area between these two applications.

An MMC simulation is presented with the aim of filling some gaps which are left by

the existing channel models. This starts with a definition of the environment and system model, and then moves on to explain the algorithms used to build the simulator and present detailed steps for simulation. This is followed by comparing the simulator with different configurations studied previously, and with experimental results.

4.2. System Model

Random sampling is used to extract an answer to the problem. This is called MMCA which is based on MC numerical simulation. Ray tracing methods trace rays of light transmitted from the source to the receiver.

For modelling the OW communication channel, the first step is to define the input and output variables.

The input variables are:

Environmental parameters, *i.e*. the sequence of the waveguide structure, namely mathematical equations, normal vectors and dimensions.

Waveguide material parameters, which are the reflection coefficient, percentage of incident ray reflected diffusely and the directivity.

Simulation parameters, i.e. time resolution and number of time bins which form the

total simulation time.

Source parameters, namely the position vector, direction vector, mode number and transmitted power.

Receiver parameters, given by position vector, direction vector, receiver area and receiver FOV.

The output parameters are contained in the impulse response table which is a table where the number of rows is equal to the maximum reflections that the ray undergoes, and number of columns equals the number of time bins. This table is the key to get the rest of output parameters which help in identifying the channel performance. The parameters studied are:

Total received power: is the summation of the impulse response quantities which is the power received over the time

$$P_R = \int_{-\infty}^{\infty} h(t)dt \qquad (4.1)$$

Path loss: is the reduction in power density as the light propagates through the medium:

$$path\ loss = -10\ \log_{10}\frac{P_R}{P_T} \qquad (4.2)$$

RMS delay spread: multiple reflections lead to multipath which causes ISI. To measure multipath effect, RMS delay spread is calculated from Equation 3.23.

Bandwidth: can be derived from the Fourier transform of the impulse response, which is the frequency where the magnitude has dropped by 3dB from its maximum value.

In order to insert all the mentioned inputs correctly in the system here, it is necessary to define the coordinate system to assure that all defining positions and directions are connected correctly.

The system environment is considered to be a rectangular cross section waveguide or sequence of waveguides connected to each other. The boundaries of the waveguide are defined to be walls while the entrance and exit are opened as illustrated in Figure 4-1.

The parts of the car are mostly made out of steel and perhaps aluminium. The former follows the Phong model as its radiation pattern while the latter follows Lambertian model.

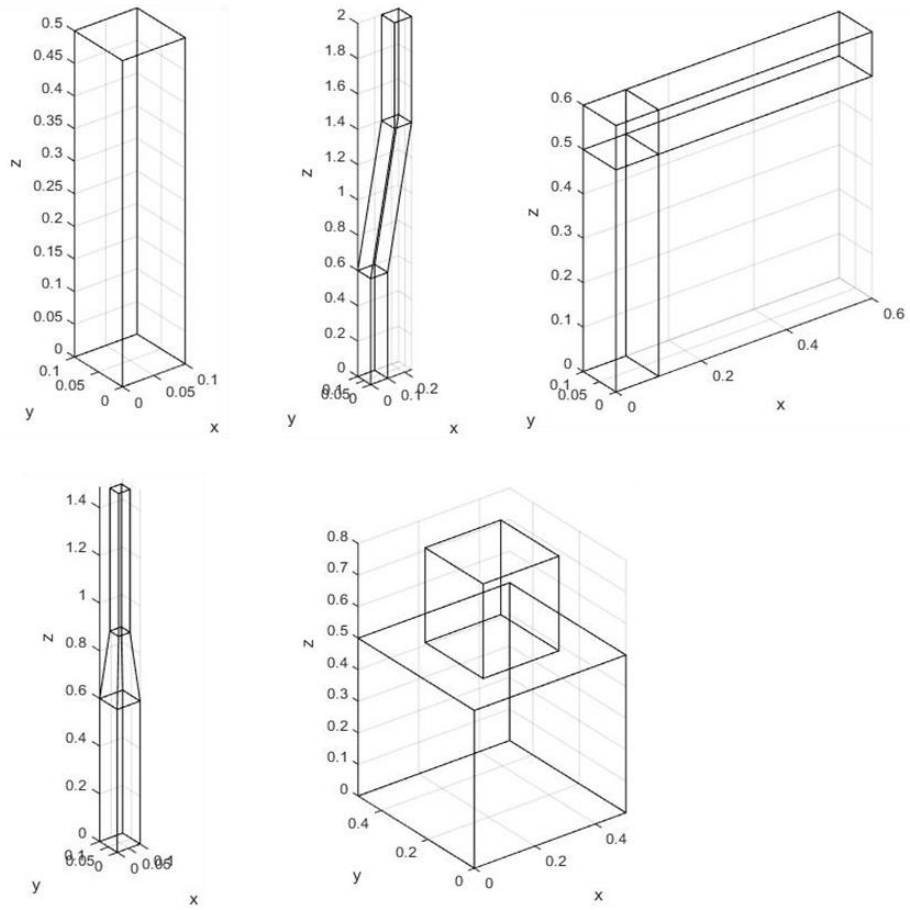

Figure 4-1 Environment structure

Section 3.3 in Chapter 3 discussed the source and reflector types and how to present them mathematically. This concentrates on their in-depth simulation.

4.2.1. Source simulation

In order to generate rays following a Lambertian radiation profile from the source, a Monte Carlo algorithm is applied [115]; a uniformly distributed random point inside a circle with radius 1 in the *x,y* plane is taken as follows:

$$x_1 = r * \cos(2\,\pi\,\theta) \qquad y_1 = r * \sin(2\,\pi\,\theta) \qquad (4.3)$$

where θ and r are random numbers between 0 and 1. The z coordinate is calculated assuming the that the ray direction is unity:

$$z_1 = \sqrt{1 - (x_1^2 + y_1^2)} \qquad (4.4)$$

If the source mode number is n > 1, then the same steps are followed and after finding (x_1,y_1,z_1) the new direction (x_2,y_2,z_2) is generated which follows a $cos^n(\theta)$ radiation pattern by applying the following equations:

$$z_2 = \sqrt[n]{z_1} \qquad k = \frac{1-z_2^2}{1-z_1^2} \qquad x_2 = kx_1 \qquad y_2 = ky_1 \qquad (4.5)$$

Ray direction = (x_2,y_2,z_2). See Figure 4.2.

If the source normal vector (***normal***) is different from the z axis (***zaxis***), then the rotated ray direction can be found using rotation matrix which is calculated via the Rodrigues formula [2] using the following method. Find the new axis direction (***axis***) by calculating the normalized cross product between z axis and the source normal vector:

$$\boldsymbol{axis} = \frac{\boldsymbol{zaxis \times normal}}{|\boldsymbol{zaxis \times normal}|} \qquad (4.6)$$

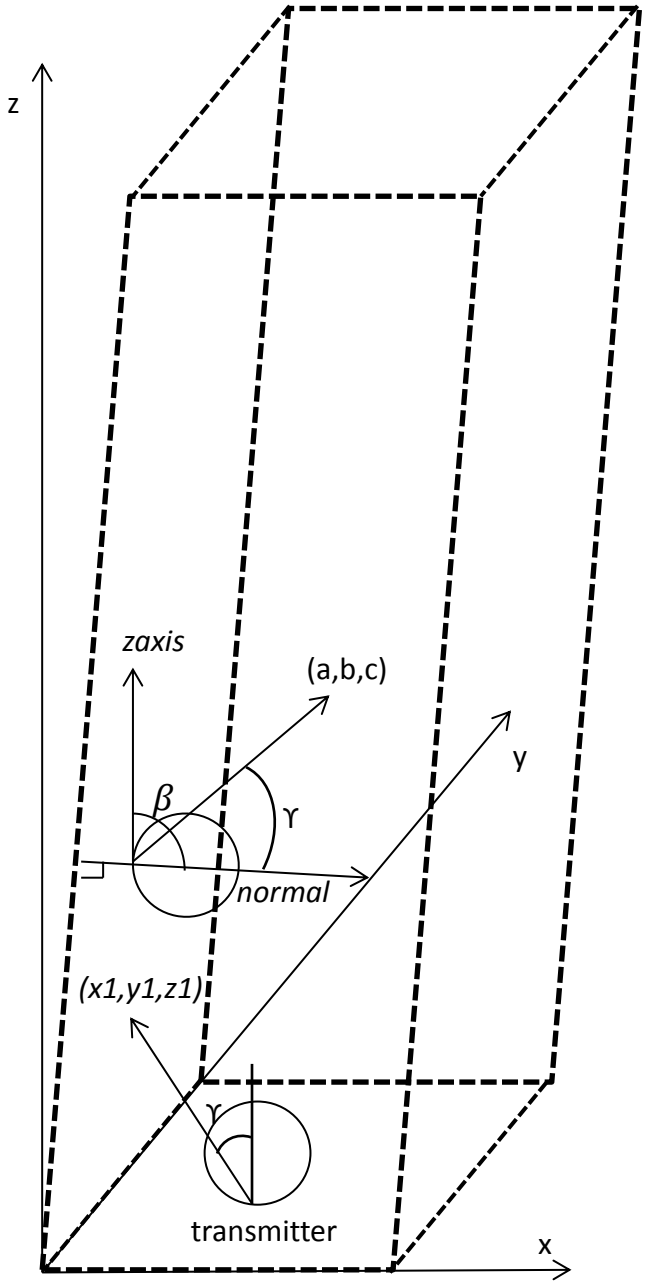

Figure 4-2 Illustration of ray rotation

A skew symmetric (*axis skewed*) representation of the normalized axis is:

$$axis\ skewed = \begin{bmatrix} 0 & -axis(3) & axis(2) \\ axis(3) & 0 & -axis(1) \\ -axis(2) & axis(1) & 0 \end{bmatrix} \qquad (4.7)$$

Rodrigues formula [116] for the rotation matrix:

$$R = I + \sin(\beta) * (axis\ skewed) + (1 - \cos(\beta)) * (axis\ skewed)^2 \qquad (4.8)$$

where β is the rotation angle. The process is illustrated in Figure 4-2 and the final ray direction components (*x,y,z*) are:

$$\begin{bmatrix} a \\ b \\ c \end{bmatrix} = R \begin{bmatrix} x_2 \\ y_2 \\ z_2 \end{bmatrix} \qquad (4.9)$$

4.2.2. Reflector simulation

To generate a reflected ray following the Lambertian model, the steps mentioned earlier are followed to generate a ray from a pure Lambertian source.

To generate a new ray that follows the Phong model, the reflected ray normal vector, $\hat{\mathbf{n}}_o$, is defined:

$$\hat{\mathbf{n}}_o = \hat{\mathbf{n}}_i - 2(\hat{\mathbf{n}}_i . \hat{\mathbf{n}}_s) * \hat{\mathbf{n}}_s \qquad (4.10)$$

where $\hat{\mathbf{n}}_i$ is the incident direction and $\hat{\mathbf{n}}_s$ is the surface normal; this is shown is Figure 4-3. Then a ray -with (x_P, y_P, z_P) direction- is generated using the procedure explained above taking into account that the normal vector is $\hat{\mathbf{n}}_o$and the Lambert mode number is m>1.

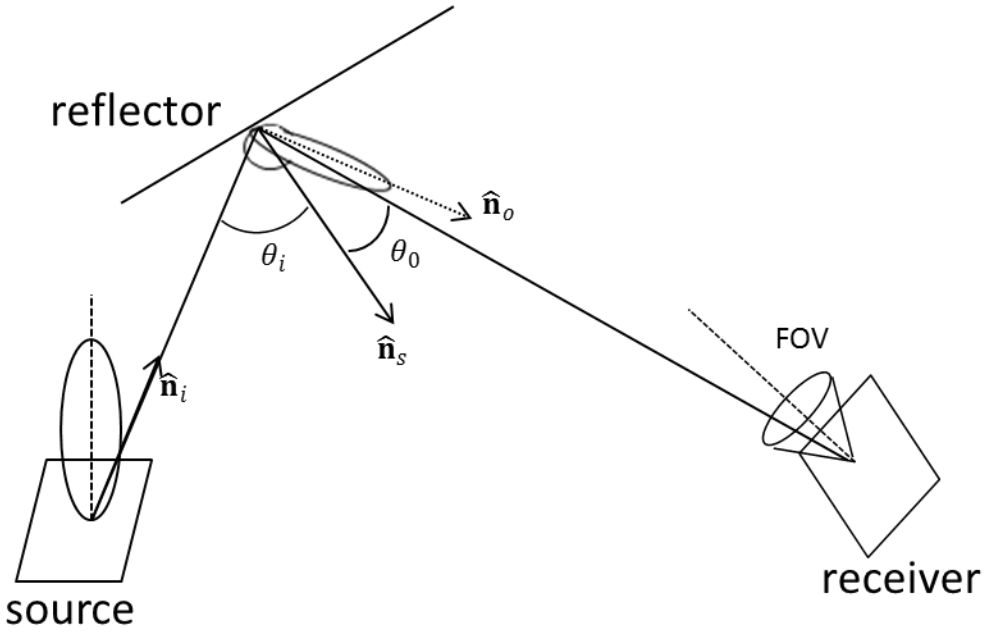

Figure 4-3 Source, receiver and reflector geometry

To generate a ray reflected from surface which follows the general Phong model, a ray that follows the Lambertian model with $n = 1$ is generated and related to the surface normal (x_L, y_L, z_L) along with another ray which is generated from the specular component with $m>1$ and related to the normal vector ….. (x_P, y_P, z_P); the final ray direction is:

$$(x, y, z) = \mathrm{r_d}(x_L, y_L, z_L) + \frac{(\mathrm{m}+1)}{2}(1 - \mathrm{r_d})(x_P, y_P, z_P) \qquad (4.11)$$

The reflected ray carries power which is equal to the power of the incident ray multiplied by ρ the reflection coefficient.

4.3. Determining Impulse Response from Simulation

4.3.1. Impulse response for LOS and multiple reflections

When there is a free unobstructed path between transmitter and receiver (the distance between transmitter and receiver is R), the whole signal will reach the receiver at approximately the same time. The impulse response is:

$$h^{(0)}(t;S;R) \approx \frac{n+1}{2\pi} cos^n(\theta)\, \mathrm{d}\Omega\, V(\psi)\delta(t - R/c) \qquad (4.12)$$

where dΩ is the solid angle subtended by the receiver's differential area (assuming $A_R << R^2$)

$$\mathrm{d}\Omega \approx \cos(\psi)\, A_R / R^2 \qquad (4.13)$$

The function $V(\psi)$ is the visibility function which will be explained in the next section. To find the impulse response results from multiple reflections, the MMC algorithm is applied [97]. The method basically generates random rays from the emitter which follows the radiation pattern. The rays then undergo several reflections and, after every reflection, contribute to the total impulse response. The algorithm keeps tracing each ray until either it reaches the receiver or the ray power goes below a defined threshold.

When a ray impinges on a surface, the impact point is calculated using the intersection algorithm explained later. After finding the intersection point, the LOS path between

the intersection point and the receiver is studied; if it exists, the contribution to impulse response is calculated depending on the surface material:

$$h^{(0)}(t; Ref; Rec) \approx E(\theta).\, d\Omega\, rect(\psi/FOV)\delta(t - d/c) \qquad (4.14)$$

where $E(\theta)$ is the surface radiation pattern and d is the distance between the reflector and the receiver.

A new ray will be generated using either the Lambert or Phong models as explained previously. The reflected ray power is calculated by multiplying the input power by ρ.

The ray journey continues until it either leaves the environment or has experienced a predefined number of reflections.

4.3.2. Intersection algorithm

While the rays travel from the emitter to the receiver through the waveguides, they undergo several reflections. To find the correct path which the ray follows, it is necessary to study the ray propagation between the emitter and the reflectors, between the reflectors, and between the reflectors and the receiver. The ray is defined by its origin point r_o (x_o,y_o,z_o) and unit direction vector r_d (x_d,y_d,z_d). It is presented mathematically by the equation:

$$r(t) = r_o + t.r_d \qquad (4.15)$$

where *t* represents the distance the ray travels.

After generating the ray from the emitter, it travels until it reaches the environment surface. To find the impact point location and the normal of the surface to which the impact point belongs, the ray equation is substituted into each surface equation which forms the current waveguide the ray travels through and the entrance and exit of the surface. The surface equation is:

$$ax + by + cz + d = 0 \qquad (4.16)$$

where *a,b,c,d* are constants.

This process produces four values from (rectangular, rhombohedrum, pyramid) waveguide surfaces, one value from the entrance surface and one value from the exit surface. The smallest positive value of *t* represents the first surface the ray would hit. To find the intersection point, *t* value is substituted in ray equation, and the appropriate normal vector is assigned. Figure 4-4 provides an illustration of the ray tracing algorithm.

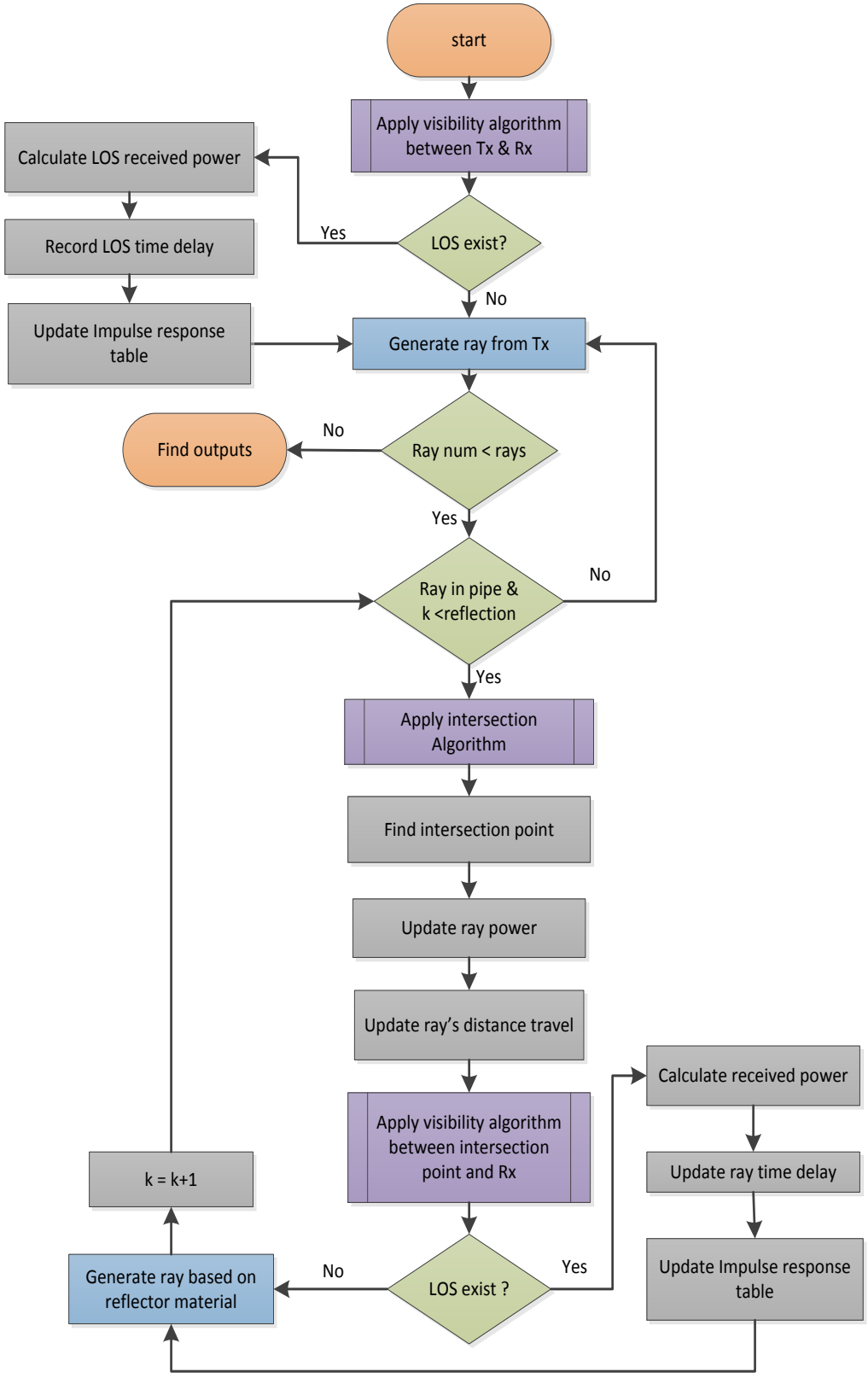

Figure 44-4 Flowchart showing the basic process for transmitting rays of light from transmitter to receiver through waveguide

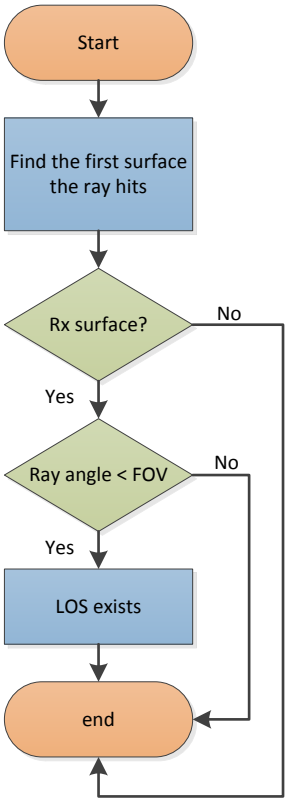

Figure 4-5 Flowchart showing visibility algorithm applied in the simulator

4.3.3. Visibility algorithm

It may be noticed that Figure 4-4 includes a visibility algorithm, shown in detail in Figure 4-5. As a result of the irregular shape of the sequence of waveguides, some points may not be visible to the receiver. In order to confirm the existence of LOS or not, the directed ray between the reflector and the receiver is considered to find whether the receiver surface is the first surface that this ray hits. If it is and the ray falls within the receiver FOV, then the reflector is visible to the receiver.

4.3.4. Steps of simulation

1- Define the environment (waveguide or sequence of waveguides) dimensions, planes equations, planes normal vectors and reflection coefficient.

2- Define transmitter characteristics (position, orientation unit vector, mode number, transmitted power) and receiver characteristics (position, orientation unit vector, FOV angle, detection area).

3- Define impulse response table where the raw represents number of reflection and the column represents time bin.

4- Calculate LOS impulse response from transmitter to receiver (LOS received power and LOS time delay) after applying the visibility algorithm to ensure LOS path between transmitter and receiver.

5- Generate a sufficient number of rays having random directions following a Lambertian radiation profile; a single ray has power $P_{ray} = \frac{P_t}{number\ of\ rays}$

6- Each ray travels from the transmitter inside the waveguide until it reaches its boundary. Calculate the intersection point by applying the intersection algorithm. The distance between the transmitter and the intersection point (d_{Tx-Ref}) is recorded in order to find the delay time ($delay = d/c$) when needed. Define $total\ distance = d_{Tx-Ref}$.

7- The power transmitted from the intersection point = ρP_{ray}, where P_{ray} is the received power at the intersection point and ρ is the reflection coefficient of the surface.

8- If the surface follows a Phong model radiation pattern, define the new reflector normal based on the incident ray direction and the surface normal. If the surface follows a Lambertian model radiation pattern, then skip this step.

9- Apply the visibility algorithm between the intersection point and the receiver in order to confirm a LOS path between the intersection point and the receiver. If LOS exists, find the received power and the distance between the intersection point and the receiver d_{Ref-Rx}. Find the delay time given by $(total\ distance + d_{Ref-Rx})/c$.

10- Add the received power to the impulse response table in the row equal to the reflection number and the appropriate time bin. Add the current contribution to previous contributions if they exist in the table.

11- Generate another ray from the impact point which follows either the Phong or the Lambertian model depending on the surface material.

12- Propagate the ray until it hits the surface. Find the new intersection point by applying the intersection algorithm. Find the distance between the two intersection points $d_{Ref-Ref}$ and update $distance = total\ distance + d_{Ref-Ref}$.

13- Repeat steps 7-12 to calculate the impulse response contributions until the ray has experienced the predefined reflection number or reaches the exit surface of the wave-guide.

14- If the number of reflections reaches the threshold, then terminate the process.

15- If the ray reaches the exit surface of the sequence of waveguides, terminate the process.

16- If there is a following waveguide, find the intersection point between the ray and the cross section of the current waveguide (exit surface). This conjunctive point is identified as the point of entry to the next waveguide.

17- Do not find the impulse response between the conjunctive point and the receiver. Find the intersection point between the ray and the new waveguide. Find the distance between the conjunctive point and the new intersection point ($d_{con-Ref}$) and update $total\ distance = total\ distance + d_{con-Ref}$.

18- Repeat steps 7-17.

4.4. Testing the Simulation Model

It is imperative to make comparisons between the simulation, previous models and

experiments carried out in the laboratory. This is to test the simulation validation and to make predictions about the system performance.

The simulation is tested against previous studies. These have a LOS configuration and a diffusive configuration; both have reflectors that follow Lambertian model. Following this, there is comparison with lab experiments for waveguide dimensions.

For the indoor environment, the received power will be compared, while for waveguide experiment path loss will be compared

4.4.1. Comparison with Recursive Model

The proposed simulator is compared with the Barry study [85] configuration A which represents a LOS link, and with configuration D which represents a diffusive link.

Both environmental parameters are shown in Table 4-1

Table 4-1 Parameters for testing against simulation

Parameter	**LOS configuration**	**Diffusive configuration**
Room: dimension	5×5×3 m	7.5×5.5×3.5 m
ρ_{NORTH}	0.8	0.58
ρ_{SOUTH}	0.8	0.56
ρ_{EAST}	0.8	0.30
ρ_{WEST}	0.8	0.12
$\rho_{CEILING}$	0.8	0.69
ρ_{FLOOR}	0.3	0.09
Source: mode	1	1
position	2.5,2.5,3	3.75,2.75,1
Elevation	-90˚	90˚
Azimuth	0	0
Receiver: area	1 cm^2	1 cm^2
FOV	85˚	70˚
position	0.5,1,0	6,0.8,0.8
Elevation	90˚	90˚
Azimuth	0	0
Resolution	0.2 ns	0.2 ns
Number of reflections	3	3

Figures 4-6 to 4-9 show the impulse responses for the original study and the proposed method. The significant numerical outputs are found in Table 4-2. High similarity in received power values is shown in the Table 4-2 between the recursive method and the proposed method with less than 1% difference in LOS environment, and less than 0.05% difference in diffuse environment.

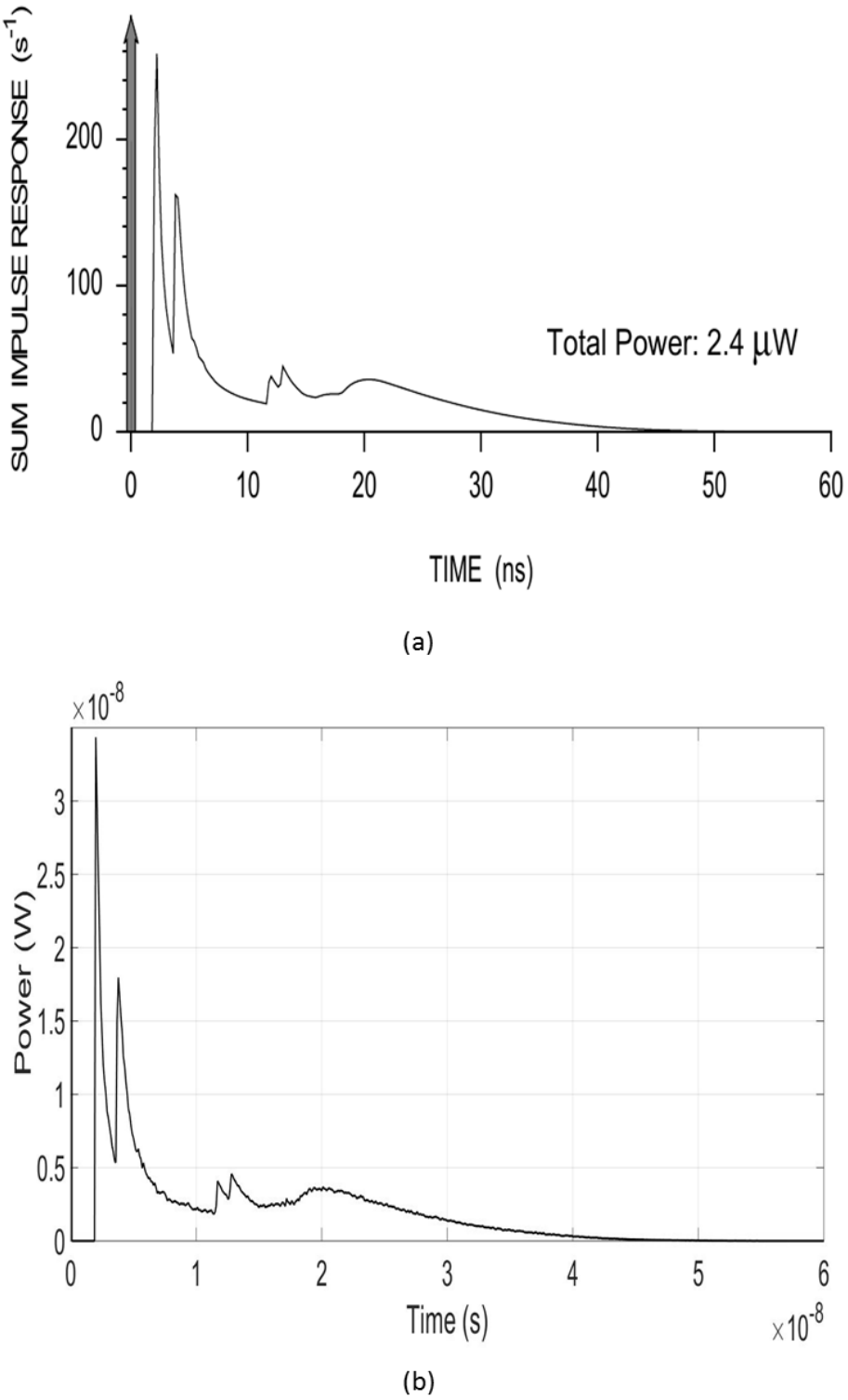

Figure 4-6 Comparison of the impulse response between: (a) Barry model configuration A; (b) simulator model.

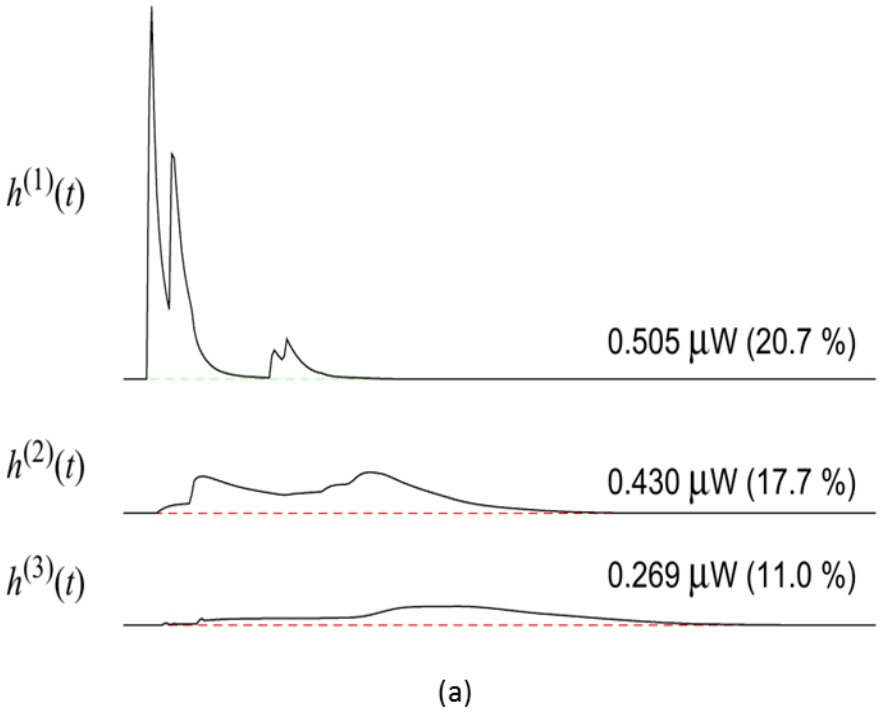

(a)

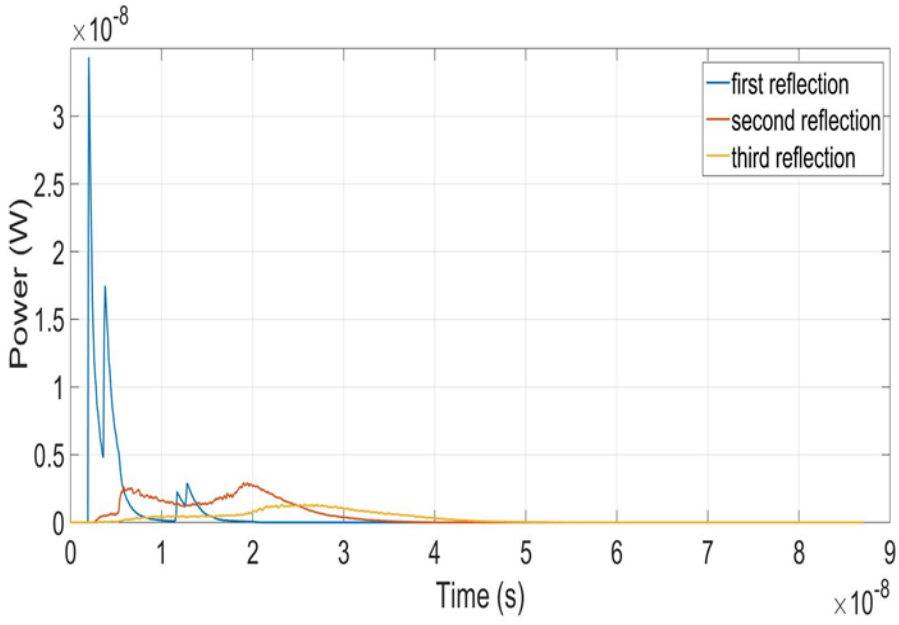

(b)

Figure 4-7 Comparison of the impulse for the first three reflections between: (a) Barry model configuration A; (b) simulator model.

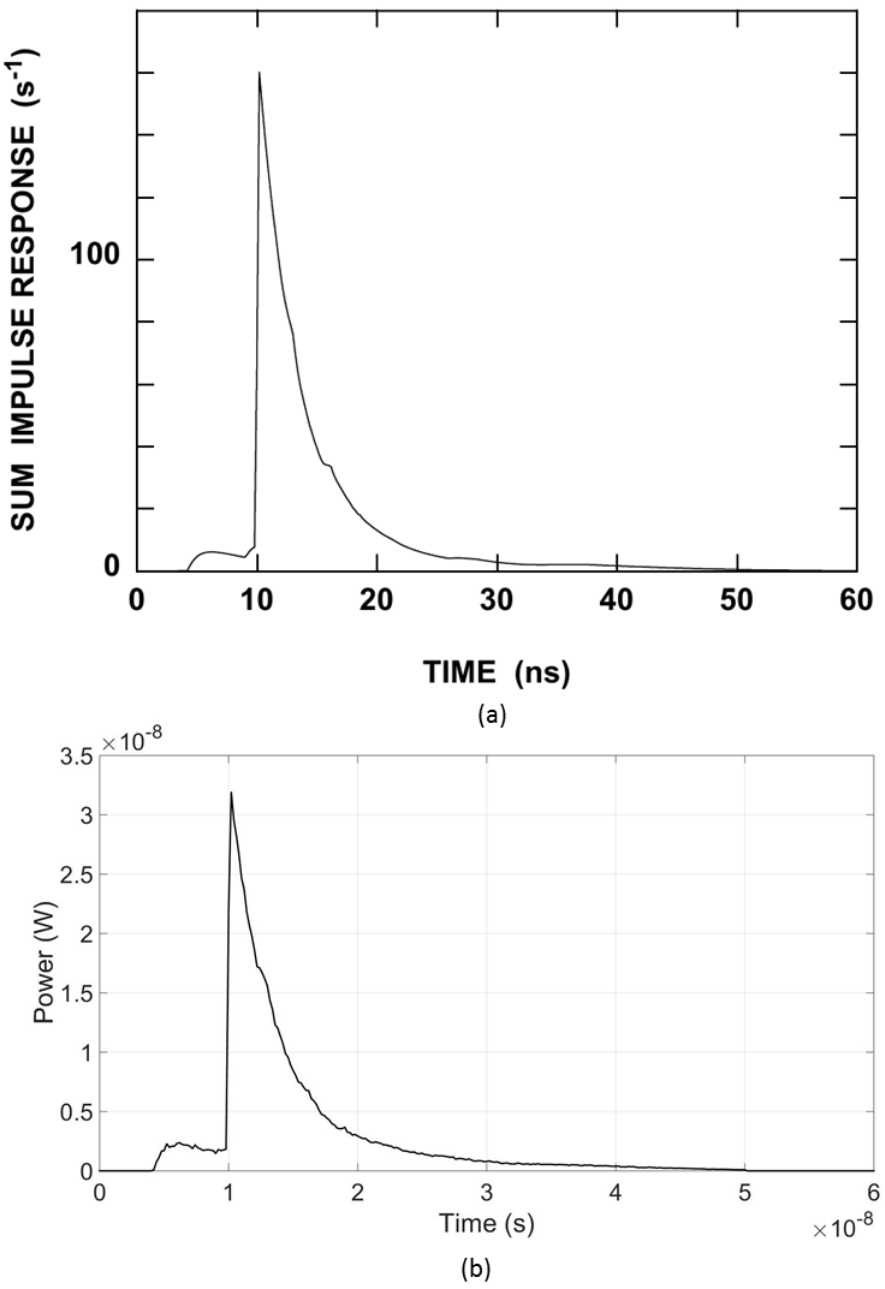

Figure 4-8 Comparison of overall impulse response between: (a) Barry model configuration D; (b) simulator model.

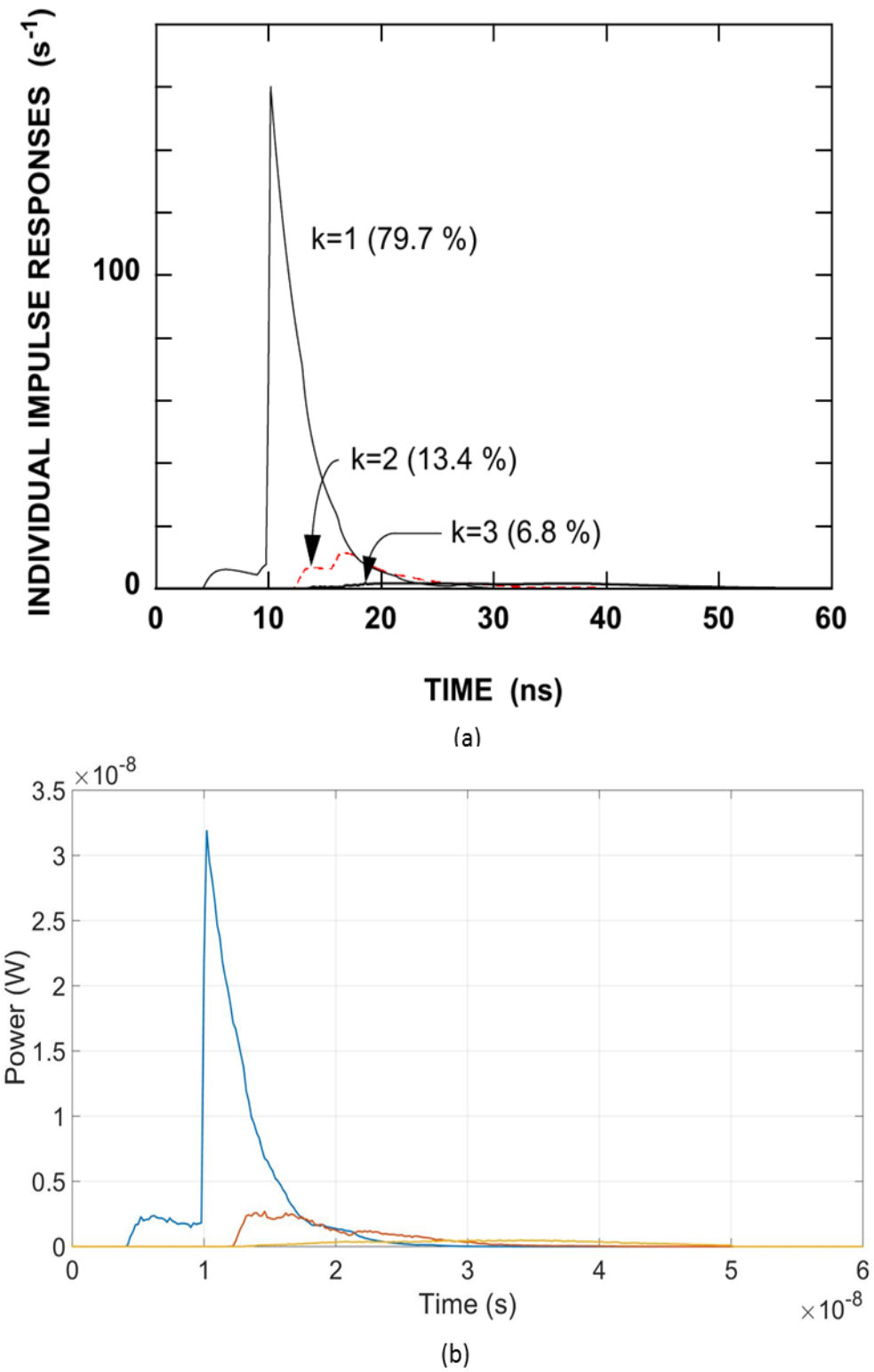

Figure 4-9 Comparing reflections impulse response between (a) Barry model configuration D (b) simulator model

Table 4-2 Summary of testing results

	LOS link (Barry)	**Proposed method**	**Diffuse link (Barry)**	**Proposed method**
Total received power	2.47 μW	2.4 μW	0.69 μW	0.68 μW
LOS link	1.23 μW	1.23 μW	0	0
Percentage	50.6%	51.25%	-	-
First reflection received power	0.505 μW	0.507 μW	0.549 μW	0.549 μW
Percentage	20.7%	21.1%	79.7%	79.5%
Second reflection	0.43 μW	0.43 μW	0.09 μW	0.091 μW
Percentage	17.7%	17.9%	13.4%	13.3%
Third reflection	0.269 μW	0.258 μW	0.046 μW	0.044 μW
Percentage	11%	11.2%	6.8%	6.4%

4.4.2. Comparison with Experimental Measurement

Experimental support for the study was provided by power measurements of the transmission of light from a VLSY5860 IrLED (radiant intensity of 11.8 mW cm^{-2}) through a straight Aluminium rectangular guide to a resistor-amplifier receiver with an SFH205F photodiode.

The environment and simulation parameters are shown in Table 4-3 and Figure 4-10 compares the simulated and measured system path losses up to 1m with good agreement obtained. It is noted that the model differs from the experiment because the model studies the path loss caused by the channel solely, while the experiment detects the signal affected from the whole system limitations.

Table 4-3 Parameters for testing against experiment

Parameter	Value
Waveguide: dimensions	4 x 4 x 50 cm
ρ	0.88
r_d	0.3
m	250
Source: mode	505
Position	2,2,0 cm
Elevation	90˚
Azimuth	0
Receiver: area	7 mm^2
FOV	60˚
Position	2,2,25 cm
Elevation	90˚
Azimuth	0
Resolution	2 ps
Number of reflections	15

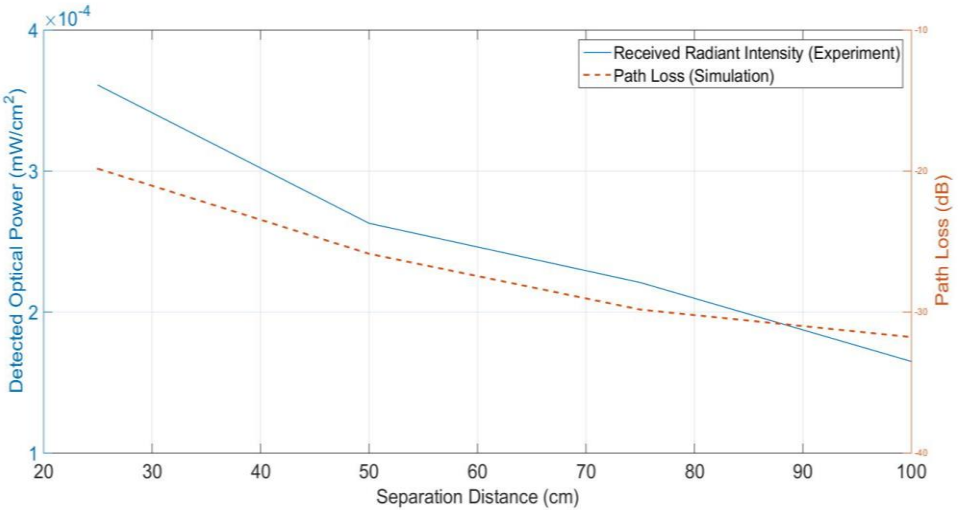

Figure 4-10 Path loss and optical received power vs transmitter-receiver distance

4.5. Conclusions

In this chapter, the operation of a simulator to predict the channel characteristics of OW links in waveguides has been described. This modelling approach helps system design engineers to propose better designs prior to practical experiments.

The simulator was tested by comparing it with calculated results from the literature and with experimental measurements. Good agreement between the model described and the other methods was obtained.

Chapter 5: Simulating Various Scenarios for Waveguide Optical Communication I (Straight and Curved Waveguides)

5.1. Introduction

In chapter 4, the simulator developed in this work has been presented and tested. This chapter examines the results produced from the consideration of different waveguide conditions, source conditions and receiver conditions. Every parameter has a potential impact on the general measured quantities, which, for optical correspondence, are typically the total received optical power and the temporal spread of the data pulses. Both of these deliberate amounts specifically influence the capacity to dependably impart information from the transmitter to the receiver.

5.2. Define the simulation variables

As a system of communication, the transmitter, receiver and environment influence

the system performance; it is very difficult to separate their effect. The technique utilised here is to characterise cases systematically, with each concentrating on specific simulation variables in order to analyse the data.

5.2.1. Waveguide parameters

A detailed theoretical study of light in indoor environment and waveguides has been provided in Chapter 4. The environment material which will be considered in the rest of the thesis is divided into two types. The first is a scattering waveguide where the light scatters randomly when it hits the boundary of the waveguide; plastic is typical of this behaviour and the radiation pattern follows the Lambertian model discussed in Chapter 3. The second waveguide material is considered as a reflective surface where the reflected light contains a specular component in addition to scattered component. Aluminium is a typical material with this behaviour and the radiation pattern follows Phong model discussed in Chapter 3. The list of material specifications are represented in Table 5.1, while Figure 5-1 illustrates the radiation pattern for both materials.

In this chapter, both straight and bent waveguides will be investigated. Bends affect the link performance as any LOS link might be blocked, and the light itself may not have the capacity to traverse the bend. The waveguide dimensions and list of bending angles are displayed in Table 5-2. The bend occurs after 50 cm of the waveguide length, as illustrated in Figure 5-2.

Table 5-1 Waveguide parameters

Coefficient	Plastic waveguide (scattering environment)	Aluminium waveguide (reflective environment)
Reflection coefficient ρ	0.6	0.88
Scattering coefficient	1	1
Percentage of incident signal that is reflected diffusely r_d	1	0.3
Directivity of the specular component m	0	250

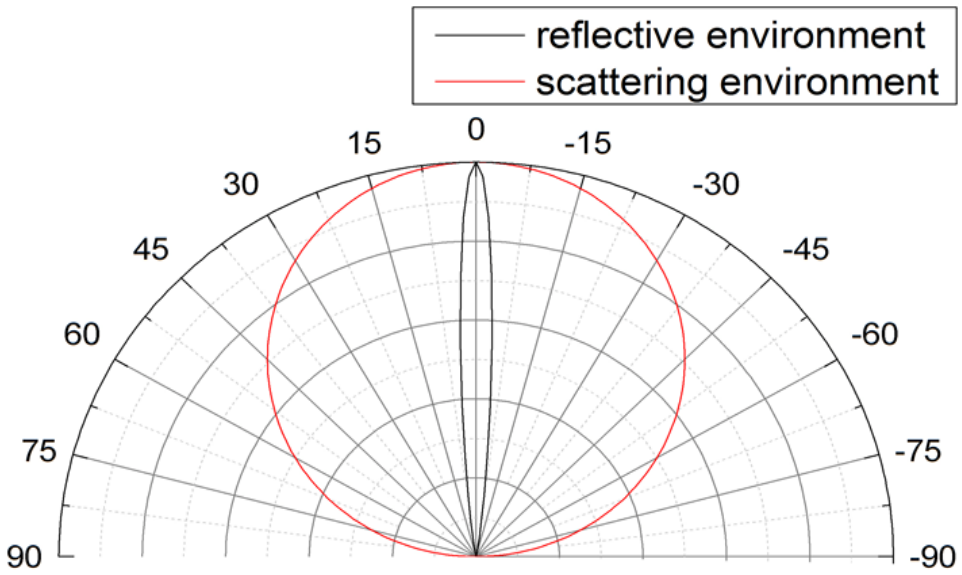

Figure 5-1 Waveguide reflective radiation pattern

Table 5-2 Waveguide dimensions and bending angles

Waveguide dimensions	*10 × 10 × 110 (cm)*
Bending angle	{0° (straight waveguide), 10°, 25°, 40°, 55°, 70°, 90° (right angled waveguide)}

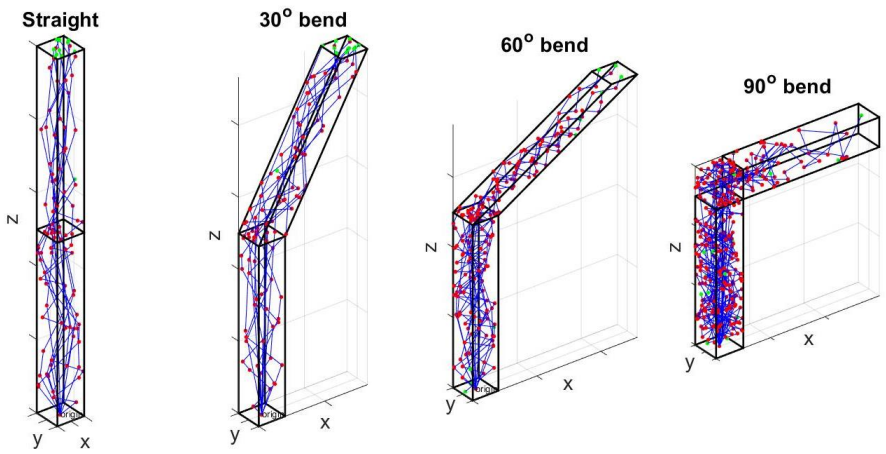

Figure 5-2 Waveguide configurations

5.2.2. Source parameters

As a source, the transmitter has been divided into two cases: pure Lambertian LED (where $n=1$) and directive LED (where $n=505$). The radiation patterns for both sources are presented in Figure 5.3. The transmitter is located in the centre of the waveguide entrance and directed vertically with transmitted power $P_T=1W$.

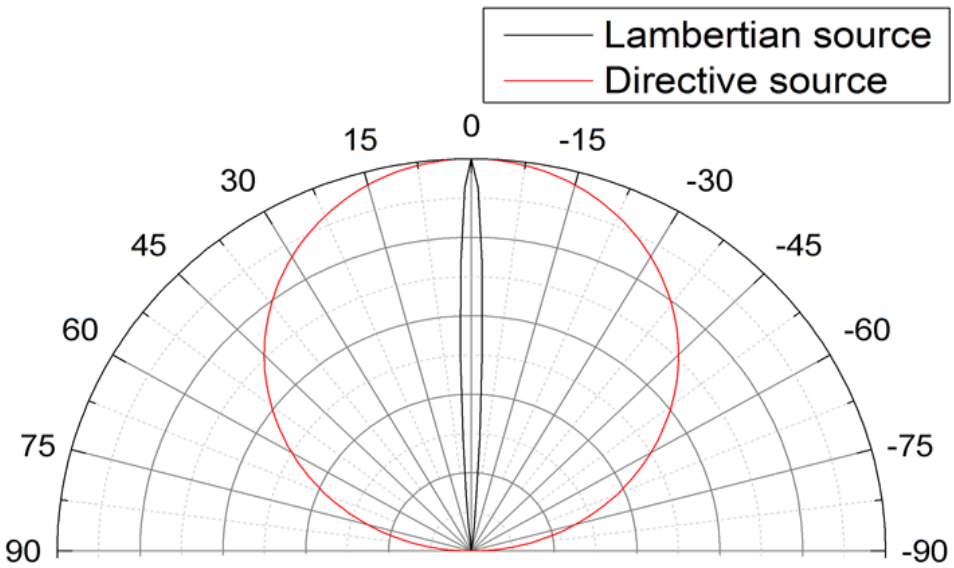

Figure 5-3 Source radiation pattern

5.2.3. Simulation variables

5.2.3.1. Receiver parameters

Notwithstanding distinctive environmental conditions and sources, simulation results are likewise delivered for a range of receiver openings and FOVs. This division produces forecasts concerning different connection setups and helps the system designer to design the receiver front-end effectively.

The minimum receiver area was chosen to be 1 mm^2 while the maximum value was set to 10 mm^2. The receiver FOV was simulated to cover the range from 10˚ to 90˚. The full arrangement of receiver FOV's and receiver apertures is recorded in Table5-3.

Table 5-3 Receiver variables

Receiver area = 1 mm^2					
Receiver FOV	10°	30°	50°	70°	90°
Receiver FOV = 70°					
Receiver area	1 mm^2	7 mm^2	10 mm^2	-	-

The receiver was located in the centre of the waveguide exit unless stated, and it was directed parallel to the bended part of the waveguide.

The summary of the simulated configurations is shown in Figure 5-4.

Other simulation variables which should be characterized before applying all cases are

time resolution, the number of simulated rays transmitted from the source and the number of reflections which contribute to the channel impulse response. A time resolution of Δt = 2 ps has been utilized to ensure that the ray does not contribute more than once to the total received power within one time bin Δt. The number of rays was 10^6 which was large enough to get accurate results.

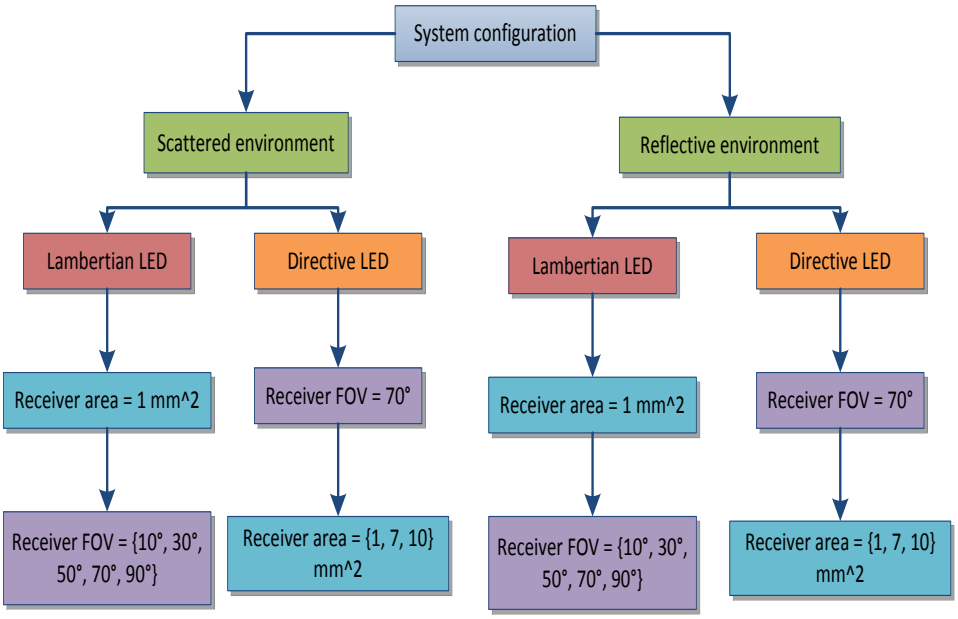

Figure 55-4 Simulated configurations

For indoor applications, it was sufficient to consider only three reflections because of the high computational time required with no significant improvement in accuracy. However, due to the waveguide dimensions, three reflections did not here convey the greater part of the transmitted power. In scattered environments where the light reflects arbitrarily with pure Lambertian transmitter, the effect of reflections has thus been studied as follows.

A set of 25 uniformly distributed receivers over the waveguide exit surface were placed in a pure diffusive environment with a reflection coefficient of 0.6. The propagation of rays through pipes with the bending angles shown in Figure 5-2 with a receiver FOV of 70° and receiver area of 1 mm^2 was simulated. Figure 5-5 demonstrates the cumulative percentage of contribution made by the reflections. As shown in the figure, LOS channels are very unlikely except for straight and small bending angles. The simulation of the 175 channels shows that for the channels where LOS exists, the first three reflections constitute more than 95% of the total received power on average, while for non-LOS channels they contribute between 50% and 80% of the final value. Based on these results, 15 reflections have been considered in the remainder of the work.

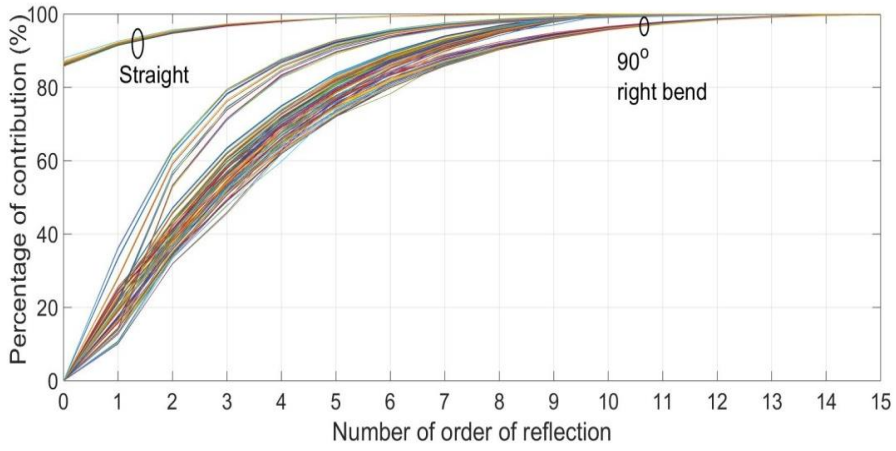

Figure 5-5 Cumulative reflection contributions for scattering environment with a Lambertian source

The following subsections will be divided as follows: the study will start with scatter-

ing environment with Lambertian source, followed by scattering environment with directive source, reflective environment with Lambertian source and, finally, reflective environment with directive source. The effect of receiver FOV for specific receiver areas and the effect of the receiver area for specific receiver FOVs will be studied. More emphasis will be on right-angle waveguides for the first configuration of a scattering environment with a Lambertian source. Received power, path loss, channel bandwidth and RMS delay spread (D_{rms}) will be examined in addition to temporal and frequency responses that will be presented for some cases.

5.3. Scattering environment with Lambertian source

This combination is such that the Lambertian radiation model makes the light reflect completely randomly through the waveguide producing a channel performance that is very hard to predict.

5.3.1. Receiver area effect

The results presented in Figures 5-6 to 5-9 show the simulated received power, path loss, channel bandwidth, and RMS delay spread versus bending angle. The smaller the receiver area is, the less the power which can be received, as expected. The power drops around 95% directly after the LOS is blocked, and the power deviation for each receiver area case is around 99%.

It can be seen that the larger the bending angle, the higher the path loss, but, for a right

angle waveguide, the path loss is less compared to the 70° bend, due to the bigger space that exists in the former case at the junction. The bend in the studied cases is sharp and it prevents the light from travelling smoothly to the next waveguide. The points where the bandwidth is not determined imply that the bandwidth at these locations is beyond capabilities of the simulator using the sampling time of 0.2 ps. As it can be seen from Figure 5-8, receiver area does not have a significant effect on the channel bandwidth. The minimum bandwidth is found in the 70° bend, and equals 130 MHz while it increases for the right angle waveguide to 220 MHz.

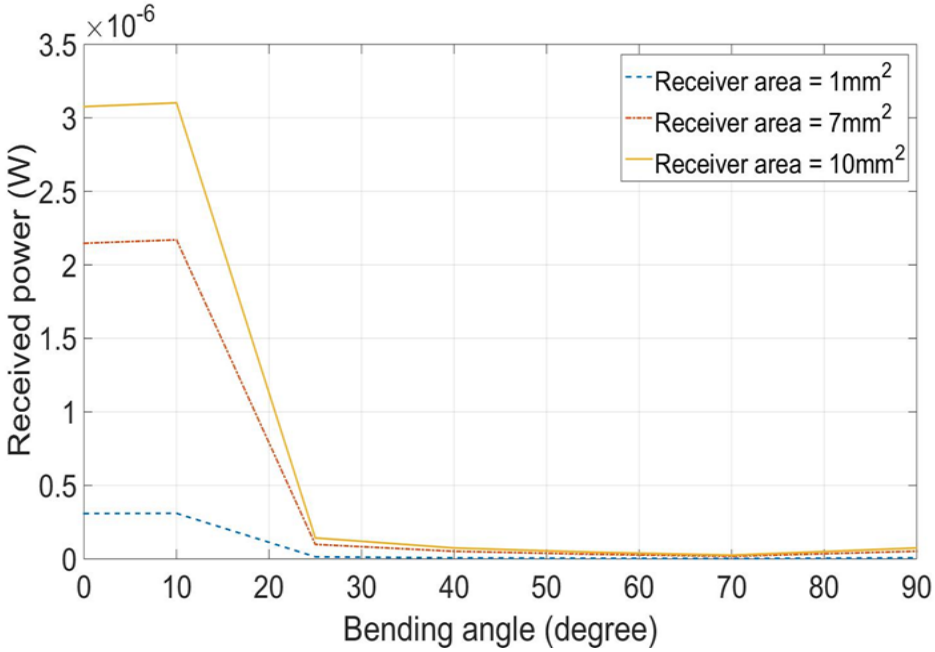

Figure 5-6 Received power versus bending angle for several values of receiver area in a scattering environment with Lambertian source

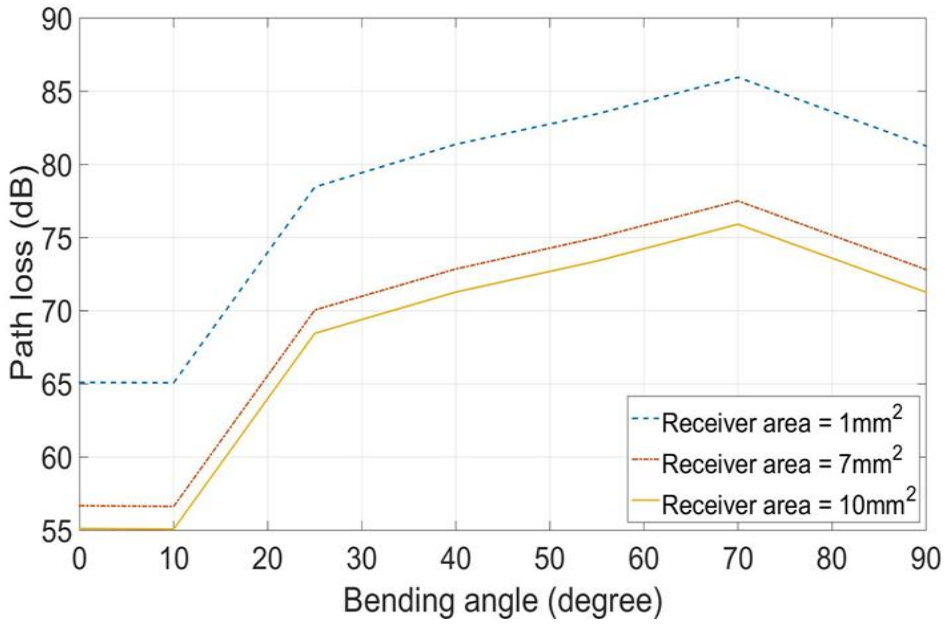

Figure 5-7 Path loss versus bending angle for several values of receiver area in scattering environment with Lambertian source

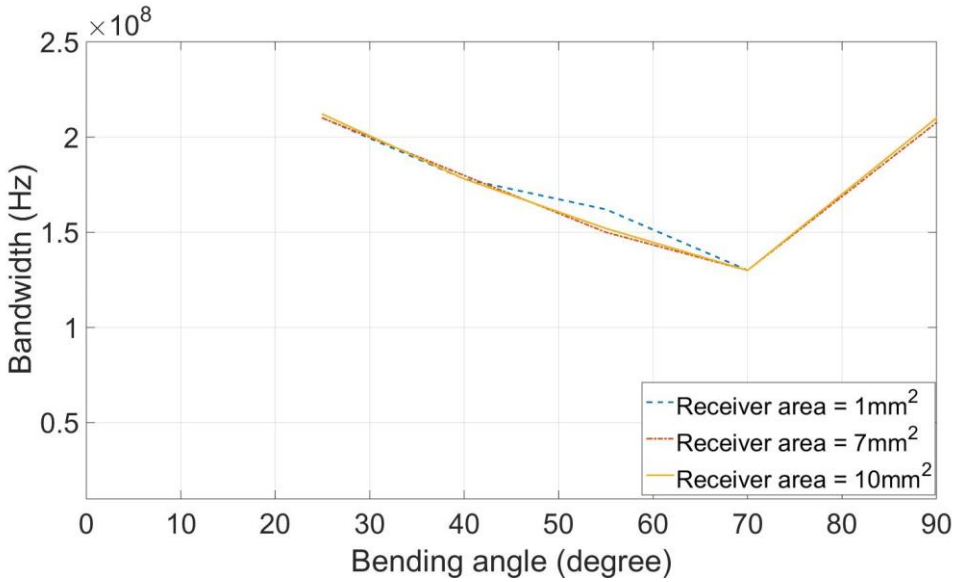

Figure 5-8 Bandwidth versus bending angle for several values of receiver area in scattering environment/ with Lambertian source

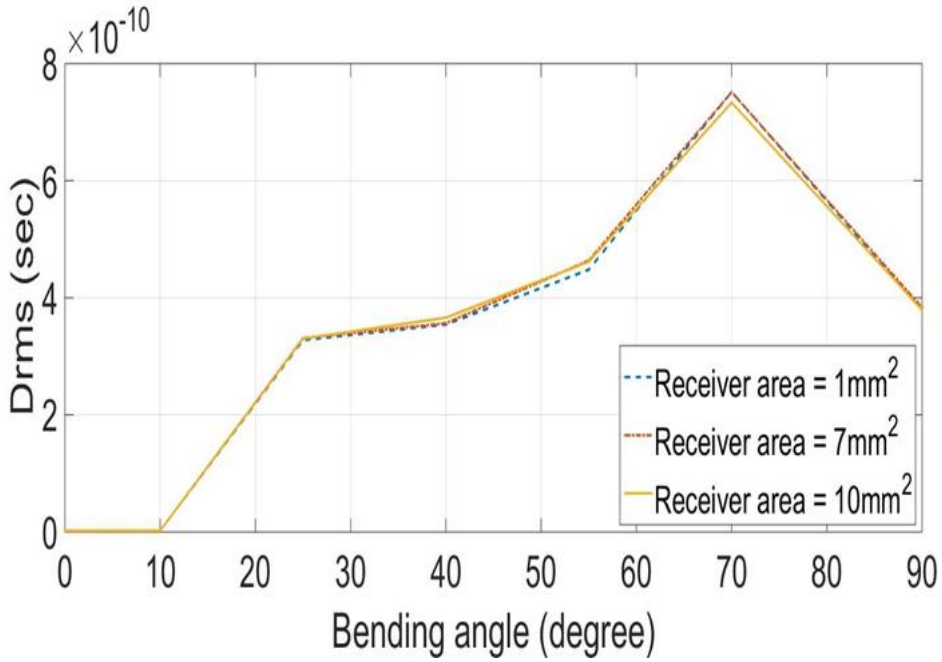

Figure 55-9 RMS delay spread versus bending angle for several values of receiver area in scattering environment with Lambertian source

5.3.2. Receiver FOV effect

Figures 5-10 to 5-13 show the receiver FOV effect over different bending angles and it is clear that this does not affect the channel characteristics. Since the minimum studied value of FOV is 10°, it is able to cover most parts of the inner surfaces of the waveguide, and because of the random movement of light in this environment, it is believed that the receiver FOV affects neither the path loss nor the bandwidth.

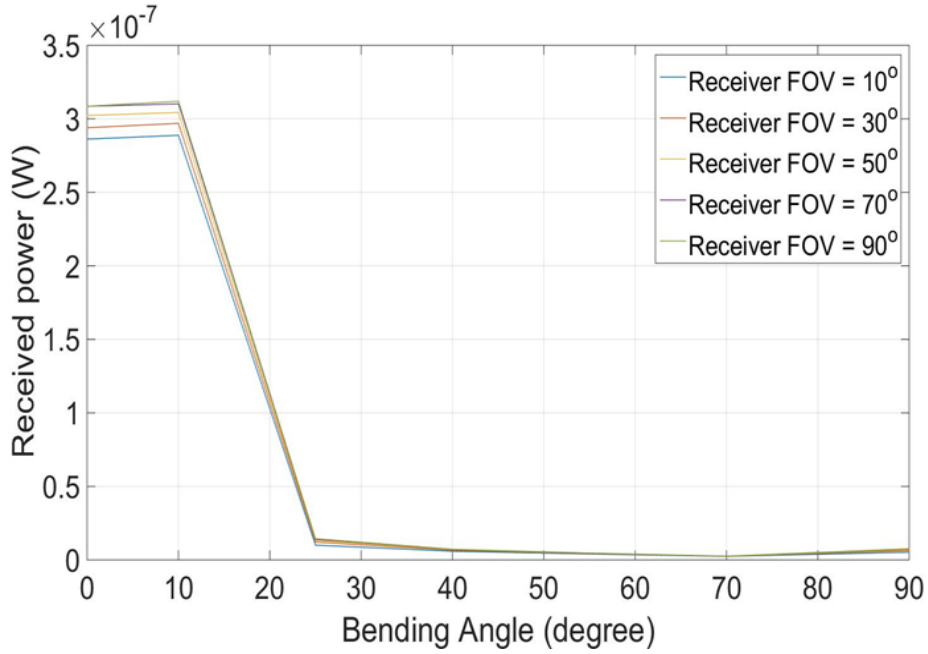

Figure 55-10 Received power versus bending angle for several values of receiver FOV in scattering environment with Lambertian source

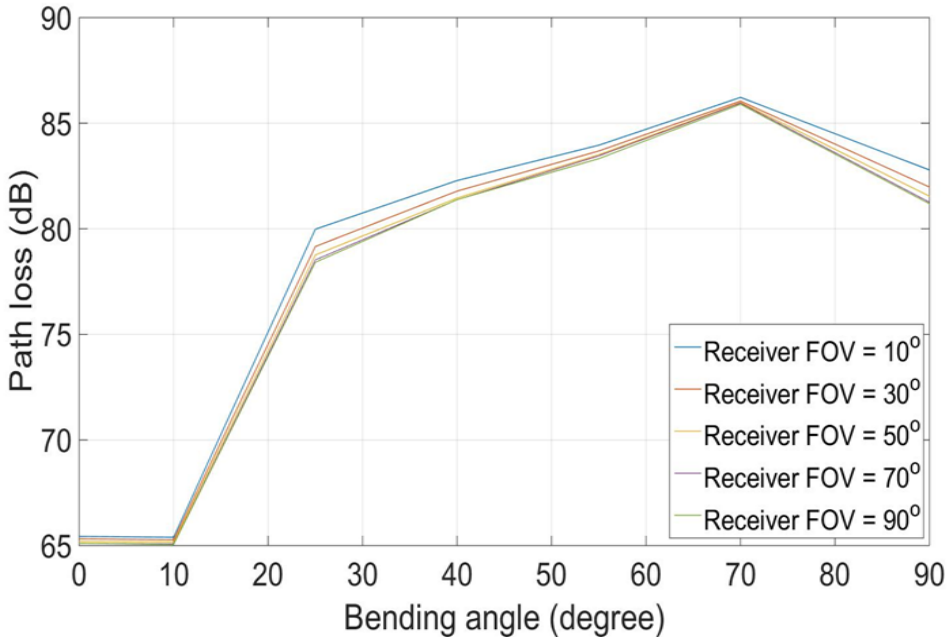

Figure 5-11 Path loss versus bending angle for several values of receiver FOV in scattering environment with Lambertian source

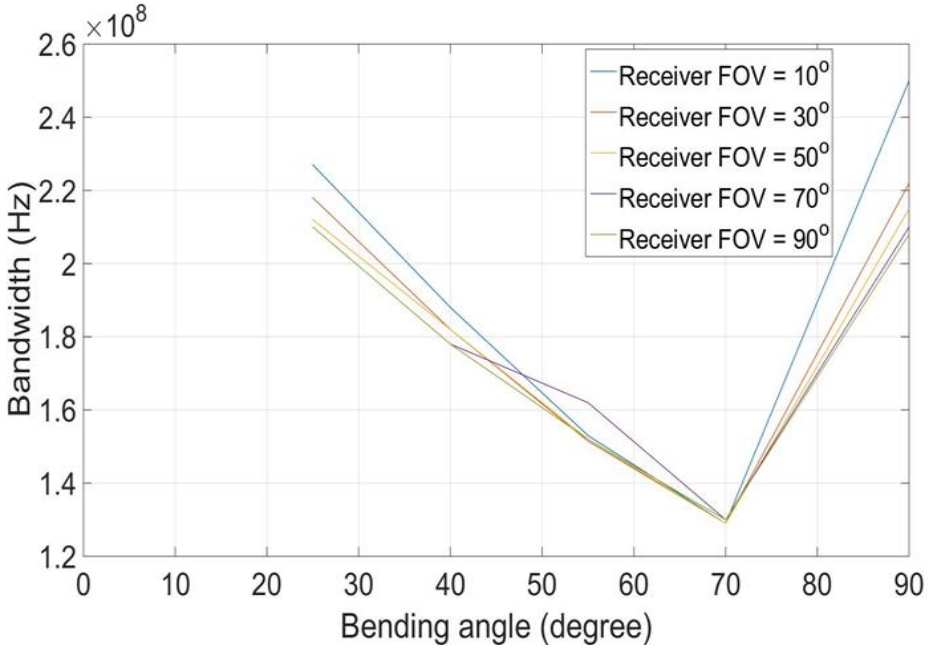

Figure 5-12 Bandwidth versus bending angle for several values of receiver FOV in scattering environment with Lambertian source

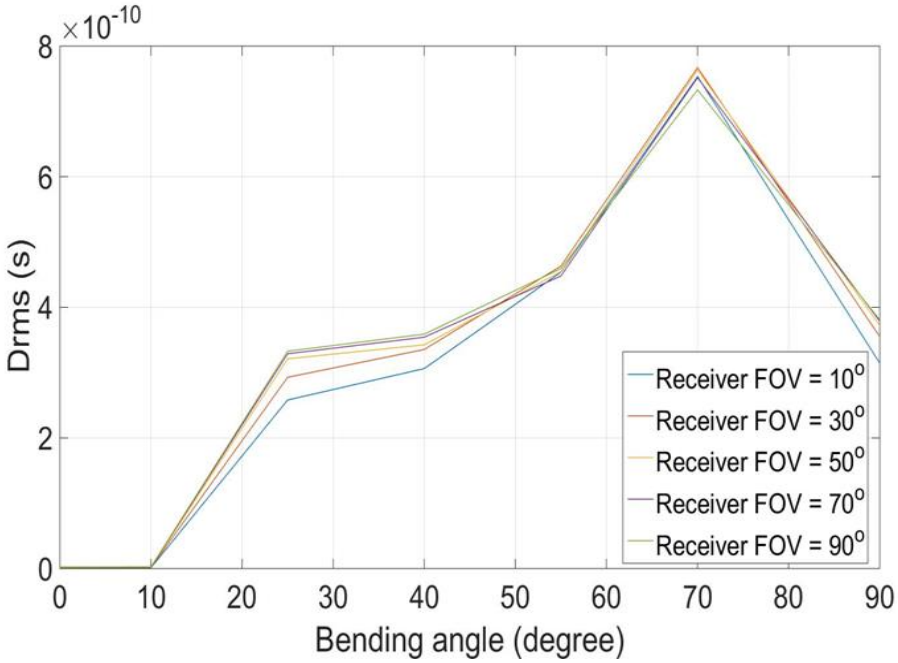

Figure 5-13 RMS delay spread versus bending angle for several values of receiver FOV in scattering environment with Lambertian source

5.3.3. Right angled waveguide

A more detailed study was undertaken for the right angled waveguide, known structure that exists within the vehicle. Figure 5-14 demonstrates the power distribution through the right angle bend waveguide. Prior to the bend, the maximum power is in the centre, while after the bend it shifts towards the inner part of the waveguide as one would expect. This distribution is maintained after the bend with a drop in the value of the received power since the LOS component has been lost. At the waveguide exit, the total received power varies between approximately 6 nW and 8 nW, a deviation of 25% from the peak. It can be seen that the bandwidth is almost constant over the exit plane with a value equal to 225 MHz.

Figure 5-15 illustrates the channel impulse response at two different locations in the right-angle pipe exit (the corner and the centre). For the former, the impulse response tail is long in contrast to the latter one where the pulse is received within shorter time.

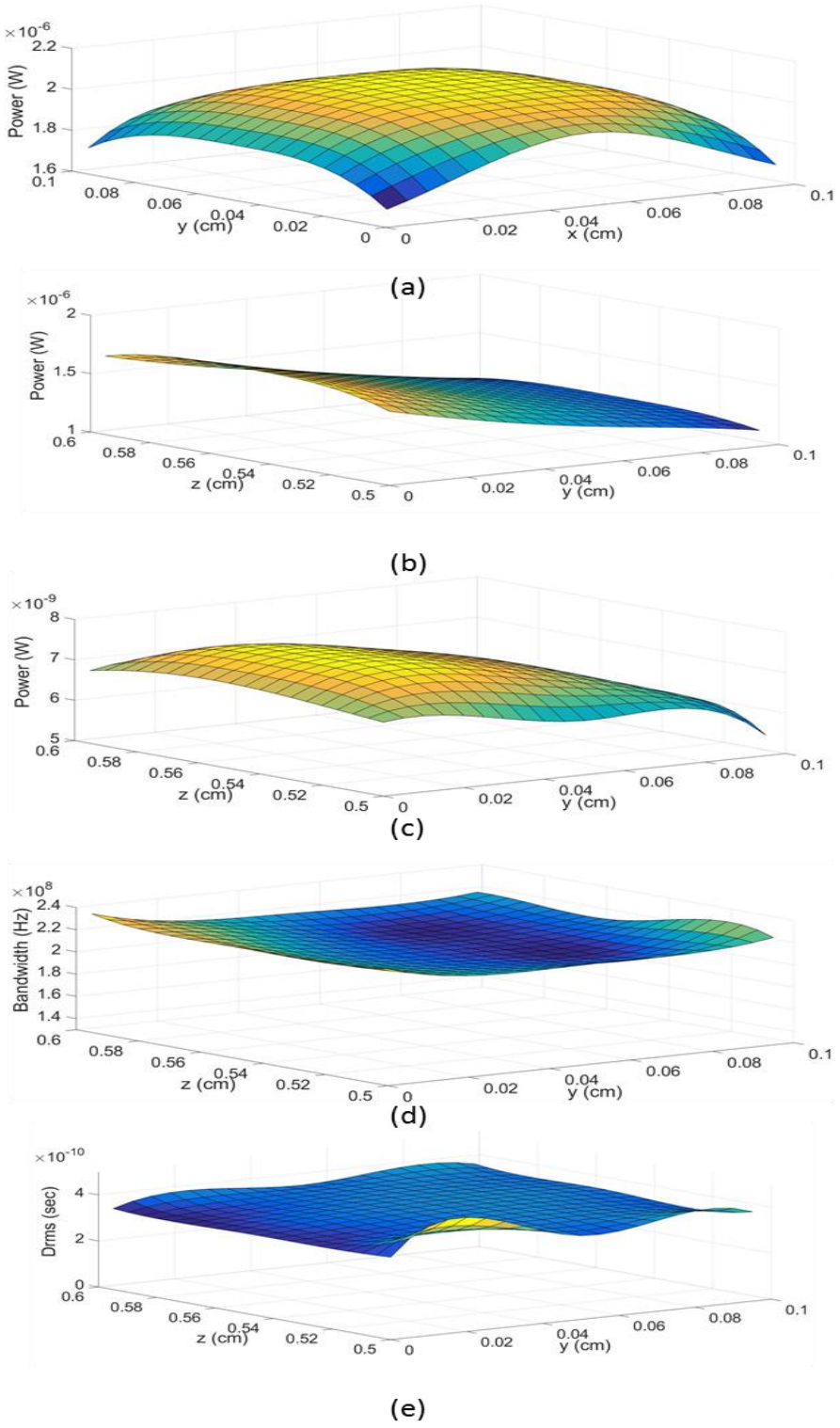

Figure 55-14 Power distribution in right angle bend waveguide: (a) before bend; (b) after bend; (c) at waveguide exit; (d) bandwidth distribution at pipe exit; (e) Drms at pipe exit

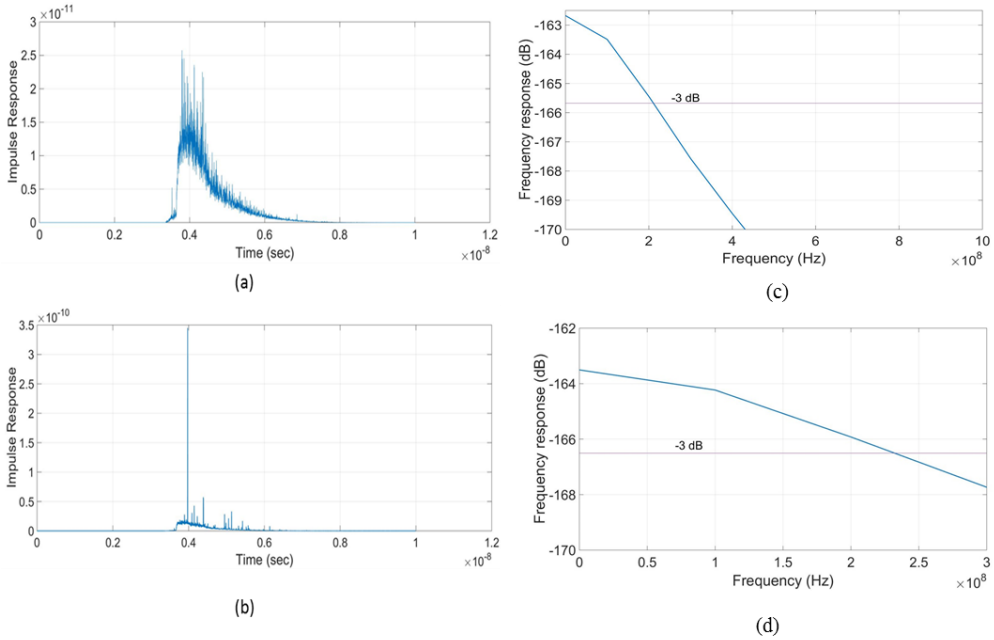

Figure 55-15 Impulse response and frequency response at the exit of the right angle bend waveguide in scattering environment with Lambertian source (a) impulse response, corner (b) impulse response, center source (c) frequency response, corner (d) frequency response, center

5.4. Scattering environment with directive transmitter

5.4.1. Effect of receiver area

Figures 5-16 to 5-19 show the channel performance through a scattering environment using a directive transmitter at the centre of the waveguide entrance surface. Similarly, to the previous configuration, the receiver area does not affect the channel bandwidth while it has an impact over the received power. The path loss drops rises by around 10 dB between 1 mm^2 and 10 mm^2 receiver area. For a straight waveguide, the received power is approximately 0.66 mW and 66 μW for 10 mm^2 and 1 mm^2 receiver area

respectively, while it drops to 3 μW and 0.3 μW for a right angled waveguide.

The minimum bandwidth which the channel can deliver is circa 158 MHz.

As can be seen, the main limitation in the environment is the power, but it is possible to increase the source power without eye and skin safety concerns in the closed pipe environment.

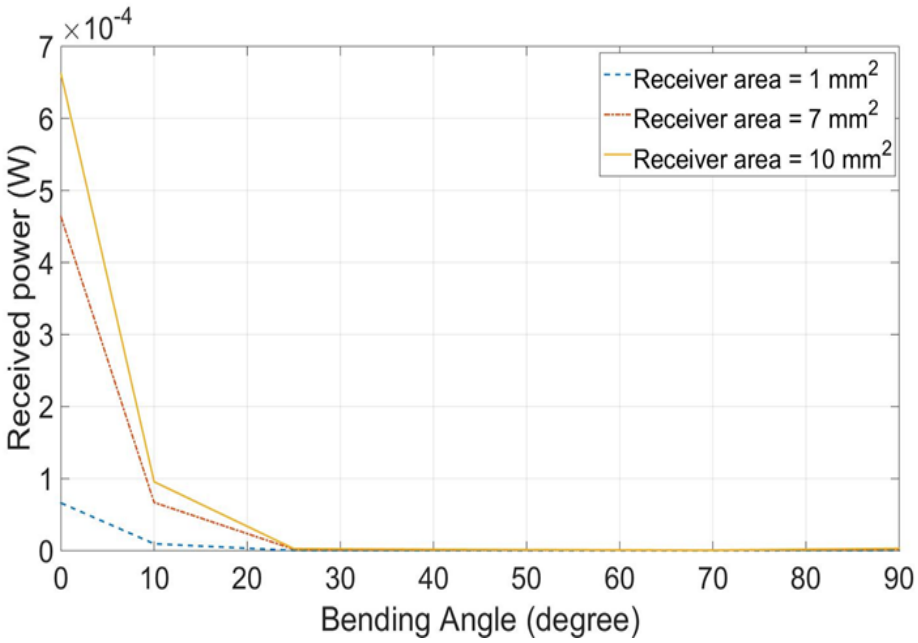

Figure 5-16 Received power versus bending angle for several values of receiver area in scattering environment with directive source

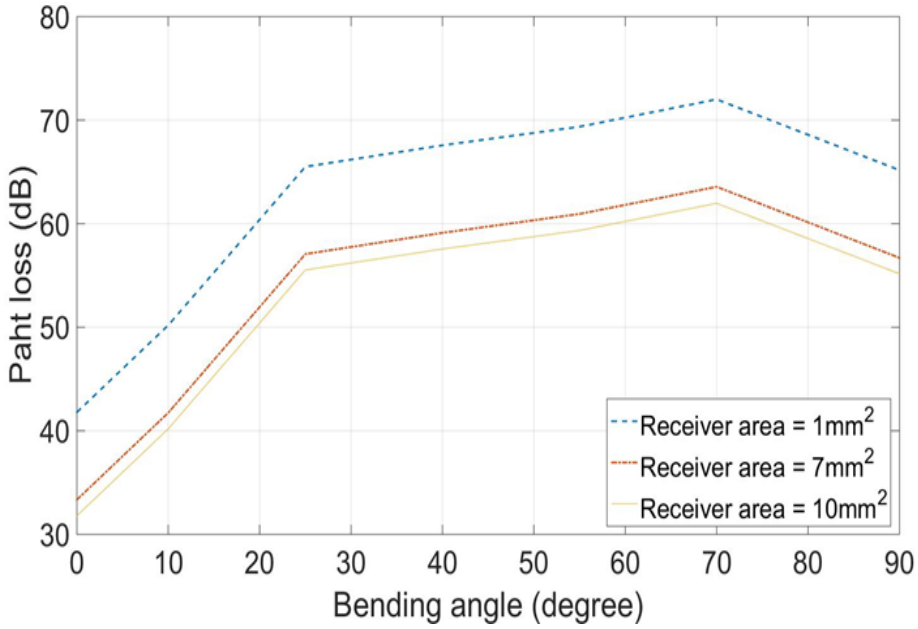

Figure 5-17 Path loss versus bending angle for several values of receiver area in scattering environment with directive source

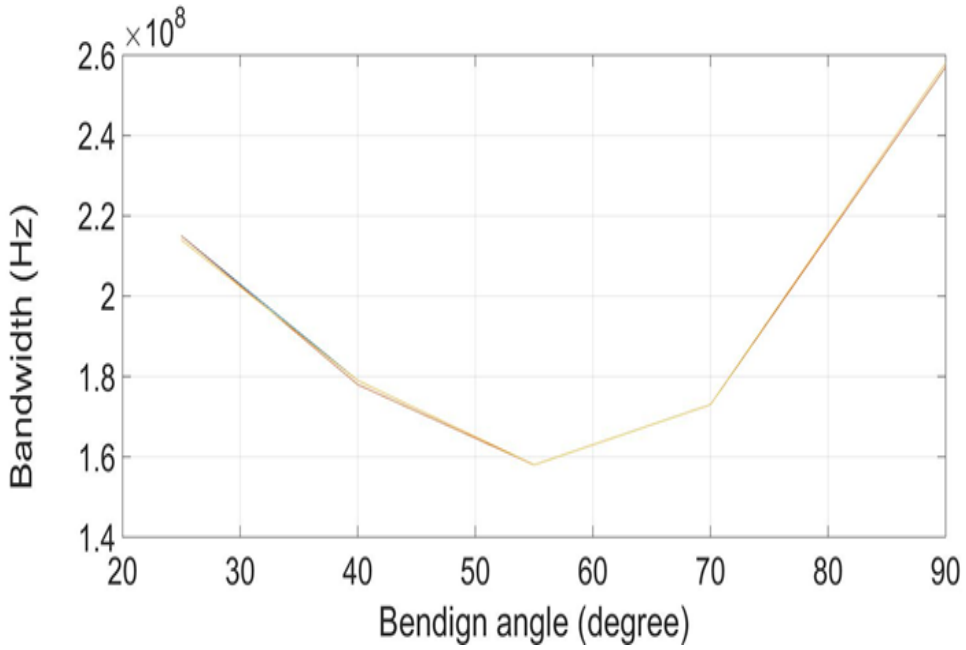

Figure 5-18 Bandwidth versus bending angle for several values of receiver area in scattering environment with directive source

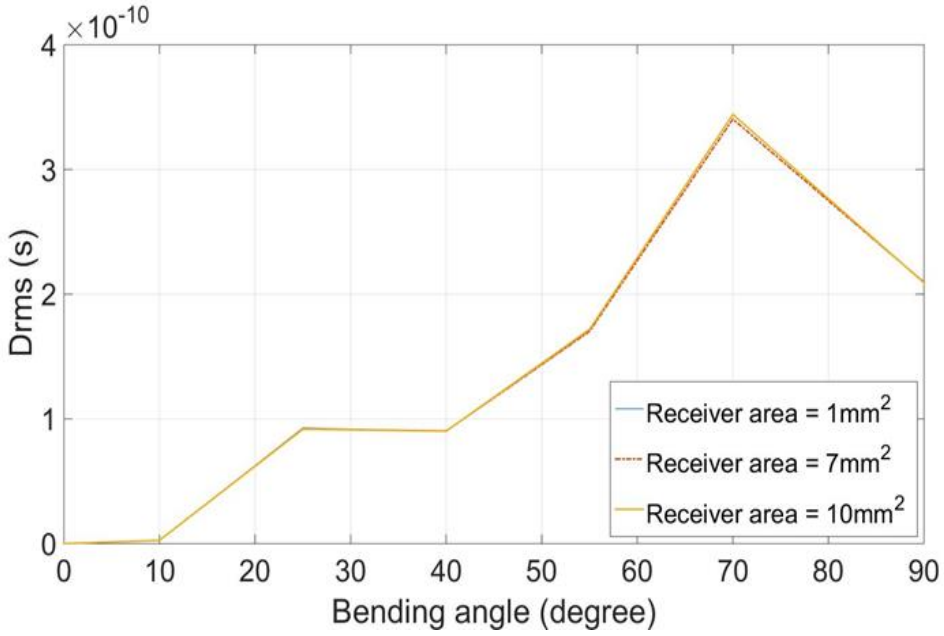

Figure 5-19 RMS delay spread versus bending angle for several values of receiver area in scattering environment with directive source

5.4.2. Receiver FOV effect

Figures 5-20 to 5-23 show the effect of the receiver FOV. This does not alter the path loss and received power except for in the right angle waveguide case, where for 10˚ receiver FOV the bandwidth is 330 MHz which decreases to 255 MHz for the 90˚ receiver area case. The path loss difference between the 70˚ bend and the straight waveguide is 30 dB, with the actual received power dropping from 66 μW for the straight waveguide to circa 60 nW for the 70˚ bend.

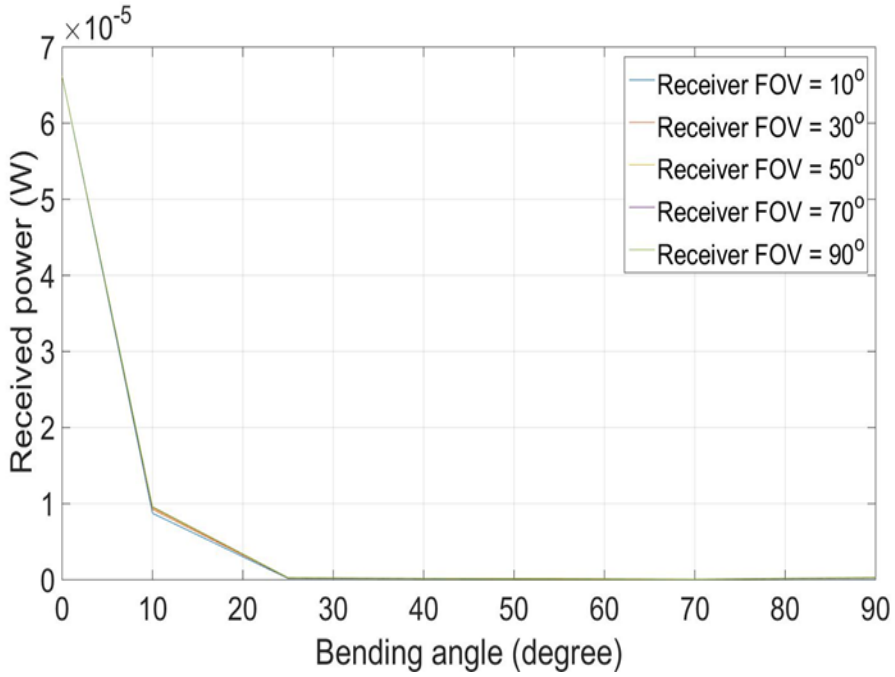

Figure 5-20 Received power versus bending angle for several values of receiver FOV in scattering environment with directive source

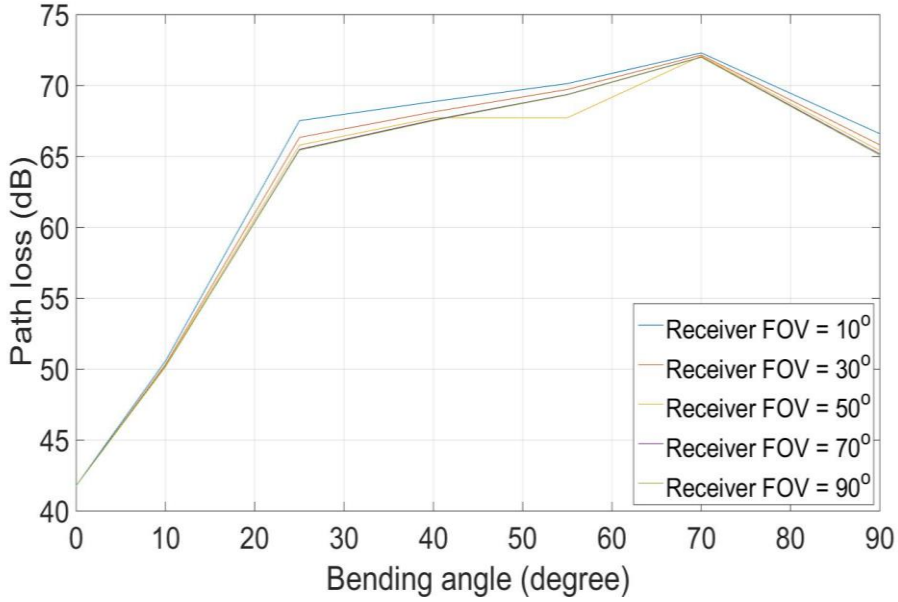

Figure 5-21 Path loss versus bending angle for several values of receiver FOV in scattering environment with directive source

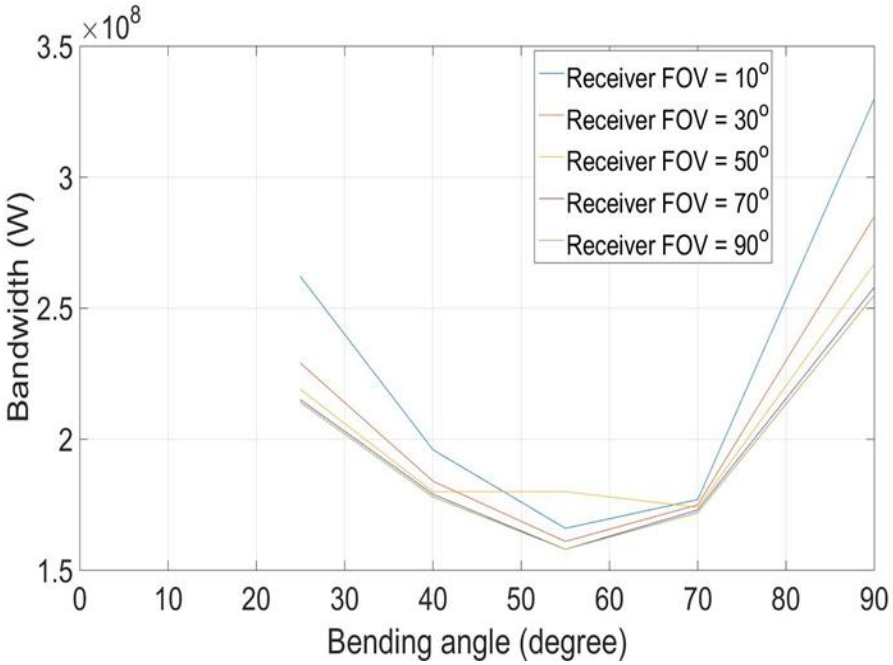

Figure 55-22 Bandwidth versus bending angle for several values of receiver FOV in scattering environment with directive source

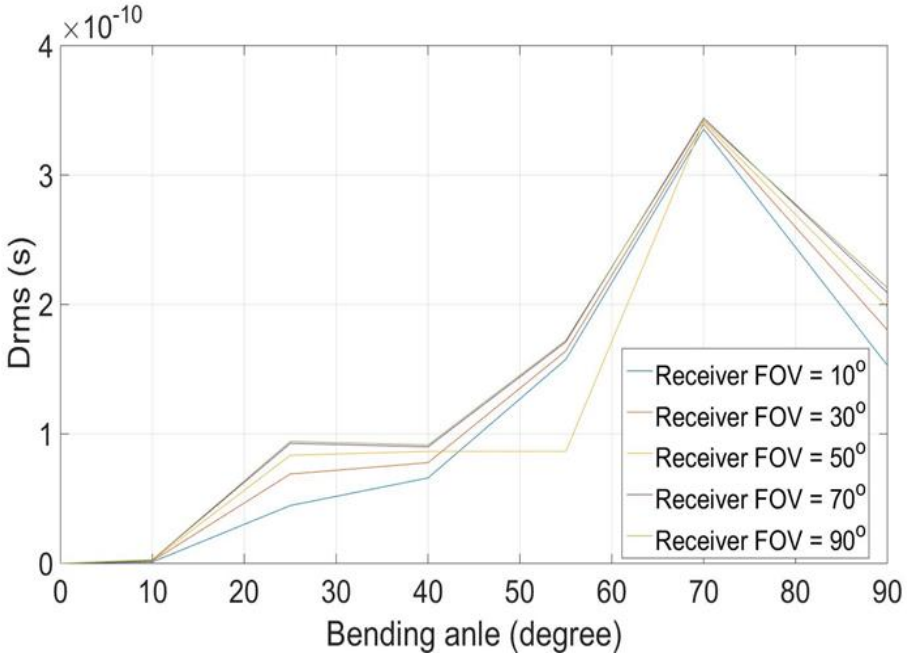

Figure 5-23 RMS delay spread versus bending angle for several values of receiver FOV in scattering environment with directive source

In general, in a scattered waveguide, it is advantageous to have a LOS link between the transmitter and receiver so that their relative position affects the performance, producing an increase of at least 10 dB in the path loss when the bend blocks the direct path. Using a directive transmitter has advantages in terms of received power, since the path loss of 65-85 dB observed when using a Lambertian decreases to 30-71 dB when using a directive source.

5.5. Reflective environment with Lambertian source

This case covers metal materials in general which form most of the vehicle chassis.

5.5.1. Receiver area effect

Figures 5-24 to 5-27 show the channel characteristics (received power, path loss, bandwidth and RMS delay spread) for a reflective environment where a Lambertian source is utilised and the receiver area is varied while the receiver FOV is set to 70˚.

The receiver area affects the received power as for 10 mm^2, the received power is 150 µW while it drops to 107 µW and 15 µW for 7 mm^2 and 1 mm^2 respectively. The power deviations for each receiver area case are: 92%, 91% and 91% for the 1mm^2, 7 mm^2 and 10 mm^2 cases respectively.

The receiver area does not affect the channel bandwidth, which varies from 200 MHz to 330 MHz with the bending angle regardless of the receiver area value.

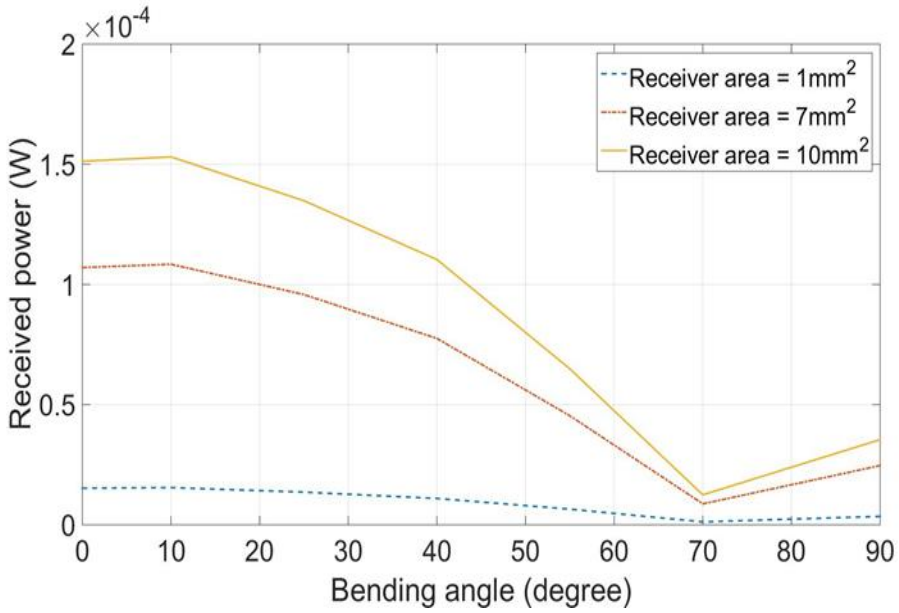

Figure 5-24 Received power versus bending angle for several values of receiver area in reflective environment with Lambertian source

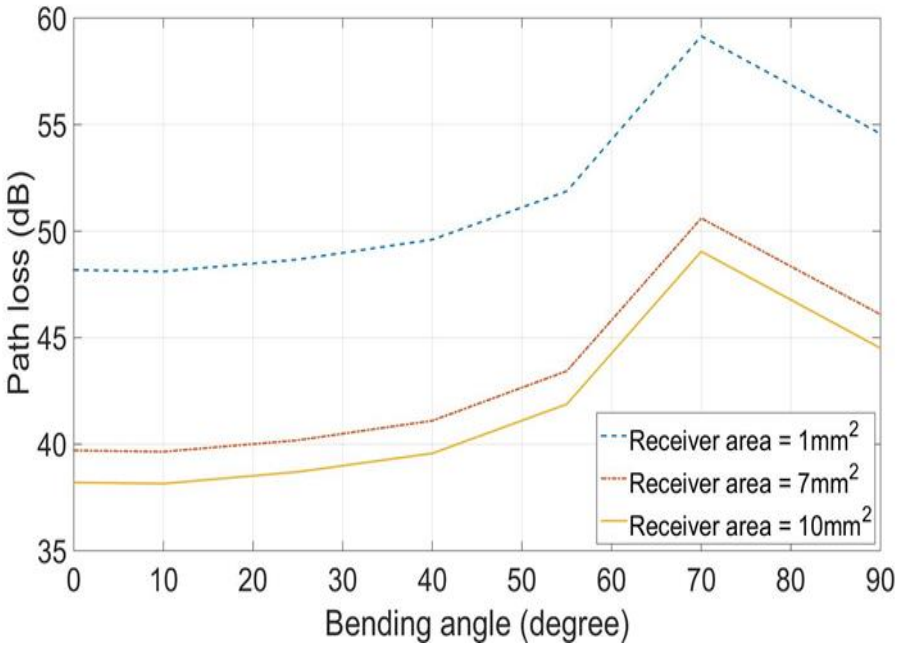

Figure 5-25 Path loss versus bending angle for several values of receiver area in reflective environment with Lambertian source

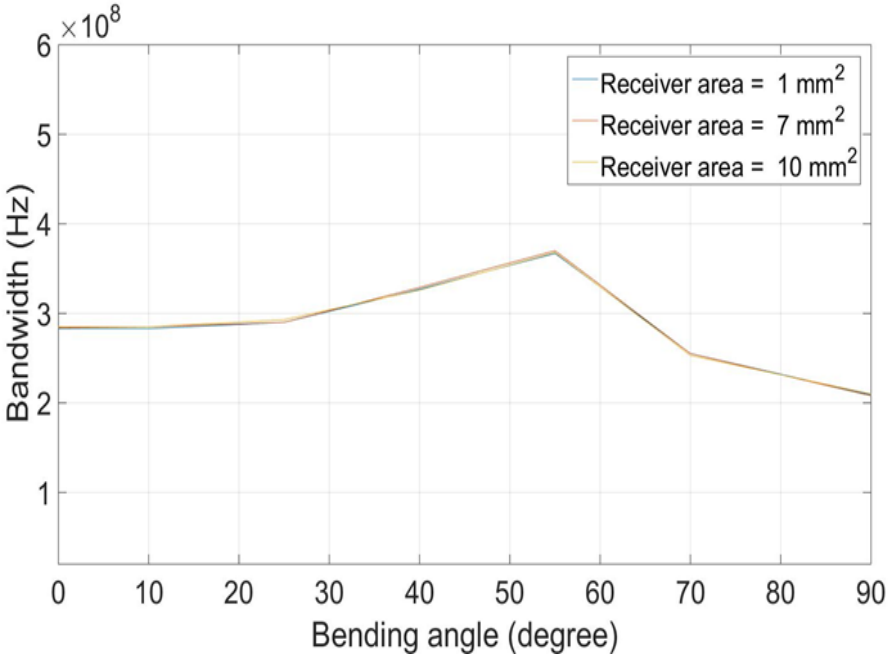

Figure 5-26 Bandwidth versus bending angle for several values of receiver area in reflective environment with Lambertian source

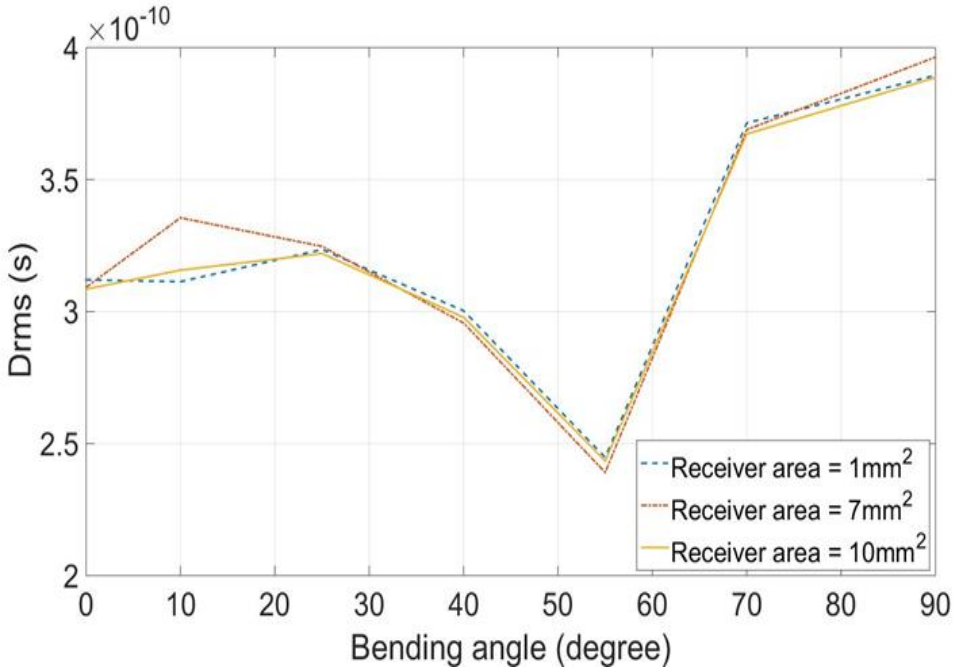

Figure 5-27 RMS delay spread versus bending angle for several values of receiver area in reflective environment with Lambertian source

5.5.2. Receiver FOV effect

Figures 5-28 to 5-31 illustrate the receiver FOV impact on the received power, path loss, bandwidth and RMS delay spread. In contrast to the previous cases, the receiver FOV affects all outputs.

The received power increases with receiver FOV where it is increased from 1.8 μW to 15 μW (87%) for straight waveguides for 10˚ and 90˚ receiver FOVs respectively, while for right angle waveguide, the received power increases from 76.6 nW to 3.67 μW.

However, for the 70˚ bend, the receiver FOV (except 10˚ FOV) does not affect the

received power which equals 1.1 μW (equivalent to a 59 dB path loss).

Regarding bandwidth, for small bending angles the receiver FOV affects the bandwidth value, whereas this influence diminishes as the bending angle increments.

Regarding RMS delay spread, for small receiver FOV values (10˚ and 30˚) the delay increases with the bending angle. While it tends to reduce for higher receiver FOV values with the bending angle until it reaches specific value where it changes the behavior and it starts to increase when bending value increases.

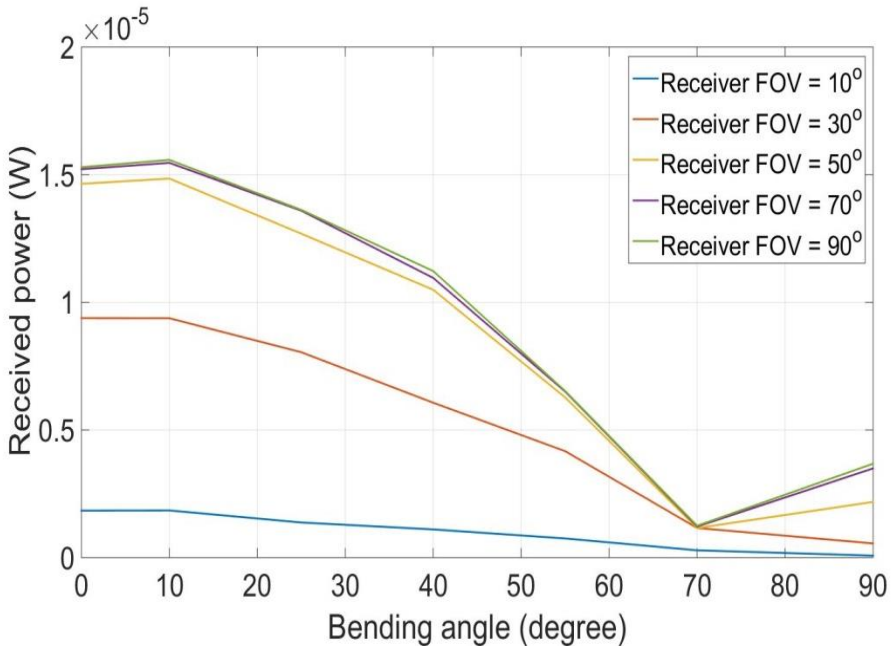

Figure 5-28 Received power versus bending angle for several values of receiver FOV in reflective environment with Lambertian source

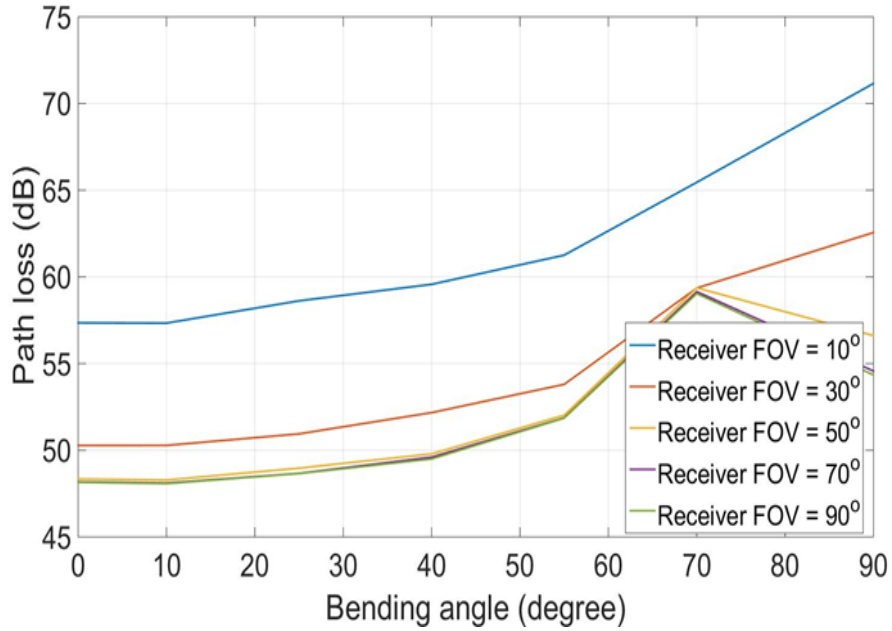

Figure 55-29 Path loss versus bending angle for several values of receiver FOV in reflective environment with Lambertian source

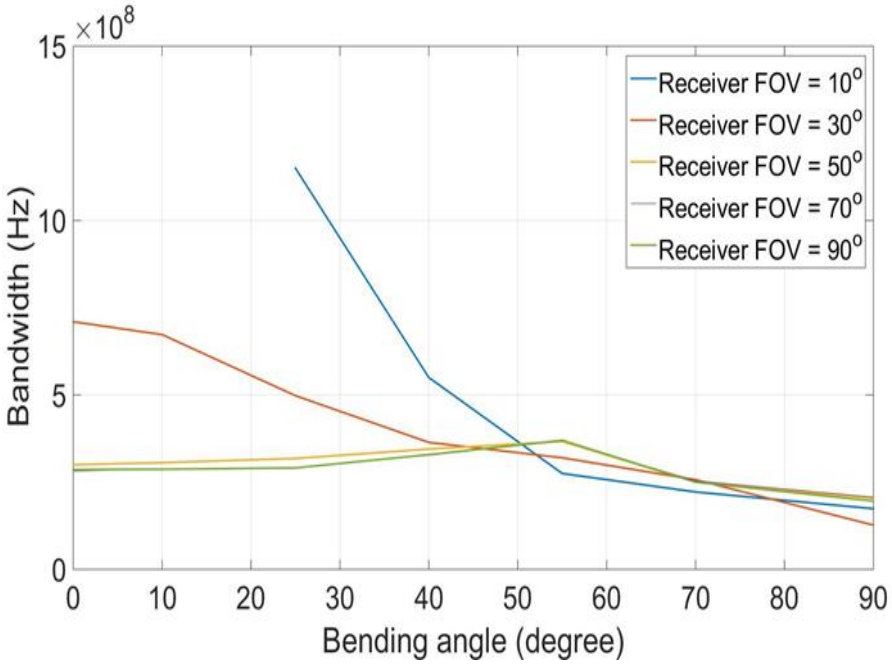

Figure 5-30 Bandwidth versus bending angle for several values of receiver FOV in reflective environment with Lambertian source

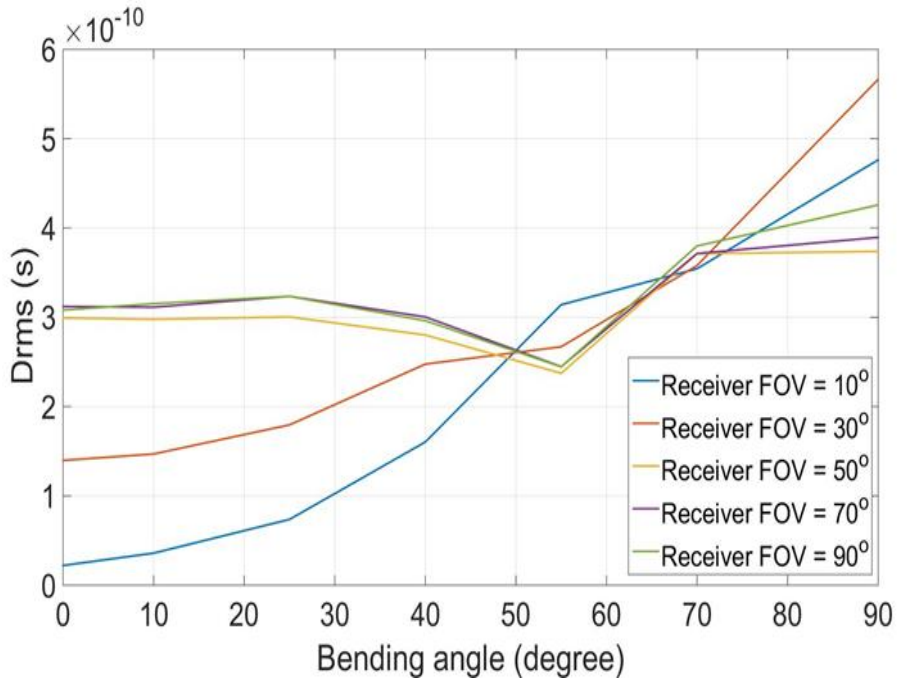

Figure 5-31 RMS delay spread versus bending angle for several values of receiver FOV in reflective environment with Lambertian source

5.6. Reflective environment with directive source

The last case represents the reflective environment whilst using directive source. The next subsections analyse the channel performance while the receiver parameters are changed. It is important to note that the bandwidth is high and was not found in most points due to sampling time limitation as explained earlier in this chapter; therefore it will not be plotted on figures for the points where it is found but rather in tables where possible.

5.6.1. Receiver area effect

Figures 5-32 to 5-34 demonstrate the received power, path loss and RMS delay spread

for the last case where the waveguides are made of reflective material and the source is directive.

The value of the receiver area affects the amount of the received light, where at its highest value (for a 25˚ bending angle), it decreases from 3.6 mW in the 10 mm^2 configuration to 0.35 mW in the 1 mm^2 configuration.

For the right angled waveguide, the received power varies from 0.24 μW (10 mm^2 receiver area) to 24.8 nW (1 mm^2 receiver area) which is still higher than in all previous cases.

Figure 5-33 displays the path loss and it can be seen that a bending angle of 25˚ can result in better performance since part of the light may reach the exit in contrast to a slightly or sharply bent waveguide.

The bandwidth is found only for the 50˚ bending angle, and it is the same over the three values of receiver area. The medium can serve up to 1.5 GHz signals.

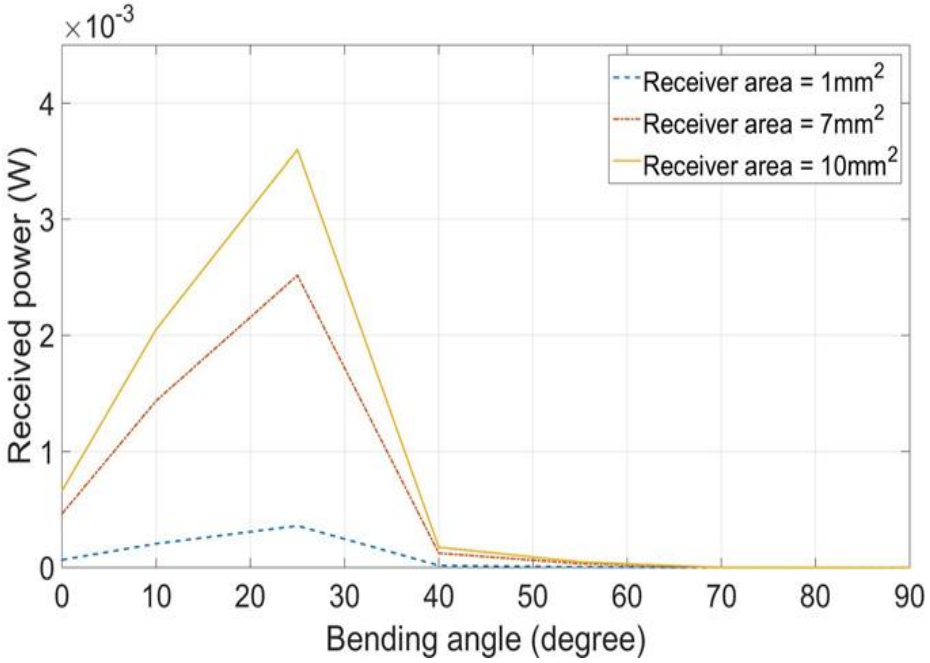

Figure 5-32 Received power versus bending angle for several values of receiver area in reflective environment with directive source

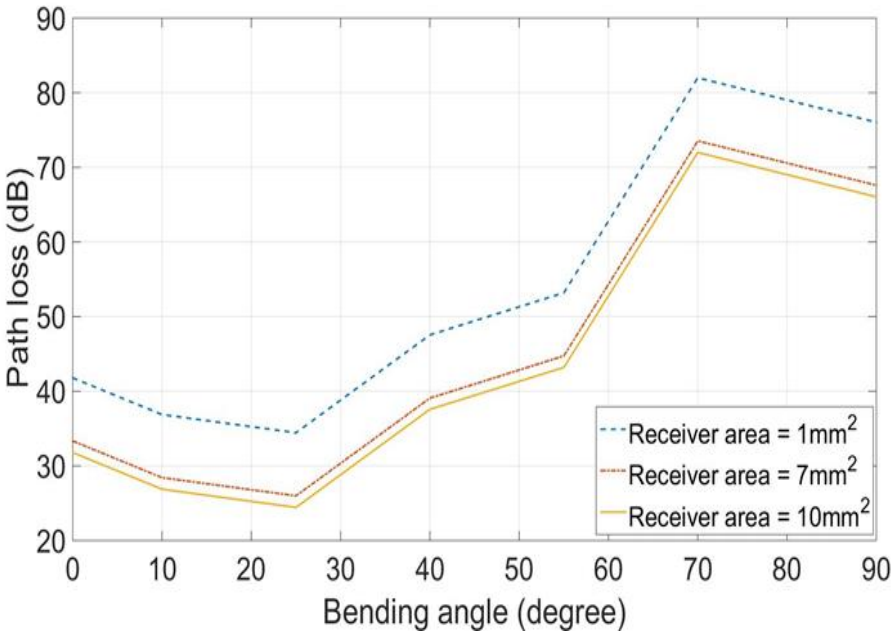

Figure 5-33 Path loss versus bending angle for several values of receiver area in reflective environment with directive source

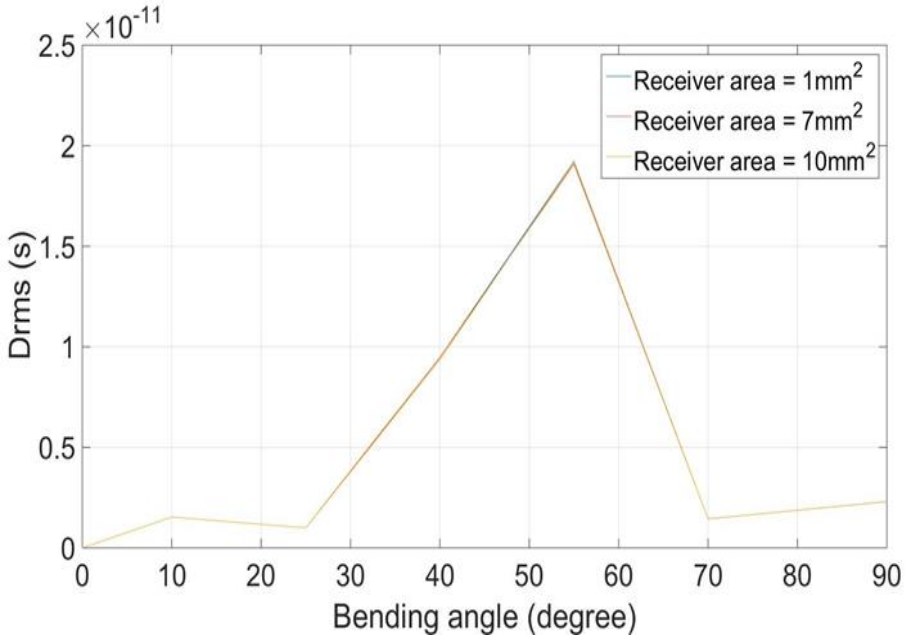

Figure 5-34 RMS delay spread versus bending angle for several values of receiver area in reflective environment with directive source

5.6.2. Receiver FOV effect

The effects of FOV are presented in Figures 5-35 to 5-37. From Figure 5-35, it is shown that the received power does not change with FOV for the situations where LOS link exists (straight and 10˚ bending angle). While for larger bending angles, the received power depends on receiver FOV for a small value (10˚ FOV), whereas the path loss (Figure 5-36) increased substantially (33 dB) while it is decreases for higher receiver FOV (2dB).

For the right angled waveguide, the received power does not change for different receiver FOVs, with the received power remaining at 24 nW, a 76 dB path loss.

The bandwidth was found for only a limited number of cases, shown in Table 5-4. for

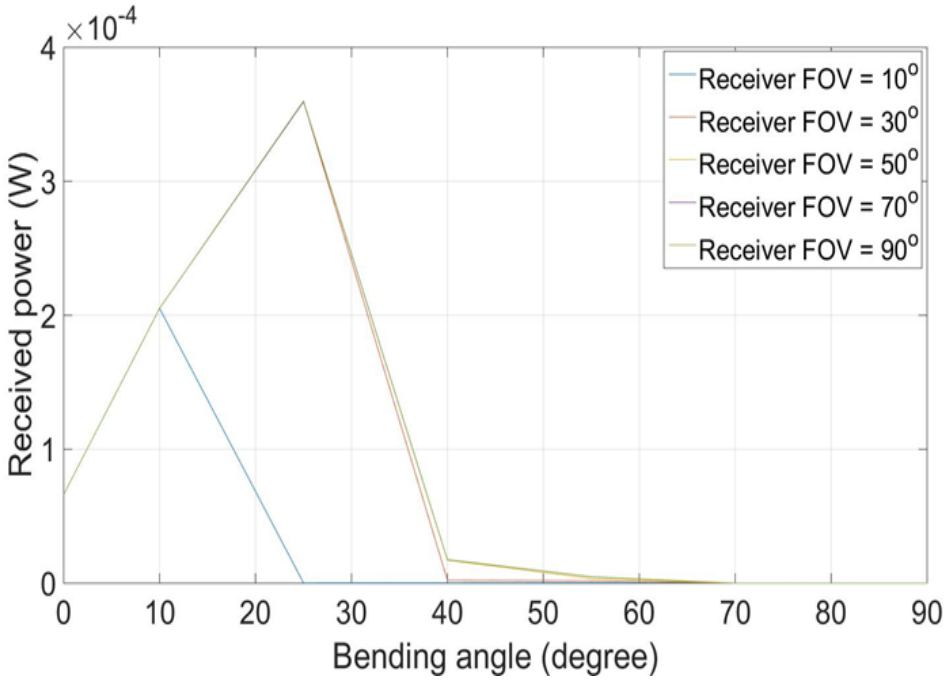

Figure 5-35 Received power versus bending angle for several values of receiver FOV in reflective environment with directive source

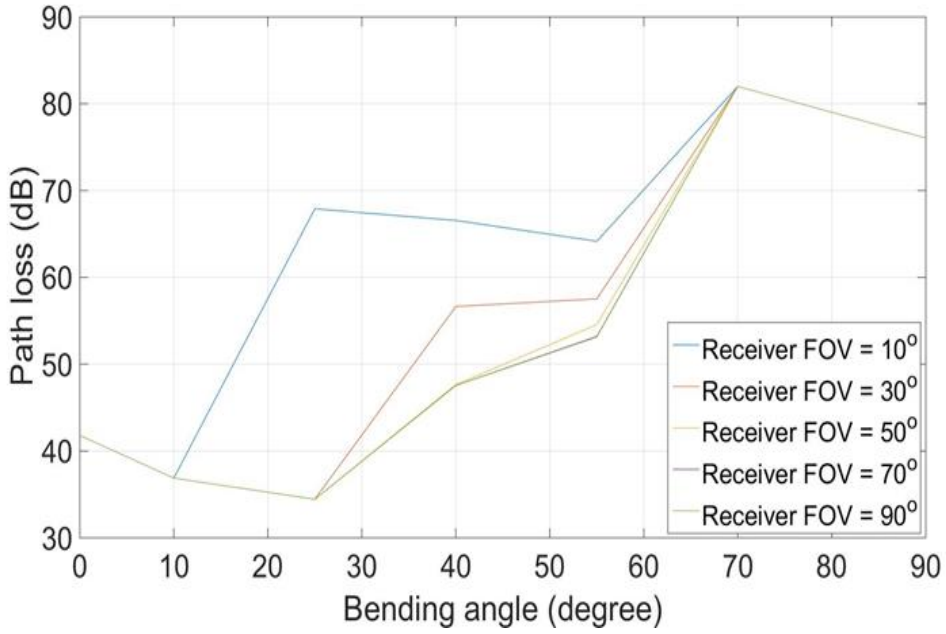

Figure 5-36 Path loss versus bending angle for several values of receiver FOV in reflective environment with directive source

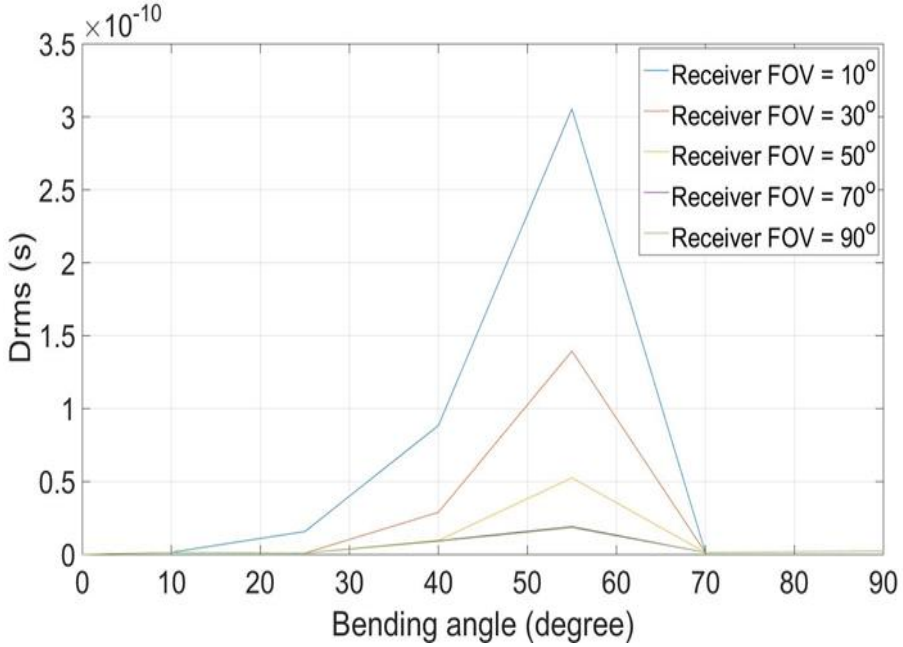

Figure 5-37 RMS delay spread versus bending angle for several values of receiver FOV in reflective environment/directive source

Table 5-4 Bandwidth for bending angle for several values of receiver FOV in reflective environment with directive source

Bending angle / Receiver FOV	0˚	10 ˚	25 ˚	40 ˚	55 ˚	70 ˚	90 ˚
10 ˚	-	5.3 GHz	1.24 GHz	450 MHz	-	-	-
30 ˚	-	-	3.2 GHz	590 MHz	-	-	-
50 ˚	-	-	-	1.07 GHz	-	-	-
70 ˚	-	-	-	1.52 GHz	-	-	-
90 ˚	-	-	-	1.55 GHz	-	-	-

5.7. Conclusions

This chapter has presented the results of the simulations conducted, and accompanying them is the analysis for a variety of communication situations in waveguides. A relatively high number of reflections have been considered (10-15 reflections) because of LOS absence in most of the cases, which leads to the high power being reflected to the receiver. For example, for right angle waveguide, the first five reflections carry only 70% of the total received power. There are four different cases in this situation, namely, scattering material with Lambertian transmitter, scattering material with directive transmitter, reflective material with Lambertian transmitter, and reflective material with directive transmitter. The chapter deals with the aspects of: power received, path loss, delay spread and channel bandwidth in all the aforementioned cases. For scattering material, whether Lambertian or directive source is used, the path loss for each case follows one pattern regardless the value of the receiver FOV and receiver area,

but all cases agree that 70˚ bending angle attenuates the transmitted signal. The bandwidth for a reflective material with Lambertian source does not change with the receiver area, and it has the highest value at 55˚ bending angle. Using directive source with reflective material leads to different behaviour, where light does not travel randomly and it is controlled by the level of transmitter directivity and the material reflective intensity pattern. Figure 5-32 shows that slightly bent waveguide allows for better reception, where the system benefits from the LOS link and the reflections which carry some of the transmitter power. However, it will be at the cost of a reduced bandwidth where the signal takes longer time to reach the receiver.

Chapter 6: Simulating Various Scenarios for Waveguide Optical Wireless Communication II (Coupling Waveguides)

6.1. Introduction

In Chapter 5, an in-depth study regarding straight and bent waveguides, which are very common structure in vehicle frames, has been presented. This introduced the received power, path loss, bandwidth and RMS delay spread for various framework setups and diverse receiver characteristics. In this chapter, coupling between two waveguides of different dimensions is investigated.

The channel performance will be surveyed for two sorts of environment and two types of transmitter. The impact of transmitter direction on received power and bandwidth will be explored.

6.2. Simulation variables

6.2.1. Waveguide parameters

The study concerns the coupling between two square cross section waveguides of dimensions $(a \times a \times L)$ cm and $(b \times b \times L)$ cm, where $a = 2b$. Both waveguides and coupling are assumed to follow either the Lambert model (plastic) or the Phong model (Aluminium) as explained in Chapter 5 section 5.2.1, material parameters are recorded in Table 5.1 and radiation patterns are illustrated in Figure 5-1.

The coupling is specified by the dimensions a and b, and the angle made by the tilted faces of the coupling with the optical axis. The waveguides measurements and rundown of coupling angles are displayed in Table 6-1. The transmitter is situated at the centre of the entrance of the larger tube as illustrated in Figure 6-1.

Table 6-1 Waveguide dimensions and coupling agles

1st waveguide dimensions	50 x 50 x 60 (cm)
2nd waveguide dimensions	25 x 25 x 60 (cm)
Coupling angle	{0˚ (no coupler),5˚, 10˚,30˚, 50˚, 70˚, 80˚}

Putting the transmitter directing upwards creates a LOS link for different configurations with various coupling angles, and different receiver characteristics, This makes receiving a strong signal very likely for any receiver FOV and any receiver area. Therefore, in this chapter, the transmitter direction effect will be contemplated, and the channel characteristics will be determined for different transmitter angles through different coupling angles.

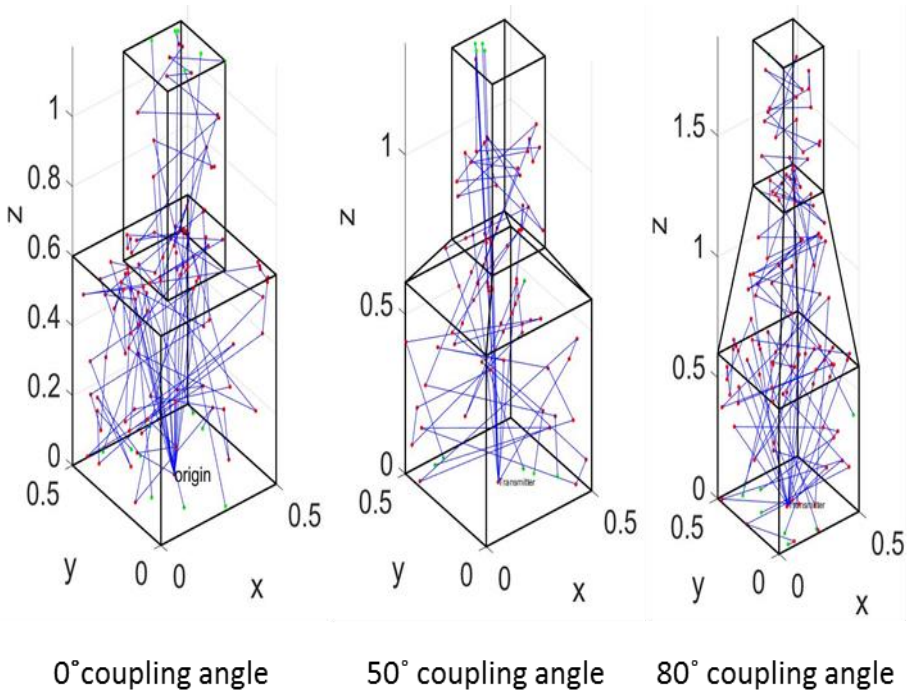

Figure 6-1 System configurations (a) 0˚coupling angle (b) 50˚ coupling angle (c) 80˚ coupling angle

6.2.2. Source parameters

Both pure Lambertian LEDs and directive LEDs are being utilized as a part of the study. The radiation pattern for both sources is that presented previously in Figure 5-3. The transmitter is located in the centre of the waveguide entrance with transmitted power P_T=1W. The simulation results are found for a set of transmitter directions. The transmitter direction is changed in the *x,z* plane only with different qualities as plotted in Figure 6-2. The list of transmitter direction angles in shown in Table 6-2.

Table 6-2 List of transmitter direction angles

Transmitter direction angle	{5˚, 20˚,40˚,60˚, 80˚, 90˚}

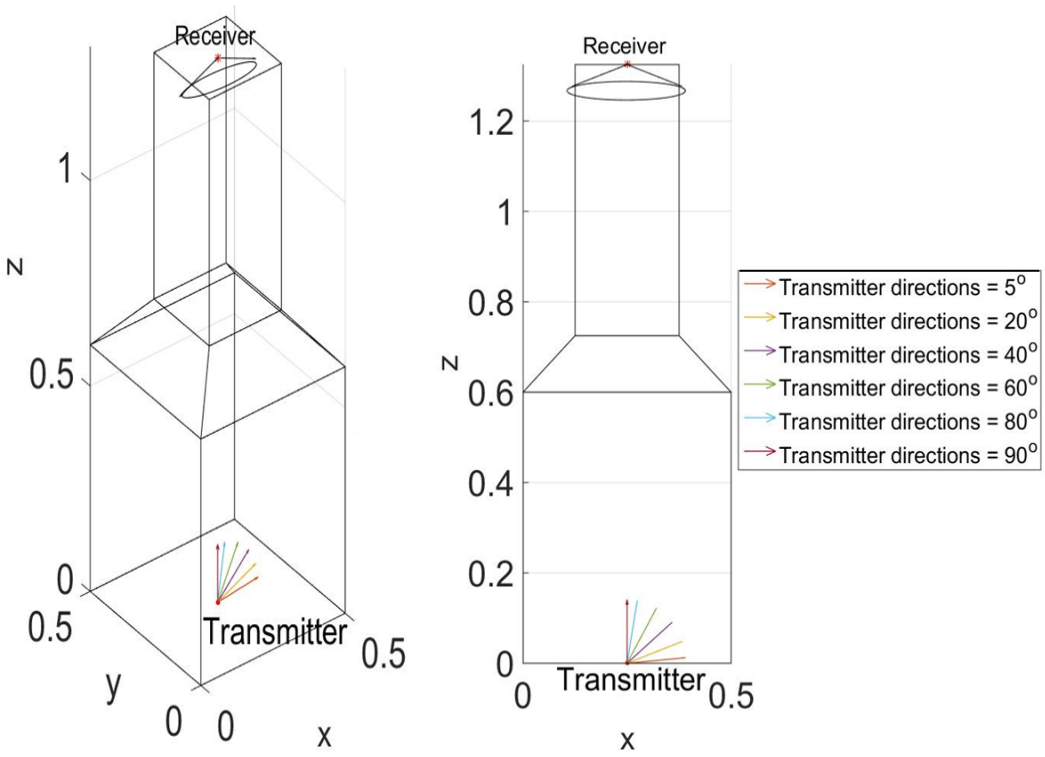

Figure 6-2 3D and 2D representation for transmitter direction

6.2.3. Receiver parameters

The receiver element is situated in the centre of the waveguide exit unless otherwise stated, and it is directed downwards. The receiver FOV is chosen to be 70˚ and its area is 1 mm^2. The rest of the simulation variables are listed in Table 6-3.

Table 6-3 List of simulation variables

Number of transmitted rays	10^6
Time resolution	2 ps
Number of reflections	15

The summary of the configurations simulated is shown in Figure 6-3

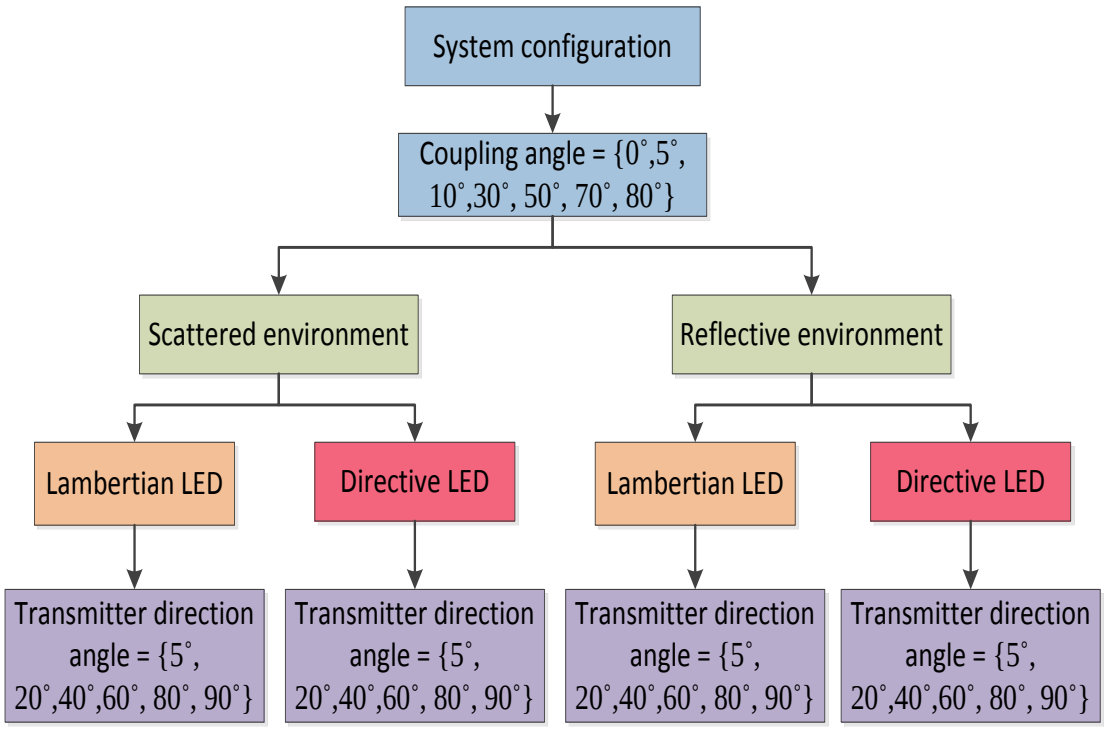

Figure 6-3 Configurations simulated

6.3. LOS effect over the configurations

A LOS link improves the channel performance in terms of received power and bandwidth. The system configurations will be classified according to the OWC link configurations which were explained in Chapter 2, Section 2.3.1.

Because the receiver FOV is wide, the configurations are either hybrid or non-directed, depending on the transmitter type and direction. The coupling angle will affect the distance between the transmitter and receiver, and will therefore affect the value of the LOS received power not the type of the configuration. Table 6-4 shows the system configuration for the Lambertian transmitter and Table 6-5 shows the system configuration for the directive source.

Table 6-4 System configuration type and LOS received power for Lambertian transmitter

Transmitter direction	System configuration	LOS received power in nW (min and max values depending on coupling angle)	
5˚	Non-directed LOS	7.6 nW	18.9 nW
20˚	Non-directed LOS	30 nW	76 nW
40˚	Non-directed LOS	56 nW	142 nW
60˚	Non-directed LOS	76 nW	191 nW
80˚	Non-directed LOS	86 nW	218 nW
90˚	Non-directed LOS	87 nW	221 nW

Table 66-5 System configuration type and LOS received power for directive transmitter

Transmitter direction	System configuration	LOS received power (min and max values depending on coupling angle)	
5˚	Diffuse (Non-directed NLOS)	0	0
20˚	Diffuse (Non-directed NLOS)	0	0
40˚	Diffuse (Non-directed NLOS)	0	0
60˚	Diffuse (Non-directed NLOS)	0	0
80˚	Hybrid LOS	9.7 nW	24 nW
90˚	Hybrid LOS	22 μW	56 μW
		(no reflections in this system)	

6.4. Simulation results: Scattering environment with Lambertian source

Figures 6-4 to 6-7 demonstrate the OWC channel characteristics (received power, path loss, bandwidth and RMS delay spread) versus coupling angles for different transmitter

directions. As expected the best signal is received when the transmitter is directed upwards towards receiver with strong LOS link regardless of coupling angle value. The maximum received power is 0.3 μW for 90˚ transmitter direction with 0˚ coupling angle. For small transmitter direction angles (the transmitter is almost parallel to the entrance plane), it is noted that the received power is almost constant (37.2 nW) except for an 80˚ coupling angle where it drops to 18.4 nW.

The received power for different transmitter directions follows the same pattern through the coupling angle values; the maximum value occurs where the two waveguides are connected directly without coupler (coupling angle = 0˚), then when the coupler exists, the received power starts to decrease and the path loss increases.

Figure 6-6 shows the bandwidth versus coupling angle relationship for different transmitter direction angles. For long couplers the bandwidth could not be defined due to time resolution restrictions as explained in Chapter 5. However, the minimum bandwidth that can be reached is 100 MHz for a 5˚ transmitter direction.

RMS delay spread is related to maximum bit rate that can be transmitted through a channel without introducing ISI and without using an equalizer at the receiver by the equation [117]:

$$R_b = \frac{1}{10D_{rms}}$$

Thus, since for a 5˚ transmitter direction and a 60˚ coupling angle, D_{rms} equals 56.2 ps

this can support a bit rate of 1.7 Gbps.

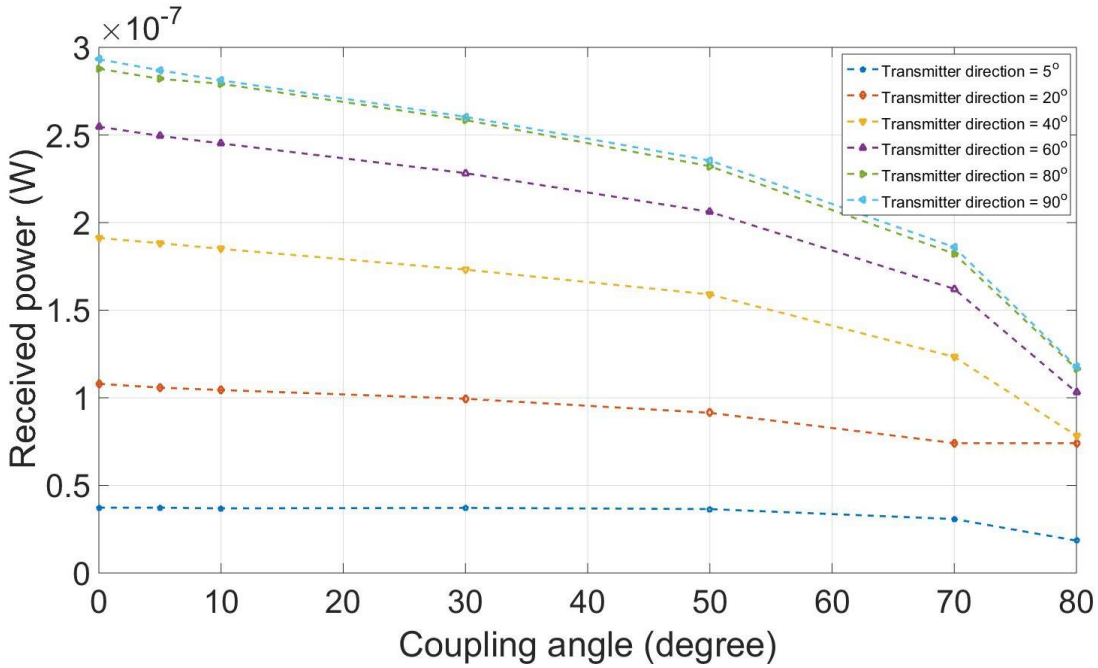

Figure 6-4 Received power versus coupling angle for several values of transmitter direction in scattering environment with Lambertian source

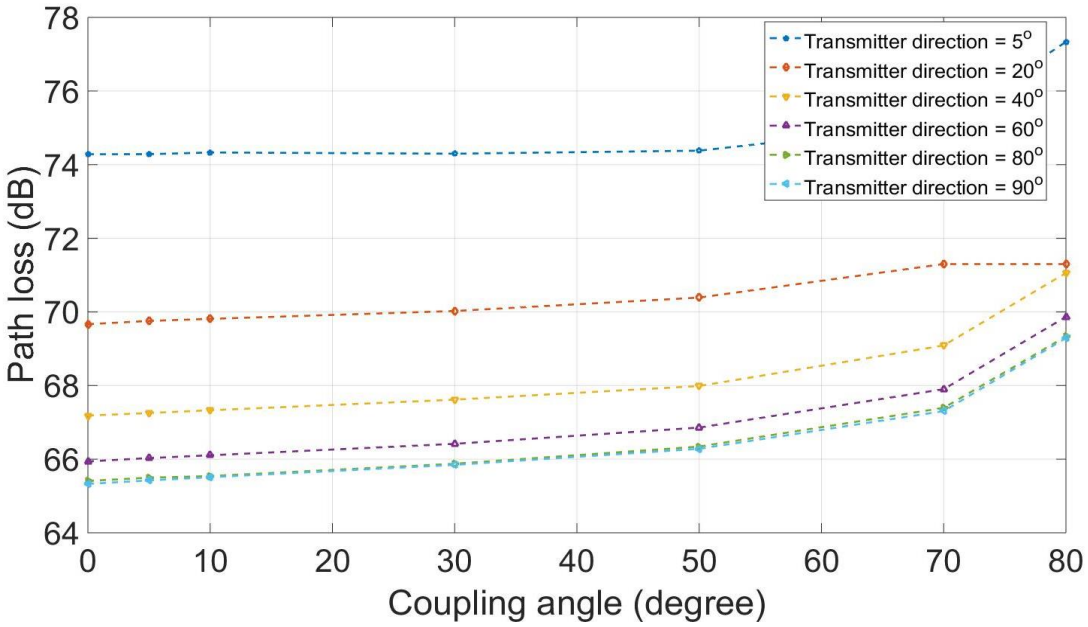

Figure 6-5 Path loss versus coupling angle for several values of transmitter direction in scattering environment with Lambertian source

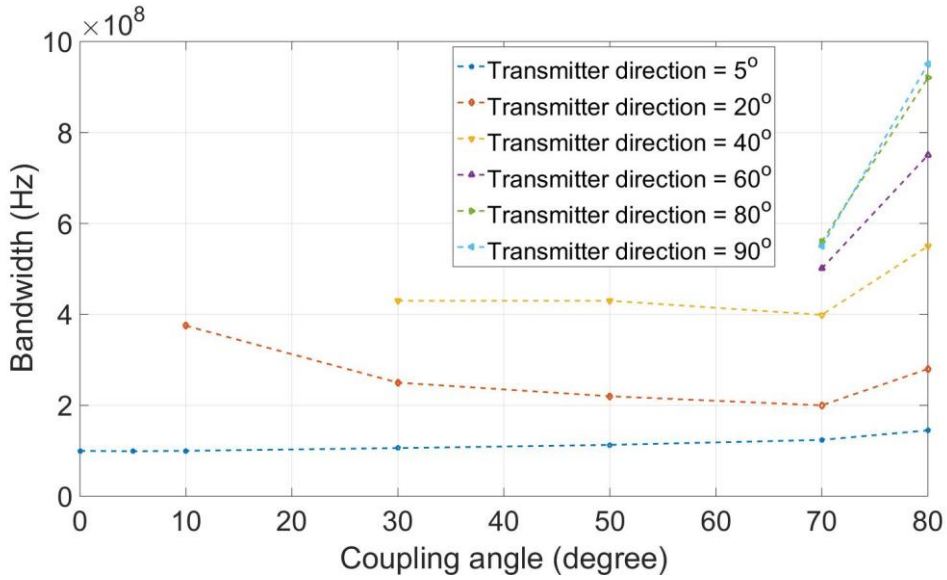

Figure 6-6 Bandwidth versus coupling angle for several values of transmitter direction in scattering environment with Lambertian source

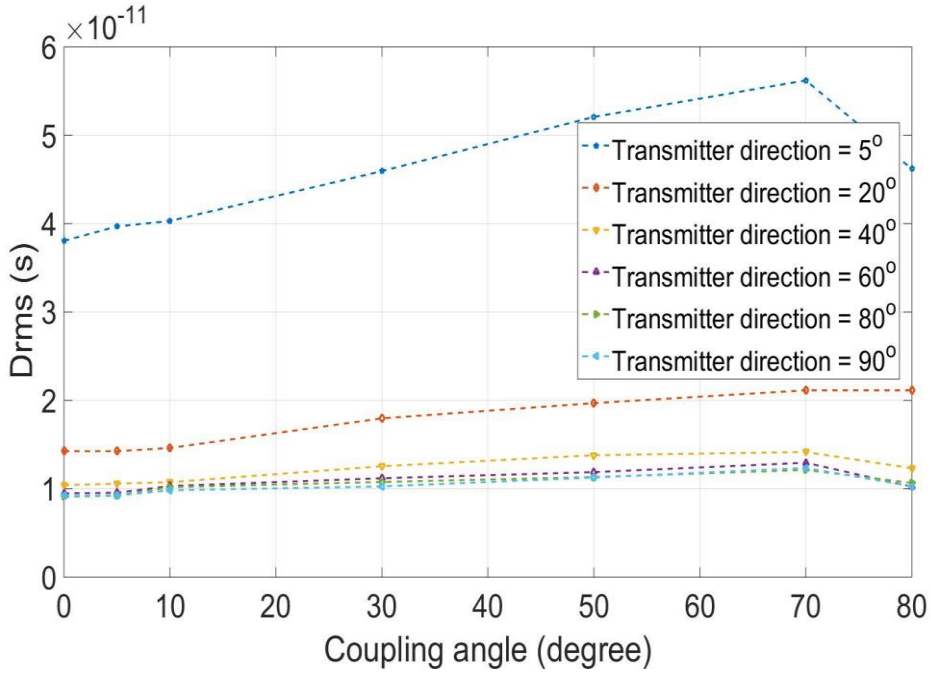

Figure 6-7 RMS delay spread versus coupling angle for several values of transmitter direction in scattering environment with Lambertian source

6.5. Simulation results: Lambertian material with directive source

Figures 6-8 to 6-11 show the channel characteristics for a scattering material while using a directive source. The performance of the hybrid LOS system (transmitter direction = 90˚) is distinguished where the received power ranges from 56 μW to 22.1 μW for short couplers and long couplers respectively. The path loss increases by at least 20 dB when the LOS link is not perfect as shown in Figure 6-9, while for the rest of the couplers the path loss ranges between 62 dB and 78 dB which is equivalent to 0.61 μW and 13.5 nW of received power respectively. The effect of transmitter direction becomes less for angles less than 60˚.

As for bandwidth, it ranges between 95 MHz and 144 MHz in general. For a 90˚ transmitter direction the bandwidth is not defined due to the time resolution limitation. For the other hybrid LOS configuration (80˚ transmitter direction angle) the bandwidth value drops after a 30˚ coupling angle.

RMS delay spread is small for non-directed LOS links which allows for high data rate signals transmission. For non-directed NLOS configurations the RMS delay spread increases significantly. Notwithstanding, the coupler assumes an essential part that every transmitter direction has a particular coupling angle where the RMS delay spread is greatly reduced. This means that for specific combinations of transmitter direction and coupling angle the light travels smoothly and rapidly to the receiver.

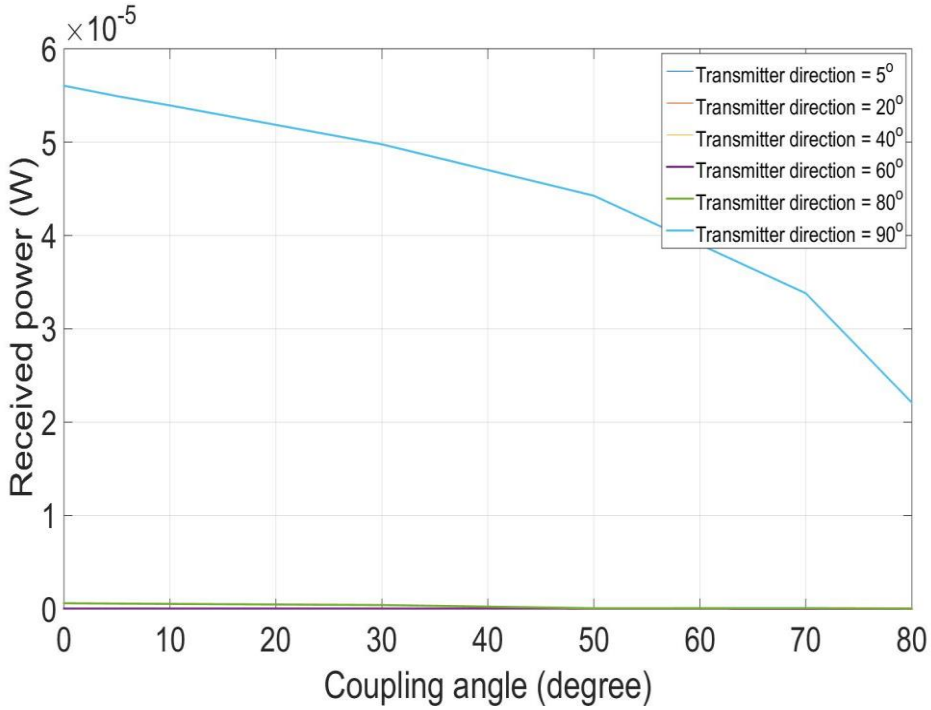

Figure 6-8 Received power versus coupling angle for several values of transmitter direction in scattering environment with directive source

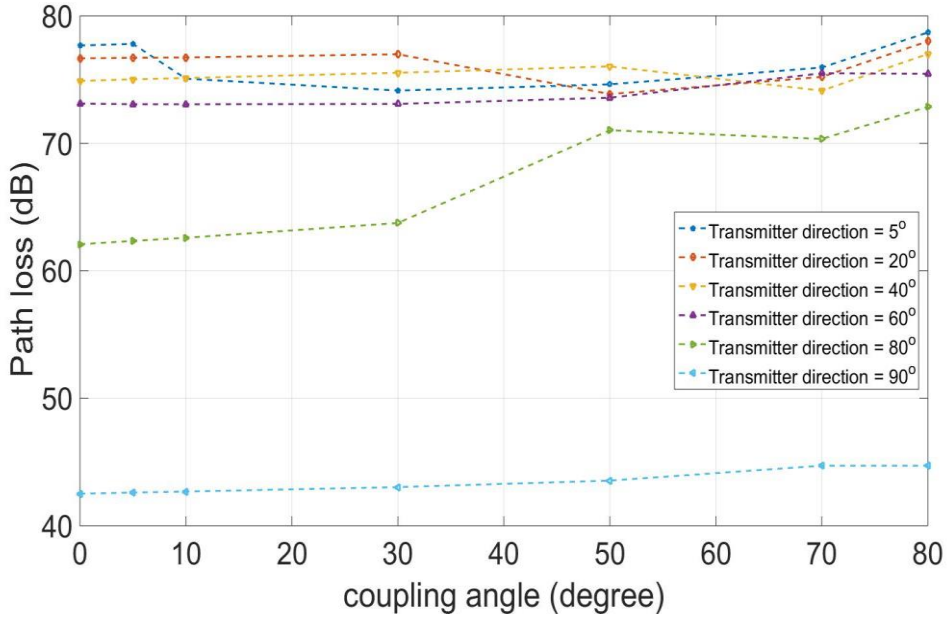

Figure 6-9 Path loss versus coupling angle for several values of transmitter direction in scattering environment with directive source

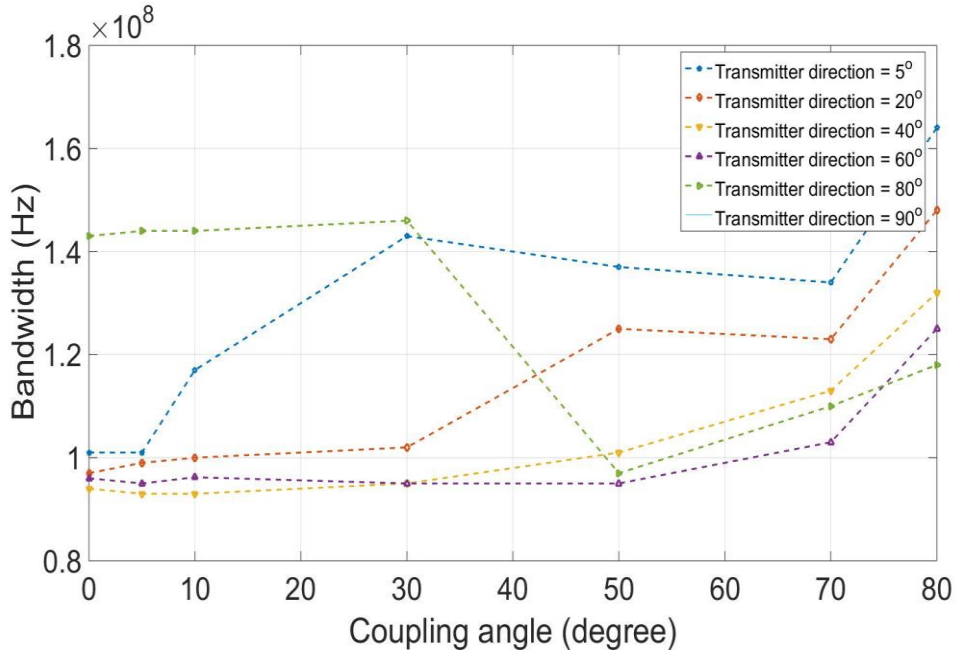

Figure 6-10 Bandwidth versus coupling angle for several values of transmitter direction in scattering environment with directive source

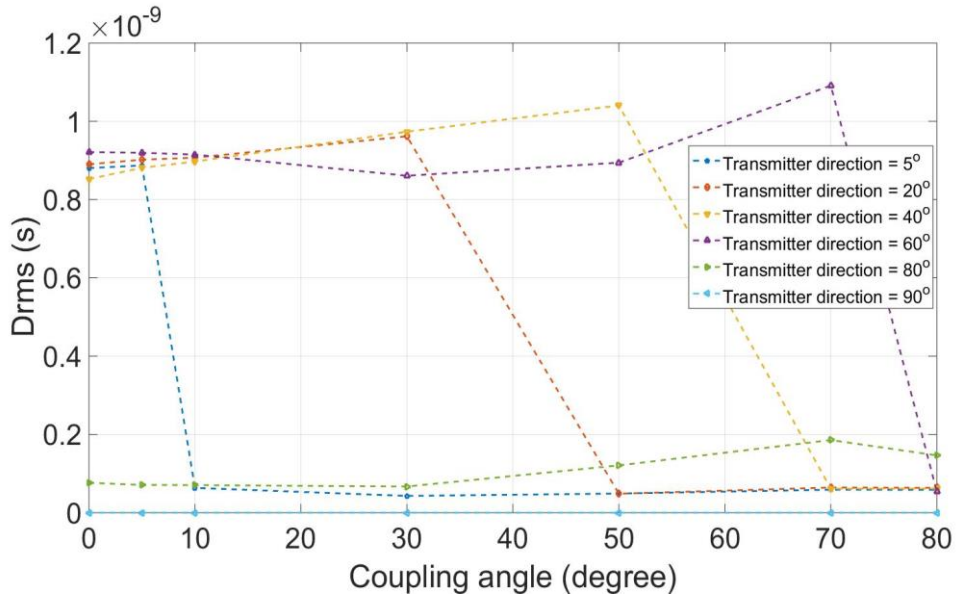

Figure 6-11 RMS delay spread versus coupling angle for several values of transmitter direction in scattering environment with directive source

6.6. Simulation results: Phong material with Lambertian source

The outcomes appearing in Figures 6-12 to 6-15 demonstrate the received power, path loss, bandwidth and RMS delay spread for an environment which contains reflective material but where the source is omnidirectional.

The LOS link performs well where 1.6 μW is received when no coupler is used while just 1 μW is received in a long coupler for a transmitter direction angle of 90˚. As can be seen in Figure 6-12, the relationship between the received power and coupling angle follows almost the same pattern as in the first case (Lambertian material with Lambertian source) with distinction in power gain value.

However, the bandwidth and RMS delay spread behaviour is totally different as shown in Figures 6-14 and 6-15. A 70˚ coupling angle allows for the best performance in terms of bandwidth, regardless the transmitter direction value. It offers at least 140 MHz of bandwidth.

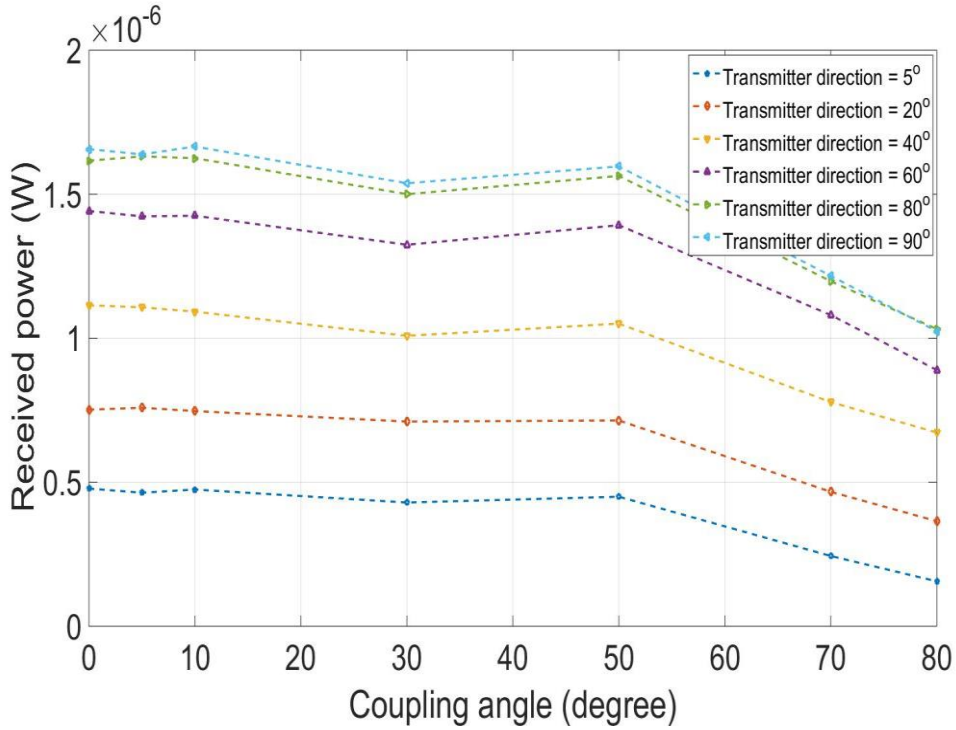

Figure 6-12 Received power versus coupling angle for several values of transmitter direction in reflective environment with Lambertian source

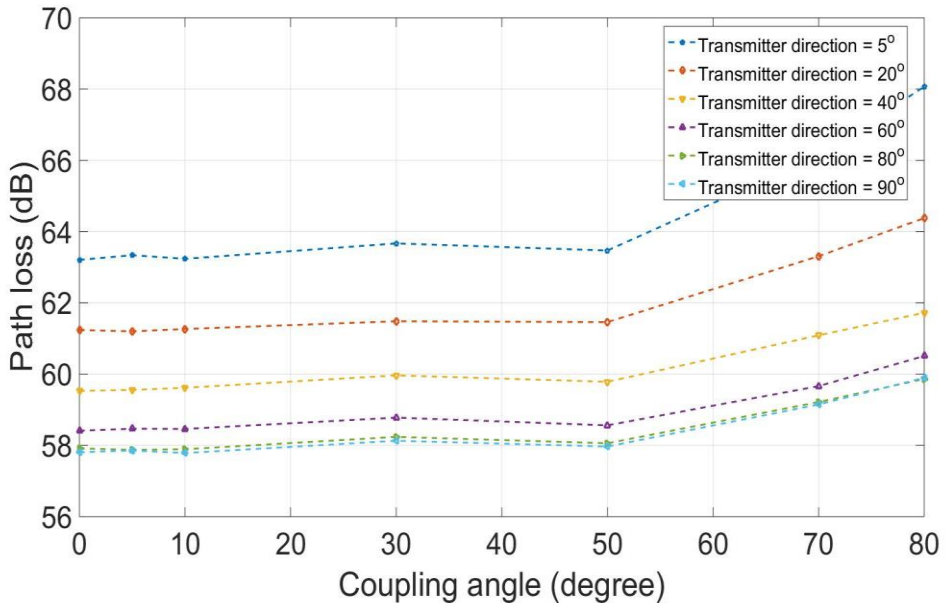

Figure 6-13 Path loss versus coupling angle for several values of transmitter direction in reflective environment with Lambertian source

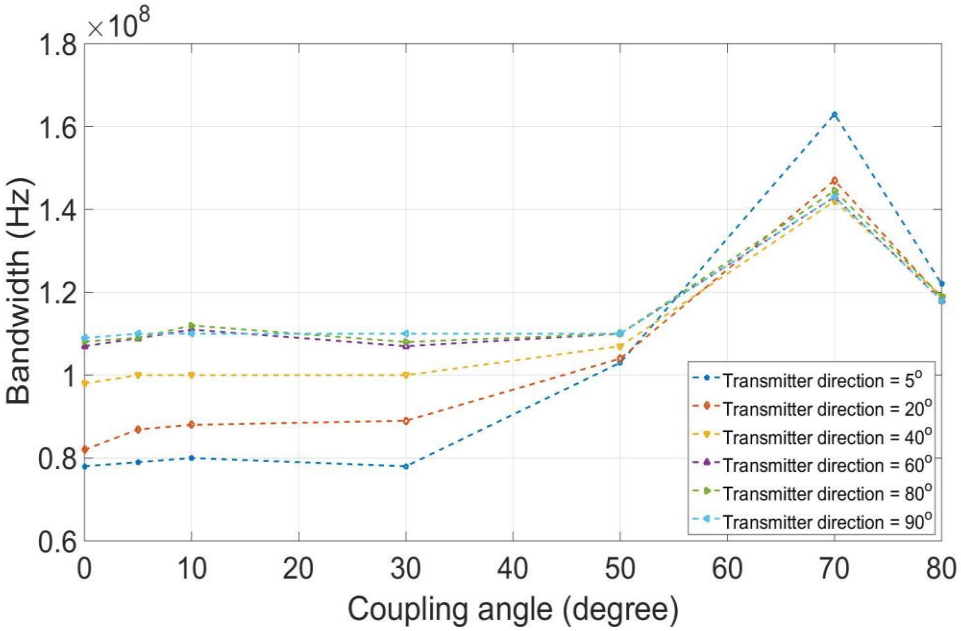

Figure 6-14 Bandwidth versus coupling angle for several values of transmitter direction in reflective environment with Lambertian source

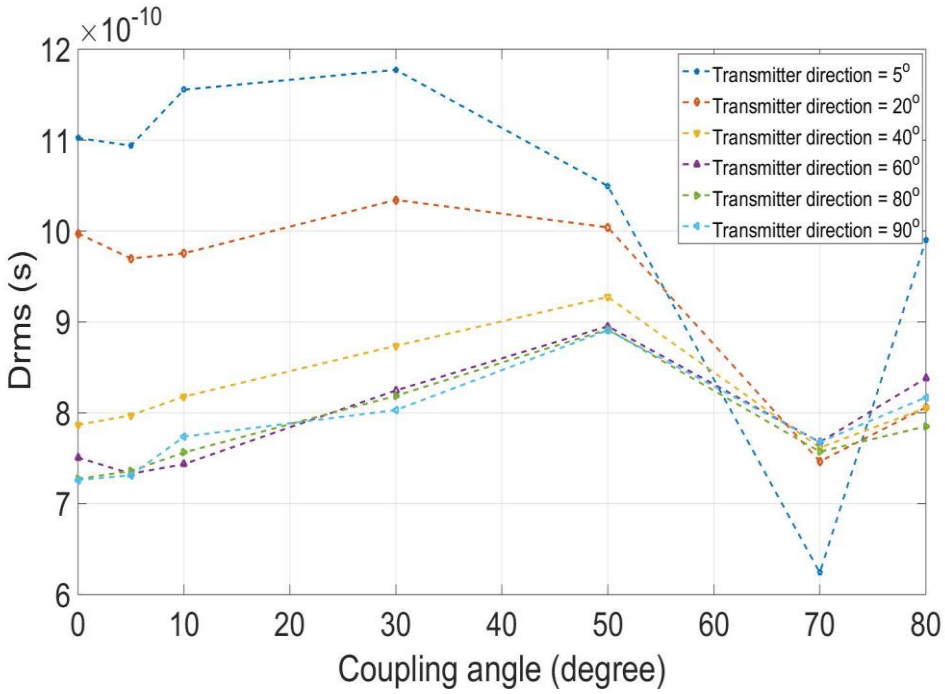

Figure 6-15 RMS delay spread versus coupling angle for several values of transmitter direction in reflective environment with Lambertian source

6.7. Simulation results: Phong model with directive source

Figures 6-16 to 6-18 show the results for an environment which contains reflective material but where the source is directional. This case is the most critical as both the material and the source are directive so the random movement of the rays is less.

As is illustrated in Figure 6-16 there is no power received for short couplers (0˚, 5˚) when the transmitter direction equals 5˚, 40˚ and 60˚, because of the high reflectivity of the material. The light is reflected back in the first waveguide and does not pass the coupler to the second waveguide. However, for transmitter direction angle of 60˚ the received power changes significantly with the coupling angle. The highest received power is at 30˚ coupling angle (0.21 mW) while it drops to 0.38 μW when the coupling angle is 70˚. A particularly clear representation of the amount of received power is illustrated in Figure 6-17 where the path loss (dB) is plotted against coupling angle for different values of transmitter direction. The path loss fluctuates with no smooth pattern as the light follows the directive radiation pattern for both waveguide material and transmitter.

The bandwidth was found for just a set number of cases, appearing in Table 6-6.

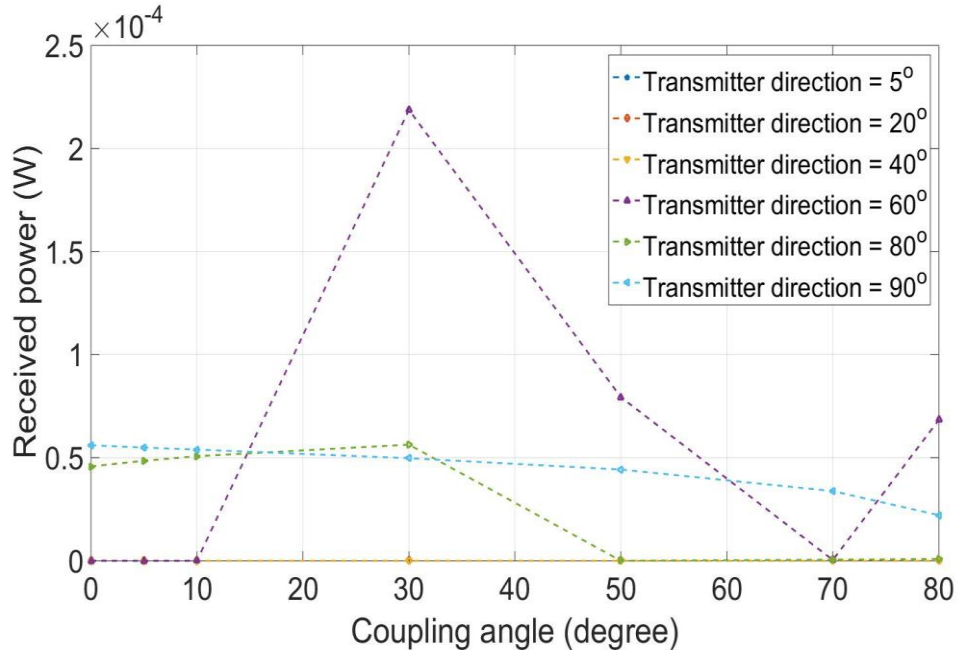

Figure 6-16 Received power versus coupling angle for several values of transmitter direction in reflective environment with directive source

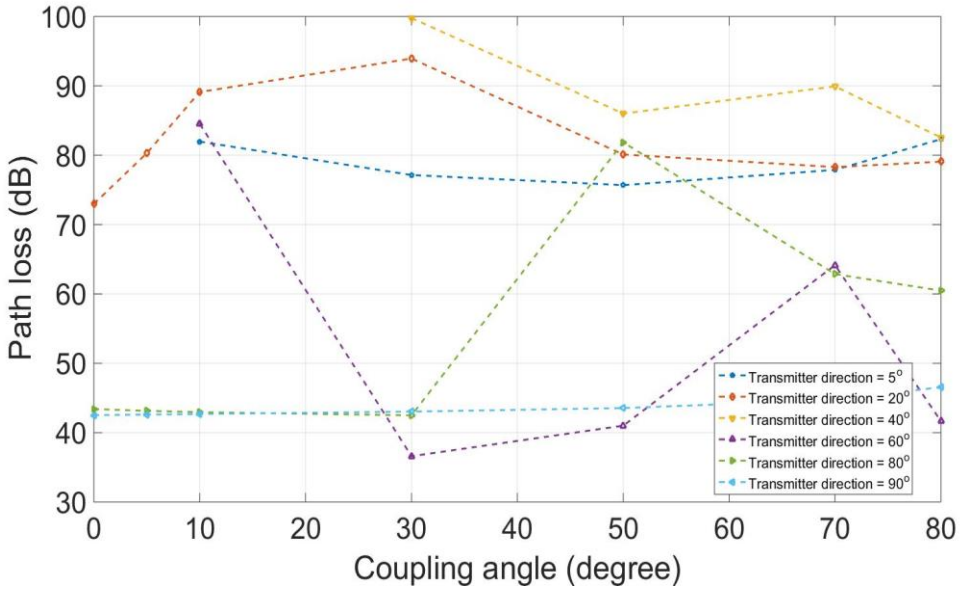

Figure 6-17 Path loss versus coupling angle for several values of transmitter direction in reflective environment with directive source

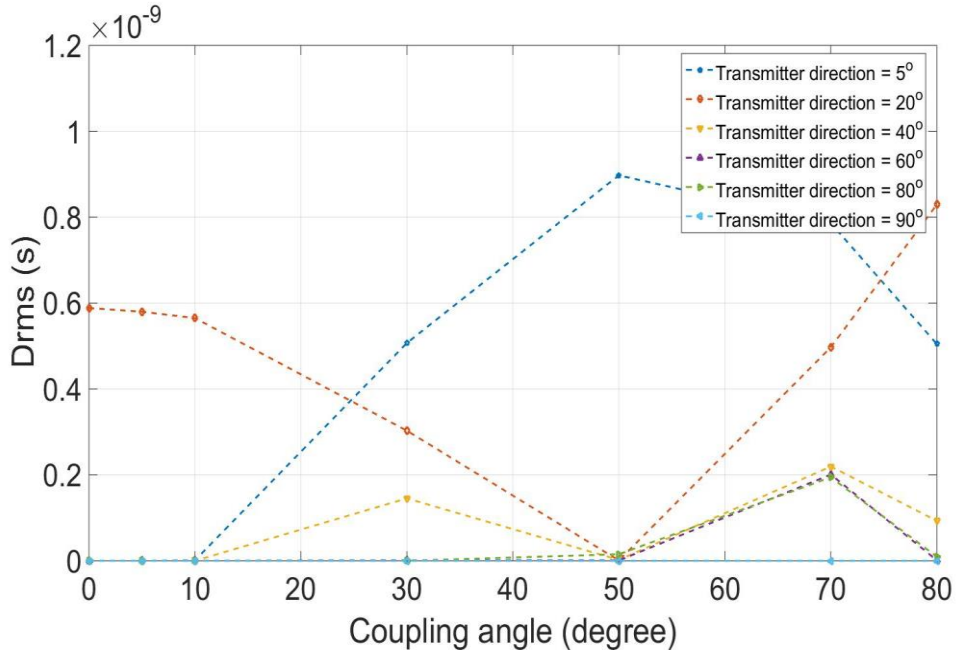

Figure 6-18 RMS delay spread versus coupling angle for several values of transmitter direction in reflective environment with directive source

Table 6-6 Bandwidth for coupling angle for several values of transmitter direction in reflective environment with /directive source

Bending angle / Transmitter direction	0˚	5˚	10˚	30˚	50˚	70˚	80˚
0˚	-	-	-	151 MHz	710 MHz	101 MHz	152 MHz
20˚	208 MHz	214 MHz	242 MHz	410 MHz	-	210 MHz	122 MHz
40˚	-	-	-	292 MHz	-	-	215 MHz
60˚	-	-	-	-	-	650 MHz	-
80˚	-	-	-	-	-	-	-
90˚	-	-	-	-	-	-	-

6.7.1. 0˚ coupling angle analysis

This configuration will be studied analytically, as using material which follows the

Phong model with high reflectivity and high directional source makes the random ray movement rare and it can be calculated.

The 2D representation of the system configuration is illustrated in Figure 6-19.

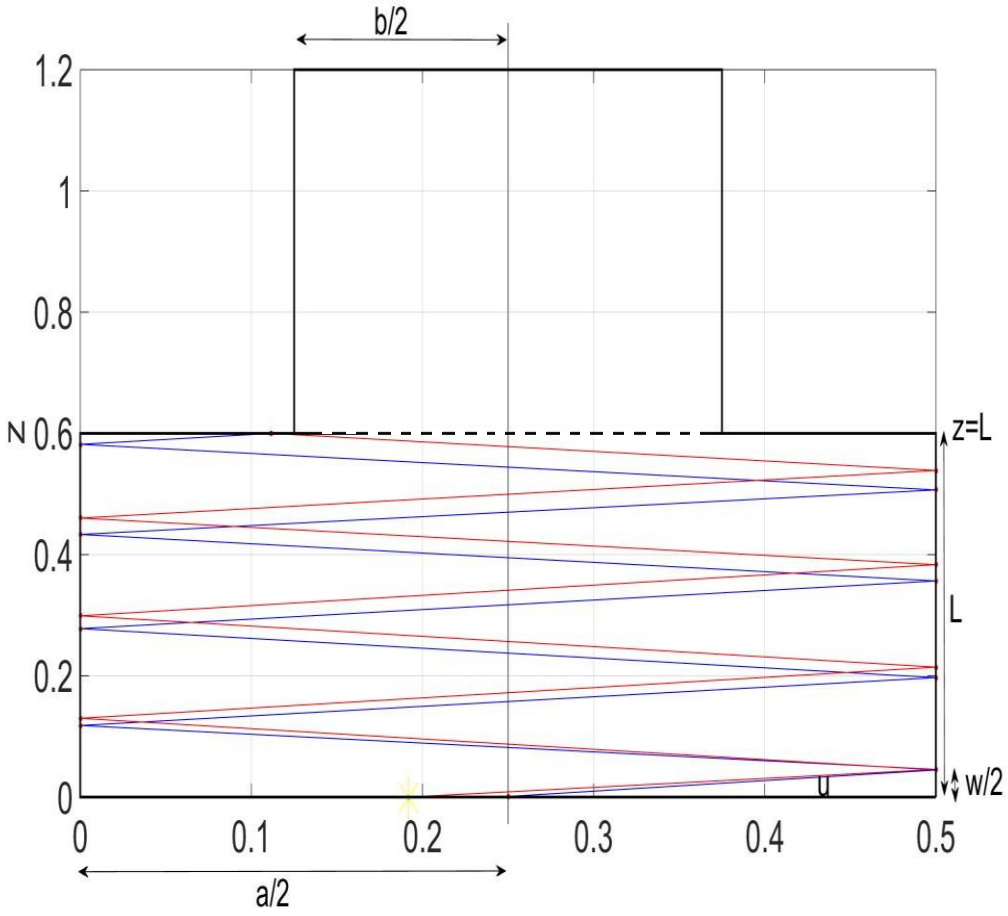

Figure 6-19 2D representation for coupling two waveguides at 0˚ coupling angle with two rays

The first waveguide length is L and width is a, the transmitter direction angle is u ($0<u<90^{\circ}$), the second waveguide width is b. The first reflection hits the surface at distance $w/2$ from the waveguide entrance, where:

$$\frac{w}{2} = \frac{a}{2} + \tan(u) \qquad (6\text{-}1)$$

The second reflection happens at distance *1.5w* from the waveguide entrance. The number of reflections the rays experiences in the first waveguide:

$$q = int\left(\frac{L}{w}\right) \qquad (6\text{-}2)$$

where q is the nearest integer number to *L/w*. The last point the ray hits the waveguide has coordinate (x_0, z_0) where

$$z_0 = \left(q - \frac{1}{2}\right) w \qquad (6\text{-}3)$$

$$x_0 = \begin{cases} a & q \text{ odd} \\ 0 & q \text{ even} \end{cases} \qquad (6\text{-}4)$$

And the ray equation after the last hit point is:

$$\begin{cases} z - z_0 = \frac{-w}{a}(x - x_0) & q \text{ odd} \\ z - z_0 = \frac{w}{a}(x - x_0) & q \text{ even} \end{cases} \qquad (6\text{-}5)$$

Then the point where the last ray intersects with the upper waveguide surface is found by substituting $z=L$ in (6-5) and finding x. If this is within the second waveguide entrance then the ray travels into the second waveguide and thence to the receiver. Otherwise it will reflect back to the first waveguide and it will not proceed.

For example:

Applying the simulation parameters with transmitter direction angle u = 5˚, a = 50 cm and b = 25 cm. L = 60 cm. Then:

$$w = 4.37\ cm$$

and the ray will undergo q =13.71 ≈ 14 reflections (even number).

$$z_0 = 58.995\ cm$$

$$x_0 = 0$$

By substituting these values in equation (6-5) with L = 60 cm

$$x\ = 11.49\ cm$$

This point does not correspond gepmetrically to the second waveguide entrance and the ray will reflect back. Figure 6-19 illustrates one ray path where the blue part represents the forward ray while the red part represents the ray after reflecting back in the wave-guide.

For transmitter direction angles 20˚, 50˚, 60˚ the ray will hit the exit surface of the first waveguide at the points *x = 10* cm*, 24.64* cm*, 40.35* cm.

This means that the beam of light transmitted from the source with transmitter direction angle = 50˚ will reach the receiver, while for transmitter direction angles of 20˚ and 60˚

it will not reach the receiver. However, because of the transmitter beam divergence and the scattering part of environment radiation pattern (Phong model), part of it might pass through, which explains the received power and path loss values in section 6.7.

6.8. Discussion

The connection of two waveguides may be achieved through various couplers with different coupling angles. Long couplers might give smooth passage for the light to travel from the transmitter to the receiver but the direct path length between them will increase. Furthermore, the waveguide material affects the way the light is reflected which might change the ray path. In general, and from the results presented, several insights are obtained; higher power is acquired from a reflective material which follows the Phong model with a directive transmitter, but the transmitter direction should be chosen carefully. While using scattering material, whether with a Lambertian transmitter or directive transmitter, the received power follows a consistect pattern: the received power decreases with the coupling angle increment and it increases with increases in the transmitter direction angle.

Regarding the bandwidth value, a high bandwidth is realisable through any configuration. The smallest bandwidth found is 71 MHz in a reflective material with a directive source when it is directed with 5˚ and the coupling angle is 50˚.

6.9. Conclusions

In this chapter an analysis of the OWC channel of various waveguide configurations has been conducted in order to connect two waveguides efficiently. There are four different cases in this situation, namely, scattering material with Lambertian transmitter, scattering material with directive transmitter, reflective material with Lambertian transmitter, and reflective material with directive transmitter. The chapter deals with the aspects of: power received, path loss, delay spread and channel bandwidth in all the above mentioned cases. After presenting the simulation results, particular attention has been taken paid to one specific case (reflective material with directive transmitter) which has been studied analytically in order to understand the light movement through the waveguide.

Chapter 7: Conclusions and future work

7.1. Introduction

This Chapter summarises the main findings of this research and presents the conclusions. It also includes suggestions for further future research.

7.2. Summary

The main idea behind this research has been to introduce a new environment for OWC systems beside indoor and outdoor environments. Waveguides are considered as potential media to transfer information through light. The main application which drove the work is to integrate OW with RF systems in the IVC network.

The cost and weight of a modern automobile's cable harness is substantial as it may weigh up to 30kg. With many modern bus systems still using redundant connections, link breaks are always a concern. On the other hand, the RF wireless medium over-

comes few disadvantages, RF susceptibility restricts the system performance. In addition, using the RF spectrum requires frequency preallocation which adds to the system cost.

OWC with all its advantages, including high bandwidth, immunity to EMI and a high security level it provides, suggests its use in IVC networks. Despite initial interest in defining OW links in the vehicle cabin [74], other vehicle parts can be used as pathways for the OW signal; for example, the vehicle frame or the engine compartment. Both the doors and the vehicle frame form potential waveguiding structures that are free of sun and ambient light. This work explores the validity of using the light through waveguides in general and vehicle frame in particular.

Chapter 2 covers recent studies regarding IVC systems with their requirements, advantages and drawbacks. Then, it moves to discuss OWC systems, comparing it with RF systems and how it started to be employed in transportation systems in various domains. However, applying OWC systems in IVC has been proposed recently within the vehicle cabin only. Therefore, the idea which drives this interesting research has been identified, namely applying OWC link within the vehicle frame, *i.e.* confined space which has been defined as waveguides through the thesis.

Chapter 3 discussed in detail different indoor OWC channel models which have been proposed until now. The theory behind each algorithm has been criticized in addition

to detailed comparison among these algorithms in order to build the simulator which will be used through the work.

In **Chapter 4**, a specific simulator has been developed in order to satisfy the proposed environment. The simulator determines all parameters needed to analyse the channel performance. It covers LOS, non-LOS and diffuse links. The simulator has been tested against previous studies and against a basic experiment. The novelty of the simulator is its ability to study materials which follow Phong model. All previous studies either concerned Lambertian model which assumes that the light scatters after hitting a surface or the surface is completely reflective where the reflected light contains only the specular component. In reality, however, the reflected light contains both scattering and specular components depending on the material specifications. Besides, the simulator handles a high number of reflections in contrast to the original indoor OWC channels where 3-5 reflections are studied. This increment in the number of reflections costs computational time. Therefore, an improvement has been made in order to keep the computational time to a minimum.

After defining the environment and building the simulator, the implementation part starts; **Chapter 5** studies the possibility of sending OW signals through waveguides, starting with straight waveguides and then moving to sharp waveguide bends. Two waveguide materials have been studied (scattering and mixed scattering-reflective ma-

terials) with the use of 2 types of transmitters (Lambertian, and directional). The receiver effect has been studied as well where different receiver FOVs were implemented besides different receiver apertures. A more detailed study has been conducted regarding right angle bend waveguide where the channel characteristics distribution over different planes have been analysed. One of the interesting results has shown that when the material radiation pattern follows the Lambertian model then the graph represents the normalized path loss versus the bending angle follows the same pattern for each case through different values of the measured variable (receiver FOV or area). In the same environments, LOS link existence makes a considerable difference on the received power value where it drops ten times when it disappears.

In reflective material, it has been shown that when using Lambertian source, the link performance degrades with bending angle increase except for 90˚ because of the bending shape chosen for this application. When using directive source, it has been shown that a slightly bending waveguide performs better than a straight one. It is believed that the existence of LOS link beside other reflections caused by the bend will increase the received power at the cost of bandwidth.

In **Chapter 6**, a different set of links have been studied. Another common structure which might be found in vehicle structure is connecting two waveguides which have different dimensions. The effect of the connection at different coupling angles has been explored for different environments. It has been shown that the coupling angle affects

the quality of the received signal. However, this system benefits from the LOS link between the transmitter and the receiver in contrast to the first set where the bending eliminates the existence of LOS link. Therefore, the concentration has been made on the transmitter direction instead of receiver characteristics.

Higher power is acquired from a reflective material which follows the Phong model with a directive transmitter, but the transmitter direction should be chosen carefully. While using scattering material, whether with a Lambertian transmitter or a directive transmitter, the received power follows the same pattern: the received power decreases with the coupling angle increment and it increases when the transmitter direction angle increases.

Regarding the bandwidth value, a high bandwidth is realisable through any configuration. The smallest bandwidth found is 71 MHz which it allows for multimedia communications.

7.3. Future work

As new research, a window is opened to carry more ideas and investigations in new applications for the OW domain.

7.2.1. Improved scenarios

To begin with, more scenarios can be investigated, namely T-shape and circular cross

section waveguides. Although it is specific application software, it could be applied to other similar purposes by changing the parameters, and running the software. T-shape configuration is presented in Figure 7-1. While circular cross section is found in Figure 7-2, finding the intersection point between the ray and the circular cross section waveguide consumes higher computational time which makes the current simulator less efficient in modelling the OWC system, and improved intersection algorithm will be desirable.

The maximum number of waveguides per case was three in the thesis, and as a proposal for future work; a more complicated set of waveguides can be implemented in order to design a full intra-vehicle communication system. Other aspects which should be studied are the effect of paint, fluids in different vehicle parts and corrosion on the optical transmission.

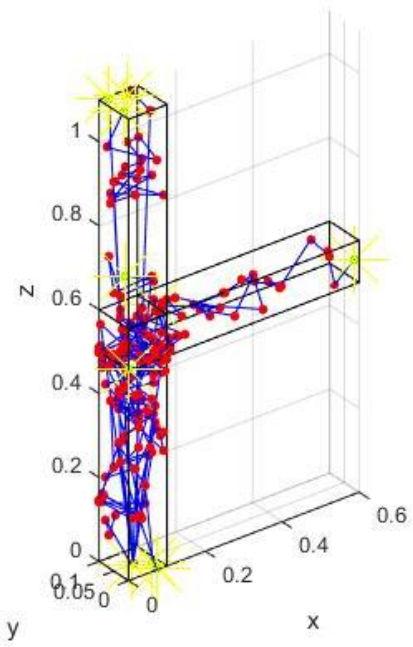

Figure 7-1 T-shape configuration

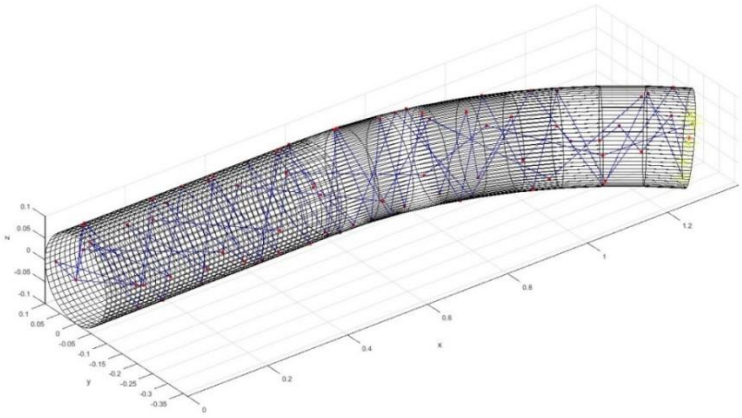

Figure 7-2 Circular cross section waveguide

Introducing this research into practical experiments will have interesting outcomes. Even though it has a relatively clear idea about how light works in waveguides, but going further to the experiment side will be interesting as a first step into proposing the idea to be a transportation standard.

Future further work in this research would target the different modulation schemes and

use it for transmitting the signals. The three major modulation schemes in the optical wireless channel will be studied: On-off keying (OOK), pulse amplitude modulation (PAM), and pulse position modulation (PPM), according to their power and bandwidth requirements.

In addition to vehicular applications, OW through waveguides can be implemented in other applications, for example, connecting rooms through light pipes instead of using fibres. Medical devices can benefit from the idea where the wires can be replaced by light traveling through the device frame.

References

[1] D. Tsonev, H. Chun, S. Rajbhandari, J. J. McKendry, S. Videv, E. Gu, M. Haji, S. Watson, A. E. Kelly, G. Faulkner, and others, "A 3-Gb/s Single-LED OFDM-Based Wireless VLC Link Using a Gallium Nitride," *Photonics Technology Letters, IEEE*, vol. 26, no. 7, pp. 637–640, 2014.

[2] R. Hou, Y. Chen, J. Wu, and H. Zhang, "A brief survey of optical wireless communication," in *Proc. of the 13th Australasian Symposium on Parallel and Distributed Computing (AusPDC2015), Australia, Jan*, 2015, vol. 2730, pp. 41–50.

[3] Z. Ghassemlooy, S. Arnon, M. Uysal, Z. Xu, and J. Cheng, "Emerging optical wireless communications-advances and challenges," *Selected Areas in Communications, IEEE Journal on*, vol. 33, no. 9, pp. 1738–1749, 2015.

[4] R. M. Sova, J. E. Sluz, D. W. Young, J. C. Juarez, A. Dwivedi, N. M. Demidovich III, J. Graves, M. Northcott, J. Douglass, J. Phillips, and others, "80 Gb/s free-space optical communication demonstration between an aerostat and a ground terminal," in *SPIE Optics+ Photonics*, 2006, pp. 630414–630414.

[5] R. Silvennoinen, K. E. Peiponen, T. Asakura, Y. F. Zhang, C. Gu, K. Ikonen, and E. Morley, "Specular reflectance of cold-rolled aluminum surfaces," *Optics and lasers in engineering*, vol. 17, no. 2, pp. 103–109, 1992.

[6] L. J. Johnson, F. Jasman, R. J. Green, and M. S. Leeson, "Recent advances in underwater optical wireless communications," *Underwater Technology*, vol. 32, no. 3, pp. 167–175, 2014.

[7] A. Sangiovanni-Vincentelli, "Automotive electronics: Trends and challenges," in *SAE CONFERENCE PROCEEDINGS P*, 2000, pp. 295–308.

[8] M. D. Higgins, R. J. Green, and M. S. Leeson, "Channel viability of intra-vehicle optical wireless communications," in *GLOBECOM Workshops (GC Wkshps), 2011 IEEE*, 2011, pp. 813–817.

[9] C. R. Lomba, R. T. Valadas, and A. de O. Duarte, “Experimental characterisation and modelling of the reflection of infrared signals on indoor surfaces,” in *Optoelectronics, IEE Proceedings-*, 1998, vol. 145, no. 3, pp. 191–197.

[10] G. Leen and D. Heffernan, “Expanding automotive electronic systems,” *Computer*, vol. 35, no. 1, pp. 88–93, 2002.

[11] N. Navet, Y. Song, F. Simonot-Lion, and C. Wilwert, “Trends in automotive communication systems,” *Proceedings of the IEEE*, vol. 93, no. 6, pp. 1204–1223, 2005.

[12] A. Sangiovanni-Vincentelli and M. Di Natale, “Embedded system design for automotive applications,” *Computer*, no. 10, pp. 42–51, 2007.

[13] T. Nolte, H. Hansson, and L. L. Bello, “Automotive communications-past, current and future,” in *Emerging Technologies and Factory Automation, 2005. ETFA 2005. 10th IEEE Conference on*, 2005, vol. 1, p. 8–pp.

[14] S. Tuohy, M. Glavin, C. Hughes, E. Jones, M. Trivedi, and L. Kilmartin, “Intra-vehicle networks: A review,” *Intelligent Transportation Systems, IEEE Transactions on*, vol. 16, no. 2, pp. 534–545, 2015.

[15] N. Navet and F. Simonot-Lion, “In-vehicle communication networks-a historical perspective and review,” 2013.

[16] O. Strobel, *Communication in Transportation Systems*. IGI Global, 2013.

[17] G. S. Bickel, “Inter/intra-vehicle wireless communication,” *Reports on Recent Advances in Networking*, p. 2006, 2006.

[18] Y. Sano, H. Fukatsu, Y. Yahata, K. Sakai, R. Hino, and T. Arashida, “Development of new in-vehicle communications system,” *Technical Review of Mitsubishi Motors*, no. 16, pp. 88–94, 2004.

[19] H. Kopetz and G. Bauer, “The time-triggered architecture,” *Proceedings of the IEEE*, vol. 91, no. 1, pp. 112–126, 2003.

[20] S. M. Mahmud and S. Alles, “In-vehicle network architecture for the next-generation vehicles,” 2005.

[21] J. Schoeters, J. Van Winkel, T. Goedemé, and J. Meel, “In-vehicle movie streaming using an embedded system with MOST interface,” in *Automotive Electronics, 2007 3rd Institution of Engineering and Technology Conference on*, 2007, pp. 1–6.

[22] M. Rahmani, J. Hillebrand, W. Hintermaier, R. Bogenberger, and E. Steinbach, “A novel network architecture for in-vehicle audio and video communication,” in *Broadband Convergence Networks, 2007. BcN’07. 2nd IEEE/IFIP International Workshop on*, 2007, pp. 1–12.

[23] P. G. ANDREAS, “MOST The Automotive Multimedia Network,” 2008.

[24] O. Strobel, “Optical data bus technologies for automotive applications,” in *ICTON Mediterranean Winter Conference, 2007. ICTON-MW 2007*, 2007, pp. 1–1.

[25] A. Grzemba, *MOST\textregistered: The Automotive Multimedia Network from MOST25 to MOST150*. Franzis, 2011.

[26] Z. Sun, G. Qin, D. Jinnan, Y. Sun, and W. He, “Design of on-vehicle radio node based on OS81050 in MOST network,” in *Computer, Mechatronics, Control and Electronic Engineering (CMCE), 2010 International Conference on*, 2010, vol. 1, pp. 222–224.

[27] F. Sethna, E. Stipidis, and F. Ali, “What lessons can controller area networks learn from FlexRay,” in *Vehicle Power and Propulsion Conference, 2006. VPPC’06. IEEE*, 2006, pp. 1–4.

[28] T. Nolte, H. Hansson, and L. L. Bello, “Wireless automotive communications,” in *Euromicro Conference on Real-Time Systems, Palma de Mayorca*, 2005, vol. 6, pp. 35–38.

[29] M. Weihs, “Design issues for multimedia streaming gateways,” in *Networking, International Conference on Systems and International Conference on Mobile Communications and Learning Technologies, 2006. ICN/ICONS/MCL 2006. International Conference on*, 2006, pp. 101–101.

[30] G. Leen and D. Heffernan, “TTCAN: a new time-triggered controller area network,” *Microprocessors and Microsystems*, vol. 26, no. 2, pp. 77–94, 2002.

[31] T. Kibler, S. Poferl, G. Böck, H.-P. Huber, and E. Zeeb, “Optical data buses for automotive applications,” *Lightwave Technology, Journal of*, vol. 22, no. 9, pp. 2184–2199, 2004.

[32] G. Leen and D. Heffernan, “Vehicles without wires,” *Computing \& Control Engineering Journal*, vol. 12, no. 5, pp. 205–211, 2001.

[33] H.-M. Tsai, O. Tonguz, C. Saraydar, T. Talty, M. Ames, and A. MacDonald, “Zigbee-based intra-car wireless sensor networks: a case study,” *Wireless Communications, IEEE*, vol. 14, no. 6, pp. 67–77, 2007.

[34] W. Niu, J. Li, S. Liu, and T. Talty, “Intra-vehicle ultra-wideband communication testbed,” in *Military Communications Conference, 2007. MILCOM 2007. IEEE*, 2007, pp. 1–6.

[35] R. de Francisco, L. Huang, G. Dolmans, and H. de Groot, “Coexistence of zigbee wireless sensor networks and bluetooth inside a vehicle,” in *Personal, Indoor and Mobile Radio Communications, 2009 IEEE 20th International Symposium on*, 2009, pp. 2700–2704.

[36] L. Liu, Y. Wang, N. Zhang, and Y. Zhang, “UWB channel measurement and modeling for the intra-vehicle environments,” in *Communication Technology (ICCT), 2010 12th IEEE International Conference on*, 2010, pp. 381–384.

[37] J. Zhang, P. V. Orlik, Z. Sahinoglu, A. F. Molisch, and P. Kinney, “UWB systems for wireless sensor networks,” *Proceedings of the IEEE*, vol. 97, no. 2, pp. 313–331, 2009.

[38] D. Porcino and W. Hirt, “Ultra-wideband radio technology: potential and challenges ahead,” *Communications Magazine, IEEE*, vol. 41, no. 7, pp. 66–74, 2003.

[39] O. Tonguz, H.-M. Tsai, C. Saraydar, T. Talty, and A. Macdonald, “Intra-car wireless sensor networks using RFID: Opportunities and challenges,” *IEEE Mobile Networking for Vehicular Environments*, pp. 43–48, 2007.

[40] U. Keskin, “In-vehicle communication networks: a literature survey,” *Computer Science Report*, no. 09–10, 2009.

[41] S. S. V. Standard, “Class B Data Communication Network Interface,” *J1850*, vol. 11, 1988.

[42] G. Cena, A. Valenzano, and S. Vitturi, “Advances in automotive digital communications,” *Computer Standards \& Interfaces*, vol. 27, no. 6, pp. 665–678, 2005.

[43] R. Makowitz and C. Temple, “Flexray-a communication network for automotive control systems,” in *2006 IEEE International Workshop on Factory Communication Systems*, 2006, pp. 207–212.

[44] J. Berwanger, M. Peller, and R. Grießbach, “byteflight—a new protocol for safety critical applications,” in *Proceedings of the 28th FISITA World Automotive Congress. Seoul, Korea: FISITA*, 2000.

[45] C. Sommer and F. Dressler, *Vehicular Networking*. Cambridge University Press, 2014.

[46] A. J. Moreira, R. T. Valadas, and A. de Oliveira Duarte, “Performance evaluation of the IEEE 802.11 infrared physical layer,” in *Proceedings of the International Symposium on Communication Systems and Digital Signal Processing*, 1998, pp. 10–15.

[47] M. Kavehrad, M. Chowdhury, and Z. Zhou, “Fundamentals of Optical Wireless Communications,” *Short-Range Optical Wireless: Theory and Applications*, pp. 11–25.

[48] Z. Ghassemlooy, W. Popoola, and S. Rajbhandari, *Optical wireless communications: system and channel modelling with MATLAB (chapter 3)*. CRC Press, 2012.

[49] J. M. Kahn and J. R. Barry, "Wireless infrared communications," *Proceedings of the IEEE*, vol. 85, no. 2, pp. 265–298, 1997.

[50] A. Boucouvalas, "IEC 825-1 eye safety classification of some consumer electronic products," in *Optical Free Space Communication Links, IEE Colloquium on*, 1996, pp. 13–1.

[51] H. Elgala, R. Mesleh, and H. Haas, "Indoor optical wireless communication: potential and state-of-the-art," *Communications Magazine, IEEE*, vol. 49, no. 9, pp. 56–62, 2011.

[52] A. Street, P. Stavrinou, D. O'brien, and D. Edwards, "Indoor optical wireless systems-a review," *Optical and Quantum Electronics*, vol. 29, no. 3, pp. 349–378, 1997.

[53] P. P. Smyth, P. L. Eardley, K. T. Dalton, D. R. Wisely, P. McKee, and D. Wood, "Optical wireless: a prognosis," in *Photonics East'95*, 1995, pp. 212–225.

[54] O. Bouchet, H. Sizun, C. Boisrobert, and F. De Fornel, *Free-space optics: propagation and communication*, vol. 91. John Wiley \& Sons, 2010.

[55] F. R. Gfeller and U. Bapst, "Wireless in-house data communication via diffuse infrared radiation," *Proceedings of the IEEE*, vol. 67, no. 11, pp. 1474–1486, 1979.

[56] J. M. Kahn, W. J. Krause, and J. B. Carruthers, "Experimental characterization of non-directed indoor infrared channels," *Communications, IEEE Transactions on*, vol. 43, no. 234, pp. 1613–1623, 1995.

[57] Z. Ghassemlooy and A. Hayes, "Indoor optical wireless communications systems-Part I: Review," *School of Engineering, Northumbria University*, 2003.

[58] S. Hranilovic, *Wireless optical communication systems*. Springer Science \& Business Media, 2006.

[59] R. Ramirez-Iniguez and R. Green, “Indoor optical wireless communications,” in *Optical Wireless Communications (Ref. No. 1999/128), IEE Colloquium on*, 1999, pp. 14–1.

[60] D. J. Heatley and I. Neild, “Optical wireless-the promise and the reality,” in *Optical Wireless Communications (Ref. No. 1999/128), IEE Colloquium on*, 1999, pp. 1–1.

[61] I. Arruego, H. Guerrero, S. Rodriguez, J. Martinez-Oter, J. J. Jiménez, J. Dominguez, A. Martin-Ortega, J. De Mingo, J. Rivas, V. Apestigue, and others, “OWLS: a ten-year history in optical wireless links for intra-satellite communications,” *Selected Areas in Communications, IEEE Journal on*, vol. 27, no. 9, pp. 1599–1611, 2009.

[62] A. H. Hashim, F. D. Mahad, S. M. Idrus, and A. S. M. Supa’at, “Modeling and performance study of inter-satellite optical wireless communication system,” in *Photonics (ICP), 2010 International Conference on*, 2010, pp. 1–4.

[63] D. O’Brien, G. Faulkner, S. Zikic, and N. Schmitt, “High data-rate optical wireless communications in passenger aircraft: Measurements and simulations,” in *Communication Systems, Networks and Digital Signal Processing, 2008. CNSDSP 2008. 6th International Symposium on*, 2008, pp. 68–71.

[64] N. Schmitt, T. Pistner, C. Vassilopoulos, D. Marinos, A. Boucouvalas, M. Nikolitsa, C. Aidinis, and G. Metaxas, “Diffuse wireless optical link for aircraft intra-cabin passenger communication,” in *Proc. of 5th International Symposium on Communication Systems, Networks and Digital Signal Processing CNSDSP 2006*, 2006.

[65] S. Dimitrov, R. Mesleh, H. Haas, M. Cappitelli, M. Olbert, and E. Bassow, “Path Loss Simulation of an Infrared Optical Wireless System for Aircrafts,” in *Global Telecommunications Conference, 2009. GLOBECOM 2009. IEEE*, 2009, pp. 1–6.

[66] D. W. Wong and G. Chen, “Optical design and multipath analysis for broadband optical wireless in an aircraft passenger cabin application,” *Vehicular Technology, IEEE Transactions on*, vol. 57, no. 6, pp. 3598–3606, 2008.

[67] C. B. Liu, B. Sadeghi, and E. W. Knightly, “Enabling vehicular visible light communication (V2LC) networks,” in *Proceedings of the Eighth ACM international workshop on Vehicular inter-networking*, 2011, pp. 41–50.

[68] S. Lee, J. K. Kwon, S.-Y. Jung, and Y.-H. Kwon, “Evaluation of visible light communication channel delay profiles for automotive applications,” *EURASIP Journal on Wireless Communications and Networking*, vol. 2012, no. 1, p. 370, 2012.

[69] A. Cailean, B. Cagneau, L. Chassagne, S. Topsu, Y. Alayli, and J.-M. Blosseville, “Visible light communications: Application to cooperation between vehicles and road infrastructures,” in *Intelligent Vehicles Symposium (IV), 2012 IEEE*, 2012, pp. 1055–1059.

[70] N. Kumar, N. Lourenço, D. Terra, L. N. Alves, and R. L. Aguiar, “Visible light communications in intelligent transportation systems,” in *Intelligent Vehicles Symposium (IV), 2012 IEEE*, 2012, pp. 748–753.

[71] R. J. Green, “Optical wireless with application in automotives,” in *Transparent Optical Networks (ICTON), 2010 12th International Conference on*, 2010, pp. 1–4.

[72] R. J. Green, Z. Rihawi, Z. A. Mutalip, M. S. Leeson, and M. D. Higgins, “Networks in automotive systems: The potential for optical wireless integration,” in *Transparent Optical Networks (ICTON), 2012 14th International Conference on*, 2012, pp. 1–4.

[73] M. D. Higgins, R. J. Green, and M. S. Leeson, “Optical wireless for intravehicle communications: A channel viability analysis,” *Vehicular Technology, IEEE Transactions on*, vol. 61, no. 1, pp. 123–129, 2012.

[74] M. D. Higgins, R. J. Green, and M. S. Leeson, “Optical wireless for intravehicle communications: incorporating passenger presence scenarios,” *Vehicular Technology, IEEE Transactions on*, vol. 62, no. 8, pp. 3510–3517, 2013.

[75] M. S. Kaminski, K. J. Garcia, M. A. Stevenson, M. Frate, and R. J. Koshel, “Advanced topics in source modeling,” in *International Symposium on Optical Science and Technology*, 2002, pp. 46–57.

[76] H. Zerhau-Dreihoefer, U. Haack, T. Weber, and D. Wendt, “Light source modeling for automotive lighting devices,” in *International Symposium on Optical Science and Technology*, 2002, pp. 58–66.

[77] M. Jongewaard, “Guide to selecting the appropriate type of light source model,” in *International Symposium on Optical Science and Technology*, 2002, pp. 86–98.

[78] I. Moreno and C.-C. Sun, “Modeling the radiation pattern of LEDs,” *Optics express*, vol. 16, no. 3, pp. 1808–1819, 2008.

[79] E. F. Schunert, J. K. Kim, "Solid-state light sources getting smart," Science, vol 308, pp 1274-1278, 2005.

[80] J. Ding, Z. Xu, and others, “Indoor Optical Wireless Channel Characteristics With Distinct Source Radiation Patterns,” *Photonics Journal, IEEE*, vol. 8, no. 1, pp. 1–15, 2016.

[81] D. Wu, Z. Ghassemlooy, H. Le Minh, S. Rajbhandari, M. A. Khalighi, and X. Tang, “Optimisation of Lambertian order for indoor non-directed optical wireless communication,” in *Communications in China Workshops (ICCC), 2012 1st IEEE International Conference on*, 2012, pp. 43–48.

[82] D. Wu, Z. Ghassemlooy, S. Rajbhandari, H. Le Minh, and A. C. Boucouvalas, “Improvement of transmission bandwidth for indoor optical wireless communication systems using an elliptical Lambertian beam,” *Photonics Technology Letters, IEEE*, vol. 25, no. 2, pp. 107–110, 2013.

[83] J. Kahn, J. Barry, W. Krause, M. Audeh, J. Carruthers, G. Marsh, E. Lee, and D. Messerschmitt, “High-speed non-directional infrared communication for wireless local-area networks,” in *Signals, Systems and Computers, 1992. 1992 Conference Record of The Twenty-Sixth Asilomar Conference on*, 1992, pp. 83–87.

[84] J. M. Kahn, J. R. Barry, M. D. Audeh, J. B. Carruthers, W. J. Krause, and G. W. Marsh, “Non-directed infrared links for high-capacity wireless LANs,” *Personal Communications, IEEE*, vol. 1, no. 2, p. 12, 1994.

[85] J. R. Barry, J. M. Kahn, W. J. Krause, E. A. Lee, and D. G. Messerschmitt, “Simulation of multipath impulse response for indoor wireless optical channels,” *Selected Areas in Communications, IEEE Journal on*, vol. 11, no. 3, pp. 367–379, 1993.

[86] M. Abtahi and H. Hashemi, “Simulation of indoor propagation channel at infrared frequencies in furnished office environments,” in *Personal, Indoor and Mobile Radio Communications, 1995. PIMRC’95.’Wireless: Merging onto the Information Superhighway’., Sixth IEEE International Symposium on*, 1995, vol. 1, pp. 306–310.

[87] S. Flórez, F. L. Hdez, J. V. Álvarez, and others, “Infrared wireless indoor channels characterisation in asymmetrical rooms,” in *Microwave and Optoelectronics Conference, 1997. Linking to the Next Century. Proceedings., 1997 SBMO/IEEE MTT-S International*, 1997, vol. 2, pp. 492–497.

[88] C. R. Lomba, R. T. Valadas, and A. de Oliveira Duarte, “Propagation losses and impulse response of the indoor optical channel: A simulation package,” in *Mobile communications advanced systems and components*, Springer, 1994, pp. 285–297.

[89] R. Perez-Jimenez, V. M. Melian, and M. J. Betancor, “Analysis of multipath impulse response of diffuse and quasi-diffuse optical links for IR-WLAN,” in *INFOCOM’95. Fourteenth Annual Joint Conference of the IEEE Computer and*

Communications Societies. Bringing Information to People. Proceedings. IEEE, 1995, pp. 924–930.

[90] A. Mihaescu, A. Songue, P. Besnard, O. Bouchet, and Q. Liu, "Reduced model channel method for impulse response: characterization of indoor wireless optical channels," in *Communication Systems, Networks and Digital Signal Processing, 2008. CNSDSP 2008. 6th International Symposium on*, 2008, pp. 544–547.

[91] P. H. Patil and D. Shah, "Performance analysis and channel characterization of indoor infrared wireless communication system," in *Electronics Computer Technology (ICECT), 2011 3rd International Conference on*, 2011, vol. 3, pp. 89–93.

[92] C. R. Lomba, R. T. Valadas, and A. de Oliveira Duarte, "Efficient simulation of the impulse response of the indoor wireless optical channel," *International Journal of Communication Systems*, vol. 13, no. 7–8, pp. 537–549, 2000.

[93] J. B. Carruthers and J. M. Kahn, "Modeling of nondirected wireless infrared channels," *Communications, IEEE Transactions on*, vol. 45, no. 10, pp. 1260–1268, 1997.

[94] F. Lopez-Hermandez and M. Betancor, "DUSTIN: algorithm for calculation of impulse response on IR wireless indoor channels," *Electronics Letters*, vol. 33, no. 21, pp. 1804–1806, 1997.

[95] R. Perez-Jimenez, J. Berges, and M. Betancor, "Statistical model for the impulse response on infrared indoor diffuse channels," *Electronics Letters*, vol. 33, no. 15, pp. 1298–1300, 1997.

[96] F. Lopez-Hernandez, R. Perez-Jimeniz, and A. Santamaria, "Monte Carlo calculation of impulse response on diffuse IR wireless indoor channels," *Electronics Letters*, vol. 34, no. 12, pp. 1260–1262, 1998.

[97] J. Lopez-Hernandez, R. Perez-Jimenez, and A. Santamaria, "Modified Monte Carlo scheme for high-efficiency simulation of the impulse response on diffuse IR wireless indoor channels," *Electronics Letters*, vol. 34, no. 19, pp. 1819–1820, 1998.

[98] F. J. Lopez-Hernandez, R. Perez-Jimenez, and A. Santamaria, “Ray-tracing algorithms for fast calculation of the channel impulse response on diffuse IR wireless indoor channels,” *Optical Engineering*, vol. 39, p. 2775, 2000.

[99] S. Rodr’\iguez Pérez, R. Pérez Jiménez, F. J. López Hernández, O. B. González Hernández, and A. J. Ayala Alfonso, “Reflection model for calculation of the impulse response on IR-wireless indoor channels using ray-tracing algorithm,” *Microwave and Optical Technology Letters*, vol. 32, no. 4, pp. 296–300, 2002.

[100] N. Hayasaka and T. Ito, “Channel modeling of nondirected wireless infrared indoor diffuse link,” *Electronics and Communications in Japan (Part I: Communications)*, vol. 90, no. 6, pp. 9–19, 2007.

[101] V. Pohl, V. Jungnickel, and C. von Helmolt, “A channel model for wireless infrared communication,” in *Personal, Indoor and Mobile Radio Communications, 2000. PIMRC 2000. The 11th IEEE International Symposium on*, 2000, vol. 1, pp. 297–303.

[102] V. Jungnickel, V. Pohl, S. Nonnig, and C. von Helmolt, “A physical model of the wireless infrared communication channel,” *Selected Areas in Communications, IEEE Journal on*, vol. 20, no. 3, pp. 631–640, 2002.

[103] V. Pohl, V. Jungnickel, and C. Von Helmolt, “Integrating-sphere diffuser for wireless infrared communication,” in *Optoelectronics, IEE Proceedings-*, 2000, vol. 147, no. 4, pp. 281–285.

[104] J. B. Carruthers and P. Kannan, “Iterative site-based modeling for wireless infrared channels,” *Antennas and Propagation, IEEE Transactions on*, vol. 50, no. 5, pp. 759–765, 2002.

[105] J. B. Carruthers, S. M. Carroll, and P. Kannan, “Propagation modelling for indoor optical wireless communications using fast multi-receiver channel estimation,” in *Optoelectronics, IEE Proceedings-*, 2003, vol. 150, no. 5, pp. 473–481.

[106] H.-S. Lee, “A photon modeling method for the characterization of indoor optical wireless communication,” *Progress In Electromagnetics Research*, vol. 92, pp. 121–136, 2009.

[107] M. Zhang, Y. Zhang, X. Yuan, and J. Zhang, “Mathematic models for a ray tracing method and its applications in wireless optical communications,” *Optics Express*, vol. 18, no. 17, pp. 18431–18437, 2010.

[108] J.-B. Wang, Y. Jiao, X. Song, and M. Chen, “Optimal training sequences for indoor wireless optical communications,” *Journal of Optics*, vol. 14, no. 1, p. 015401, 2011.

[109] J. Wang, Y. Jiao, X. Dang, M. Chen, X. Xie, and L. Cao, “Training sequence based channel estimation for indoor visible light communication system,” *Optoelectronics Letters*, vol. 7, pp. 213–216, 2011.

[110] A. Behlouli, P. Combeau, L. Aveneau, S. Sahuguede, and A. Julien-Vergonjanne, “Efficient Simulation of Optical Wireless Channel Application to WBANs with MISO Link,” *procedia computer science*, vol. 40, pp. 190–197, 2014.

[111] M. Chowdhury, W. Zhang, and M. Kavehrad, “Combined deterministic and modified monte carlo method for calculating impulse responses of indoor optical wireless channels,” *Journal of Lightwave Technology*, vol. 32, no. 18, pp. 3132–3148, 2014.

[112] Z. Zhou, C. Chen, and M. Kavehrad, “Impact analyses of high-order light reflections on indoor optical wireless channel model and calibration,” *Lightwave Technology, Journal of*, vol. 32, no. 10, pp. 2003–2011, 2014.

[113] O. González, S. Rodr’\iguez, R. Pérez-Jiménez, B. R. Mendoza, and A. Ayala, “Comparison of Monte Carlo ray-tracing and photon-tracing methods for calculation of the impulse response on indoor wireless optical channels,” *Optics express*, vol. 19, no. 3, pp. 1997–2005, 2011.

[114] S. Elahmadi, M. D. Srinath, D. Rajan, and R. Haberrman, “Channel capacity and modeling of optical fiber communications,” in *Proceeding of the Sixth international conference on Wireless and Optical Communications Networks (WOCN’09 Proceedings)*, 2009, pp. 73–78.

[115] W. Jin-jiang, L. Wen-yao, and C. Huai-yu, “Mont Carlo simulation of surface Lambertian source,” in *Proc. of SPIE Vol*, 2003, vol. 5254, p. 245.

[116] K. Bisshopp, “Rodrigues’ formula and the screw matrix,” *Journal of Engineering for Industry*, vol. 91, no. 1, pp. 179–184, 1969.

[117] M. Kavehrad, M. Chowdhury, and Z. Zhou, “Analyses of Indoor Optical Wireless Channels Based on Channel Impulse Responses,” *Short-Range Optical Wireless: Theory and Applications*, pp. 67–109.

[118] M. Higgins, Z. Rihawi, Z. A. Mutalip, R. Green, and M. S. Leeson, “Optical Wireless Communications in Vehicular Systems,” *Communication in Transportation Systems*, p. 209, 2013.